A Multi-functional st-ELR Scaffold for Dentin Regeneration

A Dissertation

SUBMITTED TO THE FACULTY OF

UNIVERSITY OF MINNESOTA

BY

Caixia Lan

IN PARTIAL FULFILLMENT OF THE REQUIREMENTS

FOR THE DEGREE OF

DOCTOR OF PHILOSOPHY

Supervisor: Conrado Aparicio

December 2018

Acknowledgements

This thesis represents not only my work but also the great contributions of many people. I would like to express my sincere gratitude to all those people who had made my PhD candidature an experience that I will cherish forever.

Firstly, I would like to express my deepest gratitude to my advisor, Professor Conrado Aparicio, for his constant support, motivation, and patience during this period. He taught me professional skills, trained me to be a researcher, and helped me to think more critically. I am deeply grateful to him for our weekly long discussions which helped me troubleshoot problems encountered in my experiments. He was always there to listen, to discuss and to support me through thick and thin. His constant encouragement and sagacious guidance walked me through all the difficulties during my candidature and enriched me with a wealth of knowledge.

I am also thankful to my committee members, Professor Alex Fok, Professor Chun Wang and Professor Wook-jin Seong, for their insightful comments, valuable advices, and encouragement on this thesis dissertation and my research. Their advices and comments at my preliminary examination and 6-month seminar were inspiring and helped me focus my ideas better and make my work more impactful.

I would like to take this opportunity to pay my special thanks to all the members of MDRCBB. Professors Alex Fok, Conrado Aparicio, Ralph Delong, William Douglas, and Maria Pintado have created such a wonderful environment in MDRCBB and provided such great opportunities to make my journey unforgettable.

Abstract

Pulpitis is one of the most widespread diseases in the world. Current advances in dental tissue engineering have provided an interesting alternative therapeutic approach in the field of regenerative endodontics. However, there remains a strong need to develop an optimized scaffold for supporting dentin regeneration. The objective of this PhD project is to develop a dental scaffold using elastin-like recombinamers(ELRs) to stimulate dentin regeneration while exhibiting antimicrobial ability to control potential re-infection of the pulp cavity.

To provide a biomimetic scaffold that resembles the extracellular matrix in dentin tissue, we fabricated fibrous scaffold of ELRs using electrospinning technique and analyzed its ability in inducing biomimetic mineralization using the polymer-induced liquid precursor (PILP) process. The ELR scaffolds exhibited intra- and extra-fibrous mineralization, which highly mimicked the structure of mineralized native collagen in dentin.

The scaffold is expected to be applied in the pulp cavity with direct contact with the pulp tissue. Therefore, we investigated the interaction between the mineralized ELR scaffold that contains statherin-derived peptide (st-ELR) and human dental pulp stem cells (hDPSCs). Proliferation and odontogenic differentiation of hDPSCs were analyzed and the study indicated that biomimetically mineralized st-ELR scaffold supported the proliferation and odontogenic differentiation of hDPSCs.

Bacterial infection is considered as the major reason for the failure of implanted materials. Therefore, we functionalized st-ELR scaffold with antimicrobial peptides to prevent the potential infection caused by oral bacteria. A cysteine modified antimicrobial peptide GL13K(Cys-GL13K) was used in this study to achieve site-specific modification on the

developed scaffold. First, we tethered Cys-GL13K peptides on titanium surface to analyze the properties and antimicrobial ability of immobilized peptides. A homogenous and strong coating of peptides was obtained. The tethered peptides exhibited promising antimicrobial ability against *S. mutans*, *S. gordonii* and *E. faecalis*. Furthermore, we bio-conjugated the peptides to st-ELR membranes using the same modification technique. Successful peptide modification was achieved, and the peptide functionalized st-ELR membrane exerted antimicrobial ability against *S. mutans* and *S. gordonii.*

This research sheds light on the development and functionalization of scaffolds for the application of regenerating hard tissues such as dentin and bone. It allows the scaffold to highly resemble the architecture and physical properties of extracellular matrix in mineralized tissues. In addition, this research provides a new approach to modify the scaffold with diverse bioactive molecules to obtain multiple functions, while maintaining good interaction with native tissues.

Table of Contents

List of Tables

List of Figures

List of Abbreviations

ALP	alkaline phosphatase level
APTES	(3-aminopropyl) triethoxysilane
ATP assay	adenosine triphosphate assay
ATR-FTIR	Attenuated Total Reflectance Fourier-transformed Infrared Spectrscopy
BMP1	bone morphogenetic protein 1
CFU	colonies forming units
CPTES	(3-chloropropyl) triethoxysilane
Cys-GL13K	cysteine modified GL13K peptide
Cys-GL13K-R1	random sequence of Cys-GL13K peptide
DAPI	4', 6-diamidino-2-phenylindole
DMP1	dentin matrix protein 1
ECM	extracellular matrix
EDS	Energy Dispersive Spectrometry
Elisa	enzyme-linked immunosorbent assay
ELR	elastin-like recombinamer
eTi	etched titanium
FM	fluorescence microscope
GL13K-FAM	GL13K peptide tagged with a FAM molecule
HA	hydroxyapatite
HBBS	Hank's Balanced Salt Solution

HMDI	hexamethylene diisocyanate
hDPSCs	human dental pulp stem cells
OCN	osteocalcin
PCL	polycaprolactone
PEG	as polyethylene glycol
PGA	polyglycolide
PILP	polymer induced liquid precusor
PLA	polylactide
PLGA	poly(lactic-co-glycolic acid)
RCT	root canal treatment
ref-ELR	reference elastin-like recombinamer
RT	room temperature
SBS	sodium phosphate buffer
SEM	Scanning electron microscope
st-ELR	statherin incoporated elastin-like recombinamer
TCP	tri-calcium-phosphate
TEM	Transmission Electron Microscopy
TGF	transforming growth factors
TGF	transforming growth factor
VEGF	vascular endothelial growth factor
XPS	X-ray photoelectron spectroscopy

Chapter 1: Introduction and Objective

1.1 Pulpitis and pulp capping procedures

1.1.1 Tooth anatomy and pulpitis

The tooth is a small, calcified organ that has a complex structure that includes four components: enamel, dentin, cementum and pulp (Fig. 1.1A). Enamel and cementum cover the outer surface of the tooth at its crown and root, respectively, while dentin encapsulates the only soft tissue in the tooth, the dental pulp, leaving only one small apical foramen connected to the periapical tissue in each root canal. The dental pulp consists of fibers, different types of cells (e.g., odontoblasts, fibroblasts and stem cells), blood vessels and nerves that are responsible for generating the mineralized dentin tissue and maintaining tooth vitality, moisture and sensitivity to biological and pathological stimuli. Dentinogenesis is the major function of pulp tissue, which is accomplished by a monolayer of odontoblast cells that line the pulpal wall of dentin (Fig. 1.1B). During tooth development, the processes of odontoblasts cross the pre-dentin and extend into the dentin bulk up to the dentin enamel junction (DEJ), resulting in the formation of the specific dentin structure with dentin tubules[1, 2] (Fig. 1.1B). Pulp tissue and dentin are combined into a complex by these tubules and make up the fundamental part of the dentinal flow system (Fig. 1.1C) that regulates the transport of fluid and nutrients from pulp tissue to nourish dentin and enamel[3]. These tubulesparticipate in the transmission of the sensed stimulus to pulp tissue[4]. Unlike bone tissue, dentin is not vascularized, but some nerve endings are present in the dentin tubules. Fluid movement occurs in tubules when dentin is irritated, which stimulates the nerve endings in the inner part of dentin and pulp tissue[5], causing tooth hyposensitivity.
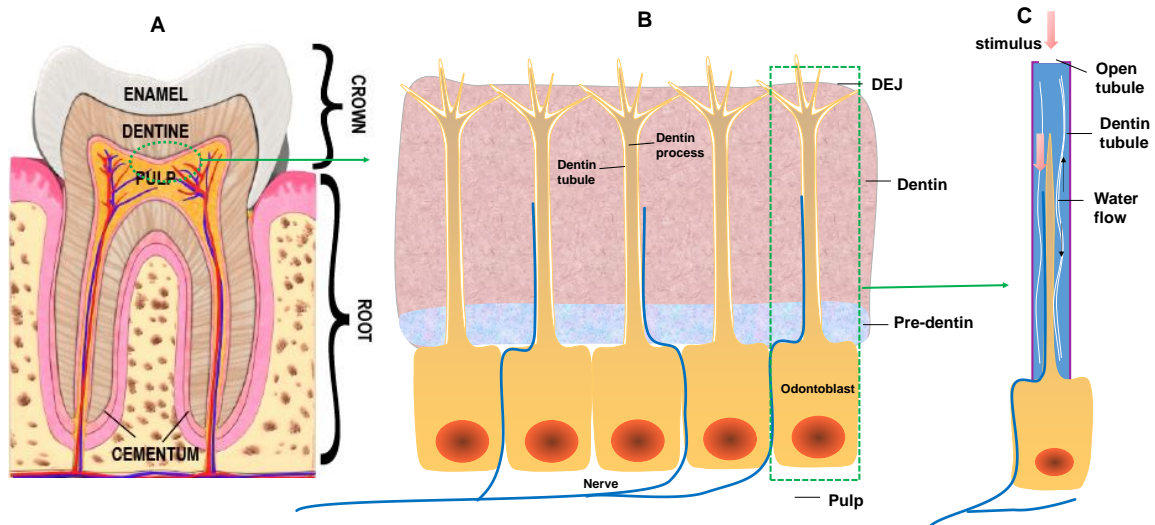
Figure 1.1 **A: Anatomy of the tooth** (adapted from

http://www.drrossdixon.com/_blog/Healthy_Lifestyle_Tips/post/anatomy-of-a-tooth/); **B: schematic of an odontoblast and dentinal tubule; C: dentinal tubule flow system.**

Although dental pulp tissue is sealed and protected by enamel and dentin, it is vulnerable to caries and mechanical trauma. Bacterial invasion from caries lesions is the most common cause of pulpal inflammation and infection. When acidogenic and aciduric carious bacteria invade the middle or deep layers of dentin, which contain 3-fold more dentin tubules than the outer 1/3 of dentin, these bacteria or their byproducts (e.g., acid) can infuse through the dentin tubules and irritate pulp tissue[6, 7] (Fig. 1.1C). In response to low levels of stimulation, odontoblasts secrete reparative dentin, a layer of poorly organized and mineralized dentin, to protect pulp tissues. However, if bacterial invasion continues to progress, it ultimately destroys the odontoblast layer and leads to irreversible pulpitis (Fig.

3

1.2). The release of immune complexes and byproducts, such as extracellular proteolytic enzymes from immune cells, aggravate the inflammation and result in high pressure within the encapsulated pulp cavity[7], causing severe tooth pain and pulp necrosis. The specific anatomical structure of the tooth limits the self-repair ability of pulp tissue, as only one tiny apex foramen is present for the drainage of body fluids, making the elimination of the infection and delivery of drugs to the affected tissue extremely difficult.
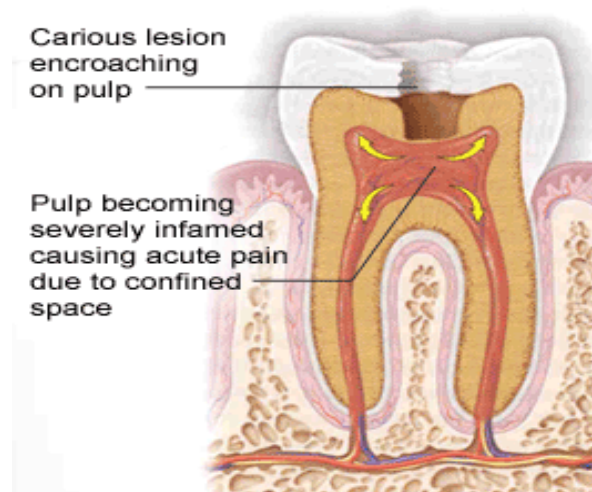
Figure 1.**2 Schematic of pulpal inflammation caused by bacterial invasion** (adapted from www.smilesforlifeoralhealth.org).

1.1.2 Endodontic therapies for pulpitis

Because of the global prevalence of dental caries, caries-associated pulpitis represents a significant problem in dental clinics. According to a report from "Dentistry today", millions of endodontic treatments were performed in 2003, accounting for approximately $8.2 billion of costs in the health care system [8]. This trend is increasing annually. The two common endodontic therapies for pulpitis, root canal treatment (RCT) and vital pulp

therapy, are used to block the progression of the disease. However, many challenges remain to be overcome, and more action is required to improve endodontic therapy.

Root canal treatment

The traditional therapy for pulpitis is RCT which includes the complete removal of pulp tissue, followed by root canal shaping, disinfection, and filling with endodontic filling materials, such as gutta percha. Despite its reported high clinical success rate, RCT has many drawbacks. First, the tooth becomes brittle and more susceptible to fracture because of the lack of a nutrient supply from the vital pulp. Actually, the loss of vitality is one of the most common reasons for vertical tooth fracture, particularly in load-bearing molars[9]. Second, RCT always leads to discoloration of the tooth, which significantly affects aesthetics. An additional investment in subsequent restoration therapy, such as veneers or crowns, is always required, posing a more substantial economic burden on the patients. Third, due to the loss of sensation, the tooth becomes less sensitive to stimuli, and thus the progression of caries is less noticeable[10]. Consequently, the preservation of the viability of healthy pulp tissues is critical for addressing the related problems and retaining the tooth for longer periods.

Vital pulp therapy

Vital pulp therapy is another endodontic therapy that focuses on maintaining the pulp viability for cases in which pulp is exposed due to mechanical trauma or caries removal. A direct pulp capping procedure involves the removal of the infected coronal pulp tissue, followed by the placement of pulp capping materials and subsequent cavity restoration. The goal of the therapy is to stimulate cells in the remaining healthy pulp tissue to generate

a layer of reparative dentin that will seal pulp tissue and thus block potential further invasion of bacteria. This approach also thereby maintains pulp vitality, as well as the moisture and toughness of the tooth. However, the application of this therapy is controversial, as it is greatly depends on the condition of tooth damage. Although vital pulp therapy has shown a high success rate when the pulp of an immature tooth is exposed due to mechanical trauma, the prognosis of carious pulp exposure is questionable. In addition, several concerns about the commercial pulp capping materials remain to be addressed. Traditional capping agents, such as calcium hydroxide and mineral trioxide aggregate (MTA), are applied because of their ability to promote the formation of a dentin bridge beneath the sealing materials[11]. These materials, however, have some drawbacks. 1) They induce potential tooth discoloration[12]. 2) MTA has low biodegradation rates that inhibit further replacement with new dentin. 3) MTA is not easy to process in clinical practice and might not completely seal the defect [13]. 4) Both MTA and calcium hydroxide have low mechanical strength[14], and 5) the degradation of calcium hydroxide leads to a high pH, which may irritate pulp tissue[15] and stimulate the hyperproliferation of scar dentin, resulting in the obstruction of the root canals[13]. Given these challenges, most teeth that are treated with direct pulp capping after pulpotomy require eventual root canal therapy after several years.

1.2 Dental tissue regeneration

Given the challenges of traditional endodontic therapy, effective approaches that help maintain or restore the health of dental tissues must be developed and are urgently needed.

With the expanding knowledge of tissue engineering, dental tissue regeneration has attracted increasing interest in the past few decades. In the field of regenerative dentistry, many studies have been conducted to investigate the regeneration of periodontal ligaments[16], dentin[17], dental pulp[18] and even the whole tooth[19] using a variety of biomaterials and techniques. Two major approaches have been described for dentin-pulp regeneration: 1) the complete regeneration of the pulp in a necrotic tooth (Fig. 1.3A); and 2) the regeneration of dental tissues using vital pulp therapy[20] (Fig. 1.3B).

Complete pulp-dentin regeneration

To date, most previous studies have focused on the regeneration of dental pulp tissue in the necrotic pulp cavity. The primary goal is to apply biomaterial-based scaffolds within the empty pulp cavity to stimulate the regeneration of dentin-pulp and restore the vitality and function of the tooth (Fig. 1.3A). The scaffolds are usually prepared as injectable formulations and can be incorporated with odontoblast inductive cells and growth factors. One strategy is to place the cell-seeded scaffold in the pulp cavity. The cells are expected to differentiate into pulp tissue-related cells, such as fibroblasts and odontoblasts, to regenerate the whole soft pulp tissue and hard dentin matrix. Another method is to fill the pulp cavity with acellular scaffolds and stimulate the migration of stem cells from the apical connective tissue to the pulp. However, the process of complete dental pulp regeneration in a non-vital tooth is much more complicated and difficult than the partial regeneration process because of the substantial challenges posed by completing the restoration of the nerves and vasculature [21, 22]. The ingrowth of blood vessels within the scaffold occurs over several days, while the cells begin to lose their activity within hours.

7

For adult teeth, the apical foramen is too narrow to allow the sufficient ingrowth of blood vessels and nerve endings from the apical tissue to the pulp cavity, representing a significant barrier to providing the necessary nutrients for the subsequent cell activity in the scaffold.

Partial dentin-pulp regeneration

The more direct and clinically practical approach is to utilize scaffolds to regenerate the lost parts in combination with the potential reparative signaling effects of the remaining healthy pulp tissues. As shown in Figure 1.3B, instead of filling the whole pulp space, biological scaffolds with odontoblast inductive properties are placed on top of the remaining healthy pulp tissue after pulpotomy. The uninfected pulp tissue in root canals is maintained to preserve the naturally established vasculature and nerves. This strategy overcomes the difficult revascularization posed by the limited apical access, making the access of nutrients easier for subsequent cellular activities. Furthermore, the preservation of some pulp tissue allows clinicians to use a scaffold lacking stem cells. The remaining stem cells within pulp tissue are stimulated to proliferate, migrate and differentiate into odontoblasts within the artificial matrix to secrete new dentin tissue. This approach avoids the use of cells from external sources, reduces side effects and simplifies the restoration procedure. The scaffold is gradually biodegraded and ultimately replaced by new tissues. The bulk replacement of the newly formed dentin structure provides better sealing of pulp tissue than commercial pulp capping materials and leads to a stronger and tougher mechanical strength of the tooth. This technique is considered permanent restoration, and potentially avoids the need for more invasive dental restoration procedures, such as a root

canal treatment and bulky composite restorations. Although artificial dental restoration materials are still needed to seal the top part of the cavity, partial regeneration represents a more conservative endodontic therapy for preserving tooth structure and function to a greater extent.
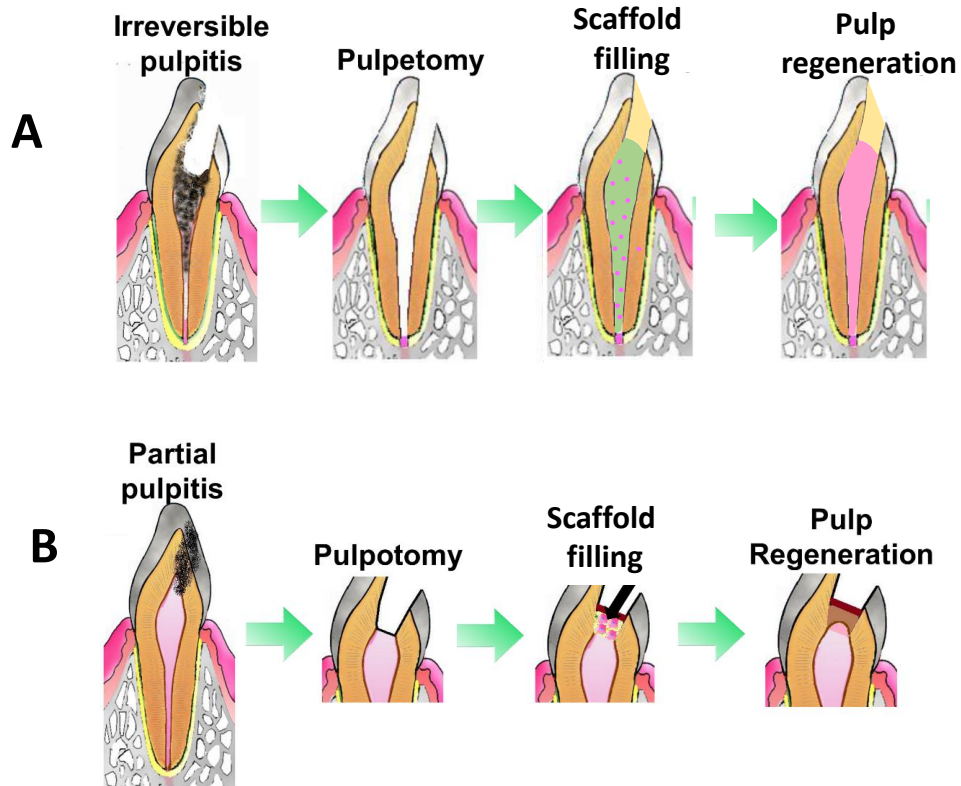
Figure 1.3 **A: Schematic of complete pulp regeneration in a necrotic root canal. B: Schematic of partial pulp regeneration after a pulpotomy**. (Adapted and modified from Iohara et al., Tissue Eng. 2011.)

Dental tissue regeneration is directed by the combination of three components: the scaffold, cell source and growth factors [23]. Scaffolds provide environments that stimulate tissue

growth and may define the shape of the newly formed tissues [23]. In this case, the cell source specifically refers to the dental pulp stem cells (hDPSCs), which are used as the progenitor cells of odontoblasts for subsequent dentin regeneration. The objective of using growth factors is to stimulate the activity and differentiation of target cells. Different growth factors, including chemicals, biological molecules and physical factors, have been used to regulate the cellular activity within the scaffolds [24]. The application of a scaffold, stem cells and growth factors is reviewed further in the subsequent sections.

1.2.1 Optimized architecture of scaffolds for dentin regeneration

In vivo, extracellular matrix (ECM) provides the structural environment for cellular growth and regulates the behavior, morphological arrangement and regenerative abilities of the cells by providing specific growth factors [25]. In dental tissue regeneration, dental scaffolds serve as the ECM and are expected to provide an ECM-mimicking environment for guiding the development of cells and subsequent tissue regeneration [25]. Scaffolds should be biocompatible and exhibit low cytotoxicity, biodegradable for the eventual replacement of natural tissues, and possess ease of customization with an optimized structure and appropriate mechanical properties [26].

Among the above requirements, the overall structure, which includes the pore sizes, density, surface area and their interconnectivity, is a critical property of scaffolds designed to regulate tissue formation [27-29]. Pore interconnectivity is extremely important for the bulk replacement of a new tissue and controls nutrient exchange, cell migration, and the invasion of blood vessels and newly formed tissues [29, 30]. Porous scaffolds have been

produced using a variety of techniques, including phase separation [31], solvent casting [32, 33] and particulate leaching [32]. However, many concerns have been raised, such as the low interconnectivity within the matrix, substantial variation in pore size and reduced thickness of scaffold walls [34]. These challenges constrain the overall tissue infiltration into scaffolds during tissue regeneration.

In this thesis, we utilized the electrospinning technique to fabricate a nano-fibrous dental scaffold. The electrospinning technique offers great advantages in controlling the porous structure and mechanical integrity of the scaffold that resembles the collagenous structure of bone and dentin matrices. This technique facilitates the production of nano-fibrous scaffolds that mimic the dentin extracellular matrix with good pore interconnectivity and a certain level of mechanical strength [35, 36]. A variety of synthetic polymers and natural materials, such as poly(lactic acid) (PLA) [37], (PCL)/gelatin [38], collagen [39], and chitosan [40], have been electrospun into fibrous scaffolds for hard tissue regeneration with the diameter of fibers ranging from 5 to 1000 nm [41]. With advantages in morphologies and mechanical integrity, plus the highly interconnected porosity in the bulk of the scaffold, these elesctrospun constructs have proved to be capable of encouraging the growth of different cells and supporting the formation of mineralized tissues [42].

1.2.2 Mechanical strength of scaffolds: Biomimetic mineralization

Scaffolds must reproduce the mechanical strength of ECM *in vivo* to provide the necessary physical cues for appropriate cellular activity. This feature is of particular relevance for cells that form load-bearing, hard tissues, such as dentin and bone [42, 43]. Cellular proliferation, migration and differentiation are affected by the mechanical strength of the

substrate with which the cells interact [44]. Cells that mainly participate in calcified tissue regeneration, such as osteoblasts and odontoblasts, are more sensitive to the mechanical changes in the scaffold than other cell types. These cells show a preference for very stiff substrates that resemble the elasticity of natural hard tissues [42, 43]. A promising method to achieve a dental scaffold with biomimetic stiffness is to induce the intrafibrillar mineralization of the dental scaffold as the collagenous matrix in dentin, which is also an intrafibrillar mineralized structure. Intrafibrillar mineralization is a key determinant of the physical, chemical, and mechanical characteristics of dentin and bone. The building blocks of these two tissues are based on the hierarchical arrangement of nano-scale hydroxyapatite (HA) crystals within collagen fibrils [45-48]. HA crystals grow within and around the type I collagen fibrils with their C-axis located approximately parallel to the long axis of fibrils [48]. However, this specific spatial relation between the organic and inorganic components of the matrix is a very challenging aspect of producing artificial scaffolds for dentin mineralization and subsequent regeneration.

Polymer-induced liquid precursor process (PILP)

In *vivo*, the mineralization of collagen is directed by non-collagenous proteins (NCPs), such as osteocalcin, dentin phosphoprotein (DSP), and dentin matrix protein 1 (DMP1) [49, 50]. All NCPs are enriched in negatively charged amino acids, such as aspartic acid and phosphorylated serine [50]. These negatively charged proteins are predicted bind to the positively charged areas in the gap zone of collagen and then trigger the crystallization of calcium phosphate [51]. The mineral nucleates preferentially within the collagen fibrils, with their alignment following the constrained space in the fibrils. The growth of minerals

eventually exceeds the size of those interstitial spaces, resulting in a homogenous coating of extra-fibrillar minerals [51, 52].

In an *in vitro* biomimetic mineralization system, poly-aspartic acid (Pasp) is used as an excellent surrogate for NCPs. Pasp inhibits hydroxyapatite crystallization in solution and effectively induces the intra- and extra-fibrillar mineralization of type I collagen [53, 54]. Pasp inhibits the precipitation of calcium phosphate in solution by stabilizing liquid-like amorphous calcium phosphate nano-complexes. These nano-complexes infiltrate into collagen fibrils through the capillary effect and create a local super-saturated environment, which initiates the nucleation of minerals within the interspace of collagen fibrils. The mineral phase transforms into hydroxyapatite and finally grows to an extent that exceeds the space constraints. The method described above for the biomimetic mineralization of collagen is called the polymer-induced liquid precursor process (PILP). The collagen structure also plays an important role in this mineralization process. The first step of mineralization is based on the electrostatic interaction between the positively charged bands on the fibrils and the negatively charged nano-complexes of ACP [52]. When ACPs bind to collagen, crystallization begins. The space constraints of fibrils also regulate the alignment of hydroxyapatite crystals by orienting the crystals t with their C axis located nearly parallel to the long axis of the fibrils [52]. All of these factors contribute to the specific hierarchical structure of minerals in bone and dentin, and provide the specific mechanical environment for appropriate tissue regeneration and responses.

This type of intra- and extra-fibrillar mineralization is a key objective of the design of scaffolds for hard tissue regeneration. Although many researchers have attempted to

supplement the scaffold with hydroxyapatite, such as blending nano-HA within the electrospun fibers [55] or inducing mineralization using stimulating body fluid (SBF)[56], these techniques fail to produce the biomimetic structure of a scaffold with the hierarchical arrangement of minerals and sufficient mechanical strength to induce proper cell activity. In this project, PILP is used as the biomimetic mineralization system to mineralize a fibrous dental scaffold composed of elastin-like recombinamers (ELRs) and is designed for the application of dentin regeneration.

1.2.3 Elastin-like recombinamers (ELRs) as dental scaffolds

In this project, we used an elastin-like recombinamer st-ELR as the dental scaffold for dentin regeneration. ELRs are a type of engineered proteinaceous polymer consisting of repeating units of pentapeptide sequences from natural elastin [57, 58]. ELRs have attracted increasing interest in applications for tissue engineering and drug delivery due to their unique and outstanding combination of properties, such as self-assembly, good biocompatibility, biodegradation, monodispersity, and a molecule-tailored design that provides specific physical/chemical and bioactive properties [59]. As the building blocks of peptide sequences are derived from natural elastin, ELRs exhibit extraordinary biocompatibility. Indeed, ELRs are less likely to induce the immune responses [60]. Furthermore, ELRs show a similar biodegradation rate to natural proteins in vivo [60].

ELRs are versatile biomaterials with thermal sensitivity, which allows them to undergo reversible self-assembly when the temperature increases above a specific value determined by the specific ELR peptide sequence [61]. Generally, at a low temperature, the ELRs form random coils in solution. When the temperature of the system is increased above the critical

transformation temperature (Tf), the polypeptide chains rearrange and form β-spirals. This property is associated with the polar-nonpolar interactions between the different peptide sequence blocks. In ELR molecules, VPGVG units represent the major hydrophobic and non-polar segments. At the initial stage of ELR self-assembly, these units aggregate together, fold ELR chains into β-sheets and separate them from hydrophilic/polar peptide segments, such as VPGKG and VPGIG[61]. This phase separation at temperatures exceeding the critical temperature results in the formation of ELR filaments and the subsequent formation a hydrogel matrix with nano- and micro-porous structures[61]. Thus, ELRs are soluble at low temperature and precipitate at temperatures exceeding the Tf through molecular self-assembly.

The structure of the ELR matrix with nano- and/or micro-pores, along with the positive charges introduced in the peptide chains by design, make ELRs a potential substitute for type I collagen in inducing biomimetic mineralization [59, 62]. The ELR matrix shares several features with the structure of type I collagen. In the PILP mineralization system, the positive charges of ELRs (mainly provided by VPGKG units) might attract the negatively charged calcium phosphate complexes through electrostatic interactions. The nano- and micro-porous structures of the ELR matrix allow the infiltration of ACP nano-droplets through the capillary effect and results in the mineralization within the bulk of the matrix. In previous studies in our lab, crosslinked ELR hydrogels were mineralized using the PILP process, and the results revealed the successful formation of needle-like hydroxyapatite crystals within the matrix [62]. Furthermore, in a study of the biocompatibility of cells cultured on mineralized ELR films, a significant improvement in primary osteoblast activities (cell attachment, proliferation and differentiation) was

observed on a mineralized ELR surface [63]. Based on these data, ELRs potentially represent a good candidate for applications in mineralized tissue regeneration.

However, those ELR hydrogel matrices display limited pore interconnectivity. The ACP complexes failed to infiltrate the core of the matrix. In addition, the poor interconnectivity may hinder the cellular invasion of the scaffold. We used the electrospinning technique to fabricate a pore interconnected nano-fibrous scaffold of ELRs to overcome this problem. The ELR we investigated is a triblock copolymer that includes a statherin-derived peptide, SNa15 (st-ELR) (see table 2.1 in Chapter 2). SNa15, a peptide analog of statherin, is added to the sequence with the aim of regulating crystal nucleation, as it has high affinity for hydroxyapatite and mediates mineral deposition in saliva [64-66].

1.2.4 Human dental pulp stem cells (hDPSCs)

Dental pulp stem cells are the main choice for dental tissue regeneration because of their capacity to undergo odontogenic differentiation and high proliferation rate[67]. In a heathy tooth, dentinogensis is achieved by odontoblasts. These cells, however, lack the self-renewal ability as they are postmitotic, terminally differentiated cells[68]. Odontoblasts damaged by a pathological stimulus are replenished by a group of stem cells residing in the "cell rich" zone of dental pulp[69]. Stem cells have been isolated from the human dental pulp tissue of third molars and investigated *in vitro* and *in vivo* to study their properties and potential applications in dental tissue regeneration. According to Gronthos et al., hDPSCs exhibit multi-linage differentiation potential into odontoblastic, osteoblastic, adipogenic and neural cell types[67]. In vivo studies found that the implantation of hDPSCs induces

the formation of dentin-pulp like tissues [70, 71]. Thus, hDPSCs are a promising and feasible cell source for applications in dentin-pulp regeneration.

The odontogenic differentiation of hDPSCs is regulated by various growth factors, such as bone morphogenetic protein 2 (BMP_2) [17] and dentin matrix protein 1 (DMP_1)[72], as well as physical/chemical cues provided by the growth environment. Supplementation of BMP_2 and DMP_1 in the differentiation medium or scaffold stimulates the odontogenic differentiation of stem cells by increasing the levels of specific differentiation biomarkers, such as dentin sialophosphoprotein (DSPP) and DMP_1[17, 72]. In addition to biological growth factors, the physical/chemical environment also influences the behaviors of stem cells, particularly the structure and the mechanical strength of the matrix. Nano-fibrous poly(L-lactic) (PLLA) scaffolds seeded with hPDSCs exhibit improved odontogenic differentiation and mineralized tissue formation compared to scaffolds with solid walls[73]. The highly porous structure of the scaffold resembles the collagenous architecture of dentin matrix and facilitates nutrient transportation and cellular migration, which promote cellular attachment and proliferation. Compared to the matrix structure and other factors, the matrix stiffness plays a more critical role in the differentiation of stem cells. As shown in the study by Engler et al., stem cells are sensitive to the elasticity of the matrix, which regulates the lineage into which stem cells differentiate [74]. A matrix with low elasticity directs stem cells to differentiate into neural cells, while a matrix with moderate elasticity induces differentiation into the muscle cell lineage [74]. When stem cells are cultured on rigid surfaces with similar elasticity to bone tissue, they differentiate into osteoblast cells [74]. Gronthos et al. investigated the difference between bone marrow stem cells (BMSCs) and hDPSCs and found that hDPSCs differentiated into odontoblast cells and formed

17

dentin-like tissues *in vivo* [67]. On the other hand, BMSCs underwent osteogenic differentiation and formed lamellar bone-like tissues under the same culture conditions [67].

Minerals such as tri-calcium phosphate (TCP) and/or nano-hydroxyapatite (nano-HA) crystals have been added to the dental scaffold to provide a better biomimetic rigid environment for the odontogenic differentiation of hDPSCs. Supplementation of nano-HA in a nanofibrous PCL/gelatin/nHA scaffold induces greater odontoblastic differentiation of hDPSCs than scaffolds without HA [70]. Zheng et al. investigated the odontogenic differentiation of hDPSCs grown on poly(lactide-co-glycolide) (PLGA) scaffolds supplemented with three different mineral components: hydroxyapatite (HA), tricalcium phosphate (TCP) or calcium carbonate hydroxyapatite [75]. The authors found that all three scaffolds promoted the odontogenic differentiation of cells and the formation of dentin-like tissues when implanted *in vivo* [75]. Consequently, the development of nano-fibrous biocompatible scaffolds supplemented with minerals might be a highly advantageous approach that provides an optimized matrix to promote the odontogenic differentiation of hDPSCs.

1.3 Antimicrobial scaffolds

1.3.1 The need for antimicrobial dental scaffolds

Post-operative infection has been considered a critical problem contributing the failure of medical devices and scaffolds[76], particularly in the human oral environment. The oral cavity is an environment that harbors greater than 700 different bacterial species that colonize the hard and soft surfaces in the mouth and form a complex microbial community in the form of a biofilm [77, 78]. These microbes are in dynamic homeostasis. Once this

balance is disrupted, environmental conditions will be changed and lead to the markedly increased growth of some pathogenic bacterial species, resulting in many dental diseases, such as caries, pulpitis, and periodontitis[79]. Among oral bacteria, *S. mutans* is a major cariogenic bacterium that is responsible for the development of caries and pulpitis[80]. *S. gordonii* is an early colonizer of oral and device surfaces and plays critical roles in the initial formation and stability of any oral biofilm[81]. *Enterococcus faecalis* is a common bacteria found in infected pulp tissues, which can survive under extreme conditions[82]. Antimicrobial agents targeting these three bacteria facilitate the control of oral biofilms, therefore inhibiting the progress of caries and its associated pulpal infection.

Given the abundant, diverse range of bacteria presented in the oral flora, an urgent need exists to functionalize the medical devices, including dental scaffolds, with antimicrobial agents to reduce the risk of re-infection. In the oral cavity, the re-infection of pulp tissue after pulptomy is potentially mediated by bacteria that remain in the root canals or contaminate dental equipment during the operation, or the invasion of bacteria from oral flora through dentin tubules[83] or micro-leakage at the dental restoration margins [84]. Due to the specific anatomical structure of pulp tissues, the normal function of pulp tissue is difficult to restore once it is infected with bacteria. Therefore, pulpal re-infection significantly affects the success of the implanted engineered scaffolds, as the eventual infection will always result in the removal of pulp tissue and additional endodontic therapy.

The functionalization of scaffolds with antimicrobial ability is an interesting but challenging approach to combat bacterial challenges. Many commercial antibiotics, such as gentamicin [85] and chlorhexidine[86], have been applied in tissue engineering to

prevent potential bacterial infections. These antibiotics have been usually blended into the scaffold and released gradually during the degradation of the scaffold. However, the increasing abundance of resistant bacterial species[87], the potential toxicity to the host tissue, and the short half-life hinder the application of many commercial antibiotics, prompting researchers to search for new alternative antimicrobial reagents that maintain the inhibitory effect on bacteria while possessing a good interaction with the host tissues.

1.3.2 Antimicrobial peptides

Antimicrobial peptides (AMPs) are considered good candidates for preventing bacterial infection as an alternative to the use of commercial antibiotics. AMPs are a large family of small amphiphilic peptides produced by diverse native tissues and cell types that display activity against various strains of gram-positive and gram-negative bacteria, viruses and fungi[88]. AMPs offer many advantages over commercial antibiotics: 1) they have lower bacterial resistance than some commercial antibiotic, 2) they have a broad spectrum of antimicrobial effects against both G+ and G- bacteria under diverse and harsh conditions, and 3) most AMPs have lower cytotoxicity towards host mammalian cells than commercial antibiotics[89]. Thus, AMPs have the potential for use as effective alternatives to current antibiotics in the clinic.

Although the detail antimicrobial mechanism of most AMPs remains unknown, AMPs are postulated to interact with the bacterial membrane by inserting into and depolarizing the lipid bilayer membrane, resulting in the eventual disruption of bacteria [90]. Many properties of AMPs are related to their antimicrobial activity, which include the overall positive charge, peptide sequence, secondary structure, hydrophobicity and amphiphilicity [90]. According to Findlay et al., the physical properties of AMPs play a more critical role

in the biological functions of AMPs than the peptide sequence [91]. AMPs are always enriched in cationic amino acids, such as lysine and arginine, which provide the high overall positive net charge of the biomolecule, and enable the peptide to attach to the negatively charged bacterial membrane through strong electrostatic interactions[91]. The amphiphilicity of the peptides enable them to undergo conformational changes once bound to the membrane. Amphiphilicity mediates the interaction of AMPs with components of the bilayer lipid membrane and thus facilitates peptide insertion. The accumulation of AMPs on the membrane leads to the depolarization of phosphate lipids, resulting in the rupture of bacteria[90]. Many biological models, such as the 'barrel-stave'[92], 'carpet'[93] or 'toroidal-pore'[94], have been presented to explain the different mechanisms underlying the bactericidal effects of AMPs [90].

1.3.3 Tethered antimicrobial peptides with antimicrobial ability

Tethered AMPs exhibit bactericidal ability[95, 96], suggesting that immobilized AMPs are good candidates for the functionalization of medical devices and scaffolds to inhibit microbial growth. To date, most studies related to AMPs have focused on investigating their soluble forms, and their antimicrobial ability, cytotoxicity, and structure-function relations have been well documented. However, the tethered AMPs do not utilize the exact same mechanisms as their soluble analogs to exert their biological functions. Tethered peptides have lower mobility and a limited ability to translocate into the bacterial membrane[97]. Researchers have suggested independent determinants for the antimicrobial ability of tethered AMPs compared to their soluble forms[97]. In addition to the traditional contributing factors, such as positive charges and hydrophobicity, several factors, including the bio-conjugation method, the linker position, and spacer and peptide

sequence, correlate with the biological function of tethered AMPs[97]. The activity is influenced by the positions of cationic and hydrophobic amino acids: higher activity is observed when the cationic residues are located closer to the linker and a better antimicrobial effect is obtained when the hydrophobic residues are located closer to the N terminus[97]. These characteristics are presumed to facilitate the optimal interaction of tethered peptides with the bacterial membrane[97], thereby regulating the antimicrobial ability.

1.3.4 GL13K antimicrobial peptide

The modification of dental implant surfaces with GL13K peptide, a small antimicrobial peptide derived from parotid secretory protein (PSP), has produced positive effects on controlling oral biofilm formation and growth [98-100]. GL13K is a positively charged, amphiphilic 13 amino acid peptide. When dissolved in solution, GL13K and its D configuration (D-GL13K) exhibit strong antimicrobial effects on both G+ and G- bacteria, such as *Pseudomonas aeruginosa* [100]*, Escherichia coli* [3], *S. gordonii* [98] and *S. mutans* [101], under different environmental conditions. In previous studies, GL13K was tethered to a titanium surface using (3-chloropropyl) triethoxysilane (CPTES) as the linker. A series of studies revealed that the tethered peptides retained the antimicrobial properties and inhibited the growth of *S .gordonii* [98], *P. gingivitis* [99] and *S. mutans* [101] biofilms *in vitro*. Thus, GL13K is an excellent reagent for protecting the dental implants and scaffolds from the challenges posed by oral flora. However, the previously used immobilization method lacked conjugation site specificity, which affected the control of the amount and location of the tethered molecules and, therefore, the antimicrobial biological function. Furthermore, the CPTES-based immobilization method is not

applicable for modifying functional biomolecules on polymeric dental scaffolds (e.g., ELR scaffold), limiting its further application in dental tissue regeneration.

Thus, we investigated an alternative, robust bio-conjugation method. We present the use of a thiol-maleimide coupling technique for peptide immobilization. The C-terminus of the GL13K peptide was modified by the addition of a cysteine amino acid to provide a specific conjugation site. In this project, we immobilized this Cys-GL13K peptide on titanium surfaces and st-ELR membranes.

1.4 Objective

The objective of this thesis is to develop a scaffold for dentin regeneration after pulpotomy by promoting adequate hDPSC activity. The optimal scaffold will be multifunctional and display intrafibrous mineralization and antimicrobial activity.

The long-term objective of this thesis is to provide valuable materials for use in implementing approaches that meet the future demands of regenerative endodontics, particularly in the regeneration of dentin after caries-induced partial pulpitis.

In Chapter 2, we developed electrospun nano-fibrous scaffolds composed of ELRs and investigated their ability to induce biomimetic mineralization using the PILP process. The ELR scaffolds overcame the drawbacks of many synthetic and natural biomaterials by stimulating the formation of a hierarchical arrangement of intra- and extra-fibrous mineralization, resulting in a significant increase in scaffold stiffness. The mineralized structure of ELRs was similar to mineralized type I collagen. Furthermore, the

biocompatibility was investigated using pre-osteoblasts. Mineralized scaffolds promoted the proliferation and differentiation of pre-osteoblast cells.

In Chapter 3, the activity of hDPSCs cultured on intrafibrous mineralized st-ELR scaffolds was assessed. The proliferation and odontogenic differentiation of stem cells were studied. Mineralized st-ELR films promoted the growth and differentiation of hDPSCs into odontoblast cells.

In Chapter 4, we developed a bio-conjugation method based on thiol-maleimide coupling to functionalize solid surfaces with the antimicrobial Cys-GL13K peptides. Surface characterization and the antimicrobial ability of the coatings with tethered peptides against *S. mutans, S. gordonii* and *E. faecalis* were analyzed. Strong antimicrobial effects against these three oral bacteria were observed.

In Chapter 5, the thiol-maleimide coupling technique was also used to functionalize st-ELR scaffolds with Cys-GL13K. Cys-GL13K peptides were conjugated to the ELR membranes and antimicrobial tests were conducted. The modification of ELR membranes with Cys-GL13K exerted antimicrobial effects on *S. gordonii* and *S. mutans*.

Future directions for this project are presented in Chapter 6.

Chapter 2: Biomimetic Mineralization of Electrospun Elastin-Like Recombinamer Nanofibers

Abstract

One of the key factors for hard tissue regeneration is to develop hydroxyapatite incorporated fibrous scaffolds. These scaffolds can provide a micro-environment resembling the structure and mechanical properties of the extracellular matrix (ECM) of hard tissues favorable for subsequent cell responses and tissue regeneration. During biomineralization, amorphous precursor phases of calcium phosphate infiltrate into collagen fibrils, and upon crystallization, the collagen fibrils are embedded with oriented hydroxyapatite (HA) nanocrystals. We previously demonstrated that hydrogels made of elastin-like recombinamers (ELRs) can template mineralization where minerals were selectively deposited into their frameworks. In this work, we focused on mimicking the nanostructure of the mineralized tissues, namely the intra- and extra-fibrillarly mineralized collagen fibrils, using the synthetic ELRs. First, we electrospun the ELRs into nanofibers and then biomimetically mineralized them via the polymer-induced liquid-precursor (PILP) process. XRD and EDS verified the mineral phase in the ELR nanofibers was HA. SEM and TEM analyses revealed that HA nanocrystals were infiltrated into and randomly oriented within the ELR nanofibers. The elastic modulus and hardness of the mineralized ELR nanofibers was increased significantly compared to unmineralized st-ELR. The mineralized nanofibers promoted the proliferation and osteogenic differentiation of pre-osteoblasts. These results supported that a scaffold obtained using this biomimetic strategy and made of mineralized ELR electrospun nanofibers with controlled mineralization and improved mechanical properties has great potential for being used in hard tissue regeneration..

2.1 Introduction

Advances in tissue engineering provide new potential in regeneration of damaged hard tissues by combining organic-inorganic hybrid scaffolds with target cells and growth factors. Ideally, the scaffold materials should be biodegradable and eventually be replaced by newly formed tissues, resulting in a transition from artificial materials to native tissues [102]. They should also be designed to mimic natural extracellular matrices (ECMs) which create an *in vivo* friendly micro-environment for cellular responses [103]. In dentin and bone, the major organic component is type I collagen, which self-assembles in fibrils. Collagen fibrils provide a structural template for mineral deposition so that amorphous calcium phosphate precursors penetrate into the gap zones of the fibrils, crystalize and grow forming hydroxyapatite nanocrystals oriented parallel to the longitudinal axis of the fibrils [104, 105]. The minerals grow and exceed the interstitial spaces within fibrils which leads to a thick extrafibrillar mineral deposition. Reproducing the fundamental nanostructure of the extracellular matrix of hard tissues, i.e. the intra- and extra-fibrillarly mineralized collagen fibrils, has been successfully achieved with various collagen sources via the polymer-induced liquid-precursor (PILP) process [53, 106, 107], a biomimetic mineralization system that utilizes poly-aspartic acid as the substitute of non-collagenous proteins (NCPs) to regulate the mineralization of the matrix . Although polymeric materials have been used to mimic the organic template of natural hard tissues, intrafibrous mineralization of nanostructured synthetic fibrillar templates has not been successfully achieved.

The electrospinning technique is a straightforward method to produce non-woven nanostructured fibrous scaffolds that mimic the natural collagen matrix. The electrospun

27

scaffolds have good pore interconnectivity, high surface area and mechanical integrity which are critical for nutrient exchange, cell migration and cell proliferation [35, 36]. Various synthetic and natural polymers, such as poly(lactic acid) (PLA) [37], poly(lactic-co-glycolic acid) (PLGA) [108], poly(glycolic acid) (PGA) [109], cellulose [110], collagen [111], elastin [112], chitosan [113] and their mixtures have been successfully electrospun to obtain fibers. Owing to the advantages in morphologies and mechanical integrity, these electrospun scaffolds can encourage growth of cells and support formation of mineralized tissues [42, 43].

Intra- and extra-fibrillar mineralization of collagen fibrils is an important structural feature for providing a physical and chemical environment specifically required for normal osteoblast/odontoblast activity [114-118]. Electrospinning polymer solutions suspended with hydroxyapatite powders have been developed to produce a ceramic-filled fibrous nancomposite structure that mimic the collagen – HA matrices for potential use as hard tissue substitutes [37, 119]. The electrospun nanocomposite fibers; i.e., HA/PLA and hydroxyapatite/polycaprolactone (PCL), significantly enhanced osteoblast attachment and differentiation [37, 119]. The presence of HA in PCL/gelatin electrospun scaffolds promoted the adhesion and differentiation of dental pulp stem cells [70]. However, the aforementioned electrospun fibers can only be obtained with a low HA content, namely less than 25 wt%. As the inorganic particles are incorporated in the scaffold as discrete additives, the fibers usually become discontinuous and form beads [120]. Electrospun nanofibers have also been used to template mineralization, yet only extra-fibrous mineral deposition was achieved [42, 56, 121]. In those cases, the surface of the polymer nanofibers was treated with an alkaline solution or was irradiated to generate hydroxyl or

carboxyl groups. During incubation of the activated nanofibers in a simulated body fluid, SBF, a layer of bone mineral-like crystals was formed on their surface.

Elastin-like recombinamers (ELRs) have great potential in the regeneration of mineralized tissues as they reproduce the chemistry and structure of the natural polymer and thus, they have good biocompatibility and bioactivity [59, 122]. They exhibit a unique inherent thermal response that allows them to undergo phase transition in response to temperature changes [123, 124]. Previously, we have demonstrated that coatings made of ELRs containing a statherin-derived peptide (st-ELR) controlled the growth of minerals on nanotopographical surfaces via an enzyme-directed biomimetic mineralization system [125]. Also, using the PILP process we produced scaffolds with hydroxyapatite nanocrystals infiltrated within the frameworks of ELR microporous hydrogels [62]. In this study, we fabricated non-woven nano-fibrous ELR scaffolds using the electrospinning technique and biomimetically mineralized them via the PILP process. We hypothesized that the electrospun ELR nanofibers can template mineralization to obtain an intrafibrous mineralized structure. With this controlled mineralization, the mineralized ELR scaffold will mimic relevant structural features and mechanical properties of dentin/bone tissues. Therefore, the mineralized electrospun ELR nanofibers will have the potential to bioactive hard tissue-related cell responses for enabling and favoring tissue regeneration.

2.2 Materials and Methods

Two recombinant polymers, st-ELR (71.5 kDa) and ref-ELR (51.9 kDa), were purchased from Technical Proteins Nanobiotechnology (Valladolid, Spain). They were synthesized using genetic engineering techniques, as described previously [126]. Table 2.1 shows that the ref-ELR, control polymer, contains the repeating pentapeptide sequences, VPGIG and

29

VPGKG, derived from the natural tropoelastin aminoacid seqeunce. st-ELR is an amphiphilic triblock polymer that includes a highly negative charged sequence, SN_A15 (DDDEEKFLRRIGRFG), derived from the salivary protein statherin [66]. Poly-*L*-aspartic acid (Mw 27kDa) was purchased from Alamanda Polymers (Huntsville, Al, USA). Fetal bovine serum (FBS), α-modified medium (α-MEM), penicillin/streptomycin (P/S), and trypsin-EDTA were purchased from Invitrogen (Grand Island, NY, USA). ALP protease inhibitor was purchased from Thermo Scientific (Rockford, IL, USA). Bio-Rad DCTM protein assay kit was purchased from Bio-Rad (Hercules, CA, USA). Mouse osteocalcin Elisa Kit was purchased from Biomedical Technologies (Stoughton, MA, USA). All other chemicals were purchased from Sigma-Aldrich (St. Louis, MO, USA).

Name	Sequence
st-ELR	MESLLP[[(VPGIG)$_2$VPGKG(VPGIG)$_2$]$_2$*DDDEEKFLRRIGRFG*[(VPGIG)$_2$VPGKG(VPGIG)$_2$]$_2$]$_3$(VPAVG)$_{20}$[[(VPGIG)$_2$VPGKG(VPGIG)$_2$]$_2$*DDDEEKFLRRIGRFG*[(VPGIG)$_2$VPGKG(VPGIG)$_2$]$_2$]$_3$V
ref-ELR	MESLLP[(VPGIG)(VPGIG)(VPGKG)(VPGIG)(VPGIG)]$_{24}$

Table 2. 1 Primary structure of st-ELR and ref-ELR

2.2.1 Fabrication of electrospun ELR nanofibers

St-ELR and ref-ELR were added in 0.6% NaCl aqueous solution at concentrations of 25 and 30 w/v %, respectively. They were stored at 4 ℃ overnight to dissolve completely and then loaded in a 1-mL syringe connected to a blunt-ended 18 gauge needle. A high voltage of 18 kV was applied to the syringe needle and the collection distance was set at 15 cm. The solutions were flowed at a constant rate of 3 μL/min during electrospinning in all experiments. Polished titanium discs with 4 mm in diameter served as collecting substrate in order to obtain the same surface area than the specimens used for cell culture tests. A thin ELR layer ofaprox. 4-μm in thickness was deposited on the discs. After air-drying overnight at room temperature, the ELR fibers on the discs were cross-linked by hexamethylene diisocyanate (HMDI) in acetone (10 v/v %) overnight to improve their physical stability. Otherwise they would dissolve in the PILP solution. The cross-linked ELR nanofibers were then washed thoroughly with acetone and then deionized water. They were lyophilized before material characterization and mineralization.

2.2.2 Biomimetic mineralization via the PILP process

The cross-linked samples were mineralized by the PILP process following the protocol described previously [127, 128]. Briefly, solutions of 9 mM $CaCl_2$ and 4.2 mM K_2HPO_4 were prepared in Tris-buffered saline (TBS, pH = 7.4 at 37 ℃) separately. Poly-L-aspartic acid (PASP, MW = 27 kDa) was added in Ca-solution at the concentration of 100 μg/mL. Then, equal volumes of these two solutions were mixed together gently to make the final concentration of Ca, P and PASP at 4.5mM, 2.1mM and 50μg/mL, respectively. St-ELR and ref-ELR samples were immersed into the mineralization solution under vacuum for 30 min to remove air bubbles within the scaffolds. After degassing, the mineralization was

conducted in an oven at 37 ℃ up to 7 days. The PILP solution was refreshed every 3 days. After mineralization, the samples were washed with deionized water for three times and lyophilized.

2.2.3 Characterization

Scanning Electron Microscopy (SEM): SEM (JEOL6500, Japan) was used to analyze surface morphologies of st-ELR and ref-ELR fibers before and after mineralization. Prior to SEM analysis, all the specimens were coated with a 5 nm think layer of platinum. All the images were recorded at an accelerating voltage of 5kV. Energy Dispersive Spectrometry (EDS) was conducted at 15 kV to evaluate chemical composition of the mineralized fibers. Some SEM images were analyzed by ImageJ (http://imagej.nih.gov/ij/) (National Institutes of Health, Bethesda, MD, USA) to determine the diameter of the fibers at predetermined mineralization times. The percentage of increase (%IFD) in fiber diameter was calculated using the following equation:

$$IFD = \frac{D - D_0}{D_0} \times 100\%$$

Where D is the average diameter of electrospun fibers at the predetermined mineralization time, D_0 is the average diameter of electrospun fibers prior to start the mineralization process.

Transmission Electron Microscopy (TEM): TEM (Tecnai T12, FEI, USA) was used to analyze the crystal structure and orientation of the minerals in the electrospun fibers at an accelerating voltage of 120 kV. The mineralized st-ELR and ref-ELR fibers were embedded into epoxy resin and cured at 60 ℃ overnight. They were then cut by an

ultramicrotome (Leica Reichert UltraCut S) at room temperature and collected on 300-mesh copper grids. Both the longitudinal and transverse sections of the mineralized fibers were evaluated. Selected area electron diffraction (SAED) was conducted to assess the crystallinity and orientation of the deposited minerals.

X-Ray Diffractometry (XRD): The crystalline phases of minerals were also determined by XRD (D8 Discover, Bruker AXS). Spectra of st-ELR and ref-ELR fibers at the different mineralization time points, as well as of a bovine dentin slab, were collected at 40kV and 40 mA with 2θ ranging from 20° to 50°. The results were analyzed using the JADE8 software (Materials Data Inc., Livermore, CA, USA).

Nano-indentation: Nano-indentation (Hysitron Triboindenter, Minneapolis, USA), was used to evaluate the mechanical properties of st-ELR nanofibers after 7 days of mineralization. Polished bovine dentin was used as control. A Berkovich tip with a radius of 150 nm was selected as an indenter. Optical imaging of the sample using a microscope allowed precise control between the sample position and the indenter to ensure that results from each test were obtained solely from the individual fiber. Each indentation used a trapezoidal load function consisting of a linear loading segment of 10 seconds followed by a 5-second holding at a predetermined peak force and a linear unloading segment of 10 seconds. 20 indents on each sample were performed. Reduced elastic modulus (Er) and hardness (H) were determined using the compliance method of Oliver-Pharr [129].

2.2.4 Cellular Response

Cell Culture: Mouse calvarial preosteoblasts (MC3T3-E1) were cultured in α-MEM, supplemented with 10 % FBS, and 1 % of penicillin/streptomycin. They were cultured in

an incubator at 37 °C with 5% CO_2 and passaged 3 times before being seeded on the ELRs samples.

Cell proliferation: Cells, at the density of 2000 cells/well, were seeded on mineralized and un-mineralized st-ELR and ref-ELR fibers that were deposited on titanium discs. 2-mm thick bovine dentin slabs from bovine incisor were used as control. Prior to cell seeding, all the samples were soaked in 70% ethanol for 40 min and then exposed to UV light for another 40 min for disinfection. The samples were then washed thoroughly with Hank's buffered salt solution (HBSS) and placed in a 48-well plate before cell seeding. Cell culture medium was refreshed every three days. After 1, 3 and 6 days of culture, cells were fixed with 4% paraformaldehyde (PFA) for 20 min in an ice bath, and then stained with 2 μg/mL DAPI for 10 min. Immunofluorescence Microscopy (Eclipse E800, Nikon, Japan) was used to determine cell number per field by counting the stained nucleus in images taken at 20X magnification.

Cell differentiation: Prior to cell seeding, all the samples were disinfected using the aforementioned protocol and then transferred to a 96-well plate (N=4 for each group). MC3T3-E1 cells were seeded on the scaffolds at the density of 10,000 cells/well and cultured with 300μl α-MEM. After 2 days of culture, cells were then in confluence and were cultured with osteogenic differentiation medium (α-MEM with 10 % FBS, 1 % P/S, 50 μg/mL ascorbic acid and 0.01M β-glycerophosphate). During cell differentiation, half volume of medium was refreshed every 3 days. The differentiation biomarkers, alkaline phosphatase (ALP) activity and osteocalcin production (OCN) were evaluated at 7, 14 and 21 days of culture. To test ALP activity, the cultured samples were washed 3 times with

PBS and immersed in 300μL lysis buffer containing 1% Triton X-100, 0.1mM $MgCl_2$, and

0.15 M Tris-base at pH 10.5. After 10 min of incubation at room temperature, the cell

lysates were collected and centrifuged at 3000 rpm for 10 min. ALP activity was tested

using an ALP assay kit. Briefly, AMP reaction buffer was prepared by dissolving one 20

mg tablet of p-nitrophenylphosphate in 5ml deionized water followed by addition of 11.25

μl 1:4 diluted AMP and 6μL 2M $MgCl_2$. 100μL of AMP buffer was added in a 96 well

plate followed by the addition of 2μL of cell lysates from each sample. The mixture was

incubated in the oven at 37 °C for 2 hours, and then a Synergy TM 2 multi-mode microplate

reader (BioTek, US) was used to measure the absorbance at 410 nm. The medium was

collected after 7, 14 and 21 days of cell culture and protein production of osteocalcin was

measured using the Osteocalcium Elisa kit following the protocol provided by the

manufacturer [125]. The data of ALP activity and OCN level was normalized using total

protein content, which was determined using Bio-Rad [DCTM] protein assay kit (BioRad,

Hercules, CA) following the manufacturer's protocol.

2.2.5 Statistical Analysis

One-way ANOVA with Tukey post-hoc tests were used to determine statistically

significant differences (p-value<0.05) for average values among different groups.

2.3 Results

2.3.1. Electrospinning and mineralization of ELR fibers

Using the electrospinning technique we obtained ELR nanofibers with diameters of several

hundreds of nanometers. Figure 2.1 shows that both st-ELR and ref-ELR nanofibers

exhibited a loose non-woven structure. The diameter of the st-ELR nanofibers $(406 \pm 74$

nm) was smaller than that of the ref-ELR nanofibers (741 $\pm$ 257) (Table 2.2). Some of the

ref-ELR fibers showed a ribbon-like shape.
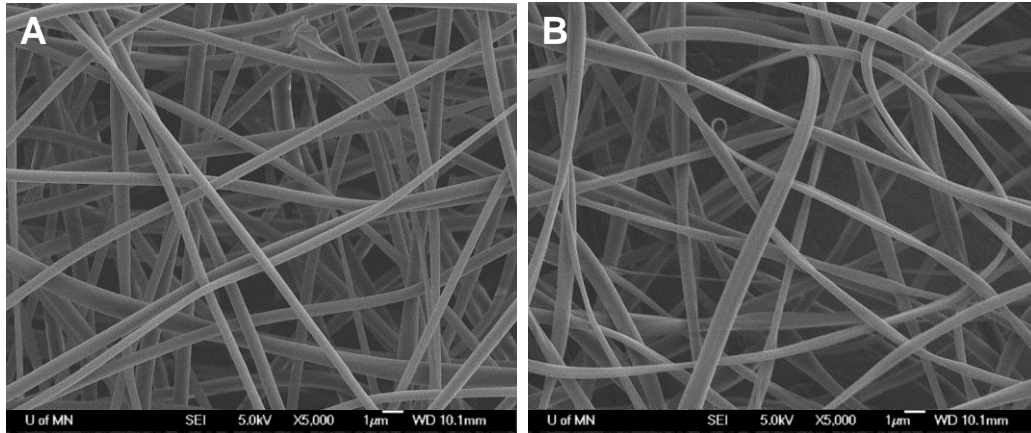
Figure 2. 1 **SEM images of electrospun nanofibers of st-ELR (A) and ref-ELR (B).**

Before mineralization, the surface of ELR nanofibers appeared smooth with small

striations (Fig. 2.2A). A Remarkable change in surface morphology was observed as the

mineralization proceeded. After 3 days of mineralization the surface of the nanofibers had

a rugged uneven appearance along the whole length of the fiber. A continuous layer of

needle-like minerals was observed on the surface of the ELR fibers after 7 days of

mineralization.   The diameters of the fibers continuously increased while the

mineralization process progressed. The average diameter of st-ELR and ref-ELR reached

805 $\pm$ 114 nm and 1143 $\pm$ 3 94 nm, respeectively after 7 days of mineralization(Table 2.2);

therefore, %IFD was significantly higher for st-ELR than for ref-ELR nanofibers after 7

days of mineralization (Fig. 2.2C).

EDS was performed to determine the chemical composition of the obtained minerals. Calcium and phosphorus were detected after 1 day of mineralization, which suggested initiation of calcium phosphate mineral incorporation in the mineralized nanofibers. The intensity of both Ca and P signals increased gradually with mineralization time (Fig. 2.2B). After 1 day of mineralization, the molar Ca/P ratio was 1.35 and 1.34 in st-ELR and ref-ELR, respectively. At day 7 of mineralization both mineralized ELRs had Ca/P ratio that increased to 1.59, which is a value comparable to the one for natural dentin (Ca/P = 1.61) [130].
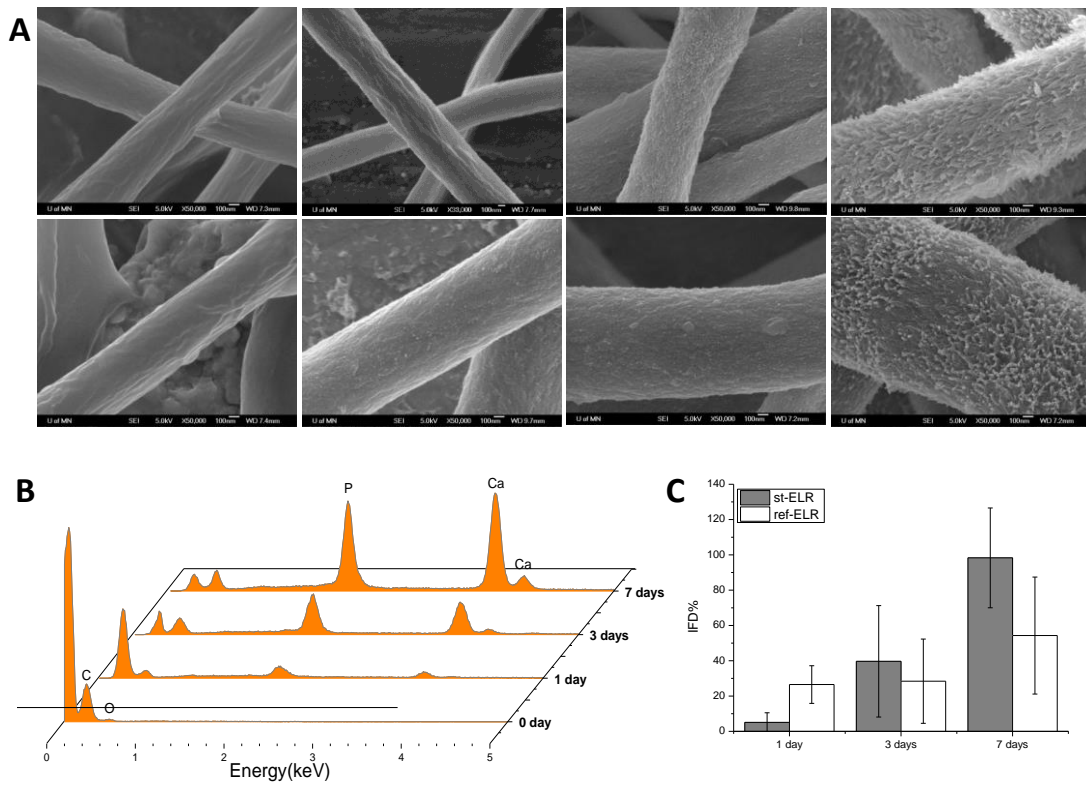
Figure 2. 2 **A:** SEM images of st-ELR (top row) and ref-ELR nanofibers (bottom row). From left to right, before and after 0, 1, 3 and 7 days of mineralization. **B:** EDS of the

mineralized st-ELR electrospun nanofibers at different periods of mineralization. **C:** rate

of fiber diameter increase for different periods of mineralization.

Day	Ca/P ratio		Diameter (nm)	
	st-ELR	ref-ELR	st-ELR	ref-ELR
0	0	0	406 ± 74	741 ± 257
1	1.35 ± 0.03	1.34 ± 0.07	417 ± 22	919 ± 174
3	1.39 ± 0.10	1.45 ± 0.03	567 ± 128	951 ± 176
7	1.59 ± 0.11	1.59 ± 0.08	805 ± 114	1143 ± 394

Table 2. 2 **Ca/P ratio of the mineral deposited in ELR nanofibers determined by**

EDS and the diameter of st-ELR and ref-ELR nanofibers measured from the SEM

images.

2.3.2 Crystallographic structure.

X-ray microdiffraction was used to analyze the crystallinity of the minerals in ELR

nanofibers. The presence of hydroxyapatite nanocrystals in st-ELR and ref-ELR

nanofibers over time of mineralization is shown in Figure 2.3. The main characteristic

peaks for hydroxyapatite appeared after 1 day of the PILP treatment —$2\theta = 26°$ and $32°$

correspond to (002) planes and overlapping (211), (112) and (300) planes, respectively.

These peaks progressively increased in intensity over the mineralization time. The formation of HA was confirmed from the spectra of both st-ELR and ref-ELR. After 7 days of mineralization, the XRD pattern for st-ELR and ref-ELR was very similar to that of dentin.
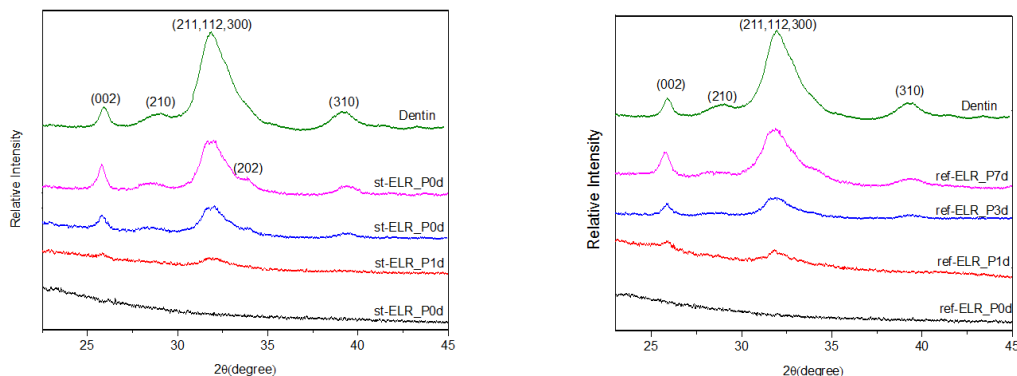
Figure 2. 3 **XRD of electrospun st-ELR nanofibers after 0, 1, 3 and 7 days of the biomimetic mineralization.** The spectrum of bovine dentin is shown for comparison.

2.3.3 Crystal distribution and orientation

We performed SEM analysis on the fracture surface of the mineralized fibers to assess the infiltration of the minerals in the interior of the ELR nanofibers (Fig. 2.4A and B). The fractured surface of the inner side of the nanofibers had similar morphology as the one for the exterior surface of the fibers, indicating the occurrence of intra-fibrous mineralization. TEM results, from both longitudinal and transverse sections of the mineralized fibers, further confirmed that evenly intra- and extra-fibrous mineralization was obtained in both st-ELR and ref-ELR fibers (Fig. 2.4C-F). In most cases, the crystals were randomly oriented in the fibers; however, alignment of hydroxyapatite nanocrystals along some of

the st-ELR fiber longitudinal axis were observed and verified by the arcing of the (002)

planes in the corresponding SAED pattern (Fig. 2.4G).
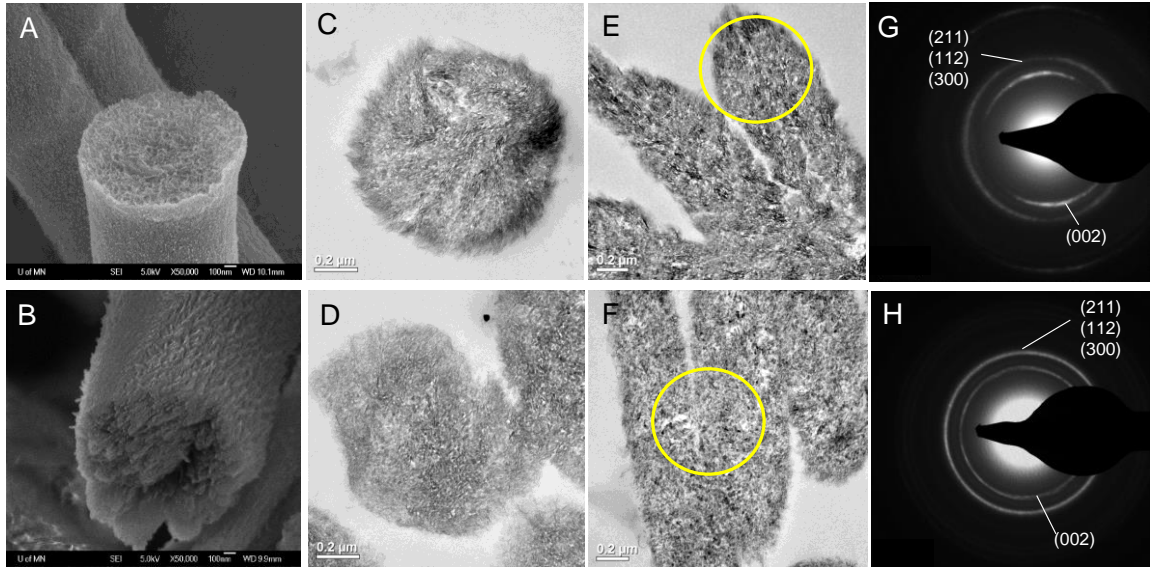
Figure 2. 4 **SEM and TEM images of ELR nanofibers after 7 days of mineralization.**
SEM images of the fractured surfaces of st-ELR (A) and ref-ELR (B) nanofibers. TEM
images of the transverse-sections of mineralized st-ELR (C) and ref-ELR (D) nanofibers.
(E) and (G) TEM image of the mineralized st-ELR nanofibers and the corresponding SAED
pattern generated from the region circled in (E). (F) and (H) TEM image of the mineralized
ref-ELR nanofibers and the corresponding SAED pattern obtained from the region circled
in (F).

2.3.4. Mechanical Properties

Table 2.3 shows reduced moduli of elasticity and hardness values for mineralized st-ELR samples and dentin in dry and hydrated conditions that were determined from the load-displacement curves at a depth of 500 nm. The mechanical properties of st-ELR fibers before mineralization were too low to be measured by nanoindentation. However, mineralization leaded to significant increase of elastic modulus and hardness of st-ELR. The elastic modulus of the mineralized st-ELR fibers, in dry and wet state, was 0.99 ± 0.77 GPa and 0.17 ± 0.20 GPa, respectively and the corresponding hardness values were 0.058 ± 0.043 GPa and 0.005 ± 0.005 GPa. Mineralized ref-ELR fibers showed comparable but lower elastic modulus and hardness than mineralized st-ELR in both wet and dry states. The values of the two ELR scaffolds are notably lower than those of dentin, which had elastic modulus of 22.7 ± 2.7 (dry) and 10.7 ± 4.2 (wet) GPa, and hardness value of 1.01 ± 0.23(dry) and 0.28 ± 0.17 GPa (wet). The values of mineralized st-ELR were also lower than that of bovine cortical bone [107], but they are comparable to the ones reported for rehydrated mineralized collagen film, which had elastic modulus of 0.177 ± 0.031 GPa and hardness value of 0.008 ± 0.003 GPa in wet state [107].

Sample	Reduced Modulus (E_r) [GPa]		Hardness (H) [GPa]	
	dry	wet	dry	wet
st-ELR_7D	0.99 ± 0.77	0.17 ± 0.20	0.058 ± 0.043	0.005 ± 0.005
Ref-ELR_7D	0.67 ± 0.56	0.146 ± 0.234	0.024 ± 0.048	0.003 ± 0.004

Dentin	22.7 ±2.7	10.7 ±4.2	1.01 ±0.23	0.28 ±0.17

Table 2. 3 **Mechanical properties of ELRs.** reduced elastic modulus (Er) and hardness (H), of the electrospun st-ELR fibers, ref-ELR fibers after 7 days of biomimetic mineralization and control samples of bovine dentin.

2.3.4 Pre-osteoblast proliferation and differentiation

Proliferation and differentiation of mouse calvarial pre-osteoblastic cells (MC3T3-E1) was determined when cells were cultured *in vitro* on non mineralized and mineralized ELRs samples. After 1 day and 3 days of culture, no significant differences in cell proliferation were observed among all groups tested and control dentin samples (Fig. 2.5&2.6). In contrast, the substrates containing minerals—dentin slabs and ELRs nanofibers after 7 days of mineralization—showed significant increase in cell number as compared to non mineralized ELRs after 6 days of culture (p-value < 0.05, N = 4) (Fig. 2.5&2.6).
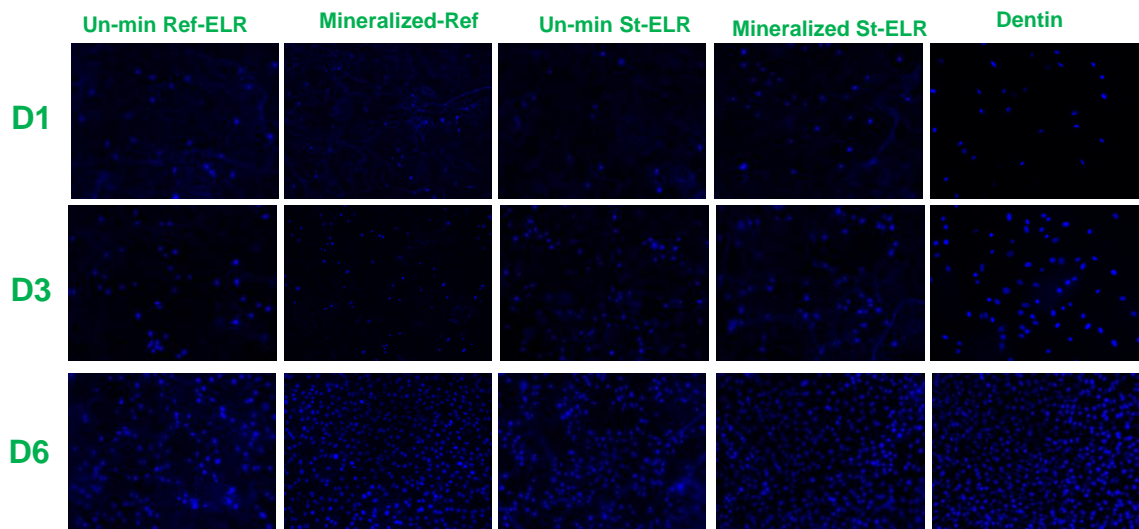
Figure 2. 5 **DAPI stained cells on scaffolds.** Cell proliferation on non mineralized (Un-min) and mineralized ELR scaffolds after 1,3 and 6 days of culture (D1, D3, D6, respectively).
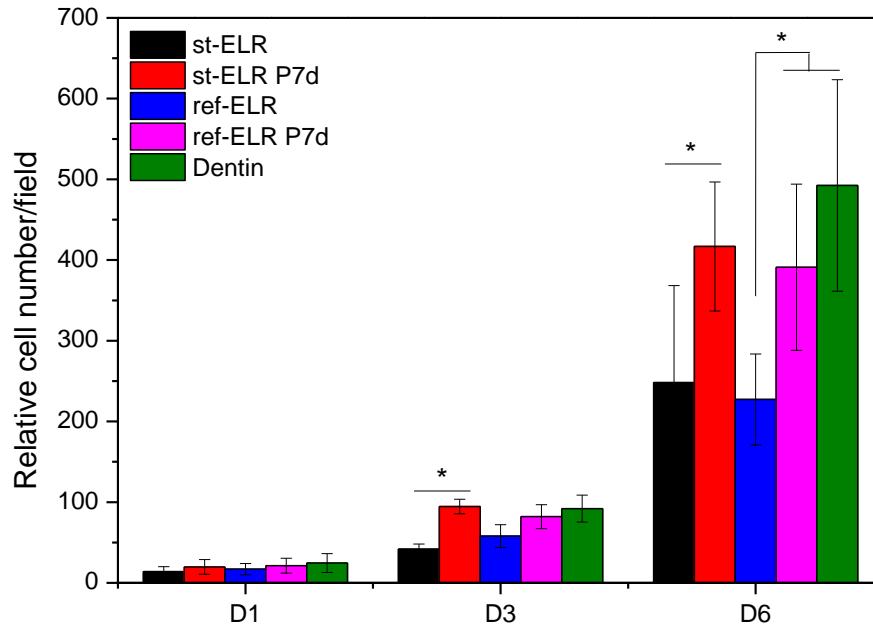
Figure 2. 6 **Cell proliferation of MC3T3-E1 after 1 (D1), 3 (D3) and 6 (D6) days of culture.** Mineralized ELR fibers for 7 days (st-ELR_P7d and ref-ELR_P7d) and bovine dentin exhibited significantly higher cell number than the non mineralized ones after 6 days of culture. Both types of mineralized ELR fibers showed similar cell proliferation results to the bovine dentin group.

Although cells showed a continuous increase in ALP activity over the 21 days of culture, except for non mineralized st-ELR samples, no significant differences in cellular ALP activity were determined between any of the tested groups at any of the time points where

cells were analyzed (Fig. 2.7A). However, cells cultured on mineralized ELRs and dentin showed a significantly higher production of OCN than non mineralized ELRs for all periods of culture (Fig. 2.7B).
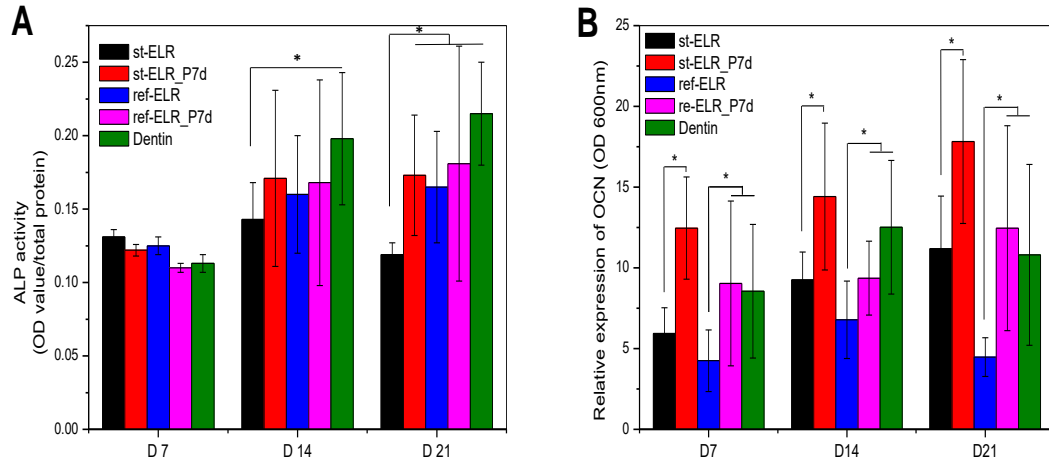
Figure 2. 7 **Osteogenic differentiation of MC3T3-E1 cells**. **(A) ALP activity**. Cells cultured on mineralized ELR nanofibers showed higher ALP activities than on non mineralized ELR scaffolds after 14 and 21days of culture with no statistically significant difference. (**B) Osteocalcin level. Cells on** mineralized st-ELR and ref-ELR produced significantly higher levels of osteocalcin than on non mineralized control surfaces after 7, 14 and 21 days of culture (p-value<0.05).

2.4 Discussion

Significant scientific and technological advances have been made to enable the use of electrospinning to produce scaffolds for hard tissue regeneration. The incorporation of inorganic nanocomponents within the polymeric nanofibers that improve the mechanical and biological properties of the scaffold is a relevant focus of investigation and

development. As a promising alternative to electrospinning composites or nucleating and growing minerals on the surface of the fibers, biomimetic intrafibrous mineralization of electrospun polymeric nanofibers is a new approach for the development of artificial matrices for hard tissue regeneration. This process mimics natural collagen fibrils mineralization and thus, recapitulates the structure of native hard tissues. In this study, we demonstrated that electrospun ELR nanofibers can be intra- and extra-fibrously mineralized using the PILP process. The minerals, hydroxyapatite nanocrystals, were homogeneously distributed and thoroughly infiltrated in the nanofibers without disrupting the original fiber morphology. As a result, the mineralized ELR nanofibers improved proliferation and osteogenic differentiation of MC3T3-E1 cells, which indicates that these scaffolds are promising substrates for hard-tissue regeneration applications.

In the pursuit of developing synthetic templates that can induce mineralization with controlled morphology that mimics natural hard tissues, others have used electropun nanofibers to template mineral growth, yet only extra-fibrous mineralization was achieved [42, 56]. However, during natural biomineralization of dentin and bone both extra- and intra-fibrillar mineralization of the collagen matrix takes place. Intrafibrillar mineralization is critical for controlling the mineral orientation and its spatial distribution in the fibrillar matrix and determining its mechanical properties. Previous work has shown that the PILP process is capable of reproducing the nanostructure of hard tissues, the mineralized collagen fibrils [53, 54]. In the electrospun ELR nanofibers, the biomimetic mineralization starts with intra-fibrous mineral deposition and is followed by the extrafibrous growth of crystals. The diameter of the electrospun fibers significantly increased with biomineralization time. Strong signals of Ca and P were detected after 3

days of mineralization, suggesting the presence of the crystals in the ELRs scaffolds. However, ELR fibers after 3 days of mineralization did not show a marked change in surface morphology. It was only after 7 days of mineralization that the surface of the ELR fibers were decorated with needle-like minerals. This suggests the initial penetration of the minerals in the fibers that eventually get thoroughly infiltrated by crystals and, eventually the minerals protrude through the fiber surface. In organic matrix-templates, mineralization takes place within defined and restricted compartments or spaces. The organic matrix should contain pores or channels to serve as sites for mineral infiltration and deposition [131]. At the same time, the mineral should be stabilized in solution as an amorphous precursor that can penetrate into the organic matrix before crystallization [52, 132]. In bone, non-collagenous proteins stabilize the amorphous calcium phosphate phase, which mediates the infiltration into the interstitial spaces of individual collagen fibrils [52, 132, 133]. ELRs exhibit microphase separation in response to the increase of temperature as a result of their reverse transition [134]. In the electrospun ELR fibers, as in our previous work with ELR hydrogels [62], the phase transition might result in formation of nano-pores to facilitate the infiltration of the minerals. However, it should be noted that here the spatial distribution of HA nanocrystals in the ELR fibers was not controlled. Biomineralization in an organic matrix is a confinement controlled process [135], orientation of HA crystals is regulated by the arrangement of the polymeric chains in the organic matrix. Collagen fibrils have a characteristic D-periodic banding pattern of 64-67 nm [136, 137]. The mineralization starts at the gap zones of the collagen fibrils and then the mineral grows into the overlap zones so the c-axis of HA nanocrystals is aligned with the fibril axis [52]. In contrast to the natural collagen structures, we only detected at the ends of the ELRs fibers

preferentially aligned HA nanocrystals with their [0 0 1] roughly parallel along the fiber axis (Figure 4E). Most of HA nanocrystals were randomly oriented in the ELR fibers as the mineral infiltrated the fiber from any point of their periphery (Figure 4F).

Mineralization rate depends on the capability of infiltration of the mineral nanoclusters into the organic matrix. st-ELR contains a peptide, SN_a15, which is a synthetic analog of the N-terminal 15 residue sequence of human salivary statherin [66]. This peptide has high affinity for calcium phosphate minerals [66] and thus, its presence in the ELR sequence may attract minerals to the fibers, thereby increasing the mineralization rate. St-ELR has a molecular weight of 71.5 kDa, while the molecular weight of the ref-ELR is 51.9 kDa. Because of the low molecular weight and less proportion of polar residues, ref-ELR exhibited higher solubility in aqueous solution and lower viscosity than that of the triblock copolymer st-ELR. In order to electrospin ref-ELR nanofibers, we increased the concentration of ref-ELR to 30 w/v %, yet the viscosity was still lower than that of the st-ELR (25 w/v %). This low viscosity and low molecular weight influenced the outcome of electrospinning, producing ref-ELR fibers with larger and more disperse diameters than the st-ELR fibers (Figure 2C). Besides, polymers with high molecular weight tend to orient their chains along the fiber axis while being electrospun as they have extensive entanglements and long relaxation time [138]. Given the difference in molecular weight and viscosity, it is reasonable that st-ELR fibers had more parallel molecular arrangements along the fiber axis than in the case of ref-ELR fibers. The parallel array of the molecules in st-ELR fibers might also contribute to the high percentage of increased fiber diameter during mineralization, pertinent to the high degree of mineralization.

Biomimetic mineralization enhanced the mechanical properties of st-ELR and ref-ELR significantly. Although elastic modulus and hardness values of mineralized ELRs were lower than that of bovine dentin and cortical bone (Table 3), the values were comparable to the mineralized crosslinked collagen at wet state. The lower mechanical strengths of ELRs are presumably due the short mineralization time and the less compacted structure than the native mineralized matrixes. ELR fibers were mineralized for 7 days while the collagen had been mineralized for 14 days as reported [107]. Consequently, ELR fibers exhibited lower mineralization degree than the mineralized collagen. In addition, the structures of mineralized st-ELR and ref-ELR are much porous than the highly compacted dentin and bone matrix, which most likely account for their lower values when compared to dentin and bone. It is worth noting thatboth types of mineralized ELRs showed values of rigidity above to 0.1 GPa, which has been proved enough to induce progenitor cells to differentiation in the be osteoblastic lineage [74].

Cell fate and functions are regulated by chemical and physical cues [127]. Surfaces with micro/nano topography and high stiffness [74, 127, 139] favor appropriate responses by mineralized tissue-related cells, such as primary osteoblast and odontoblast-like cells. Scaffolds with a nano-fibrous structure and high stiffness promote the osteogenic and odontogenic cell growth and differentiation [70, 140]. In this study, the fibrous structure and mineralization of ELR fibers led to an enhancement in cell proliferation and differentiation as the mineralized ELR fibers mimicked the mineralized collagen fibrils, the primary component of bone and dentin. Intra- and extra-fibrous mineralization resulted in significant improvement of mechanical properties (Table 2.2). Such fibrous structure, coupled with mechanical cues, created a favorable micro-environment for cell response.

The cellular OCN production on the mineralized samples was higher after 14 and 21 days of culture than on the unmineralized samples (Fig.2.7B).

2.5 Conclusion

The potential of elastin-like recombinamers to control calcium phosphate mineralization that mimics biomineralized collagen in natural calcified tissues has been investigated. We demonstrated that the electrospun st-ELR and ref-ELR nanofibers induced intra- and extra-fibrous mineralization via the PILP process, leading to an increase in proliferation and differentiation of primary osteoblasts. This study supports that mineralized electrospun nanofibrous ELR scaffolds can provide an optimized biomimetic physical and chemical environment to stimulate the activity of cells.

2.5 Acknowledgement

Chapter 3: Intrafibrous Mineralized st-ELR Supports the Proliferation and Differentiation of Human Dental Pulp Stem Cells

Abstract

The prevalence of dental pulpitis and advances in dental tissue engineering demand the further development of appropriate scaffolds for dentin regeneration. As shown in our previous study, an electrospun st-ELR scaffold was capable of inducing biomimetic mineralization. Mineralized st-ELR enhanced the proliferation and osteogenic differentiation of primary osteoblast cells. In this study, we investigated the proliferation and odontogenic differentiation of human dental pulp stem cells (hDPSCs) grown on an intrafibrous mineralized st-ELR scaffold. hDPSCs were cultured on mineralized and unmineralized st-ELR scaffolds. Cell proliferation was measured by counting stained nuclei after 1, 3, and 6 days of culture. Odontogenic differentiation was determined by analyzing the expression of ALP and DMP_1. hDPSCs continuously proliferated over time on all substrates. Significantly greater numbers of cells were observed after 3 and 6 days of culture on mineralized st-ELR than on nonmineralized st-ELR. hDPSCs in mineralized groups displayed higher ALP activity and higher DMP_1 expression after 14 days of culture than nonmineralized st-ELR scaffolds. Based on these data, st-ELR is a potential dental scaffold for dentin regeneration as it enables biomimetic mineralization of dentin and supports the proliferation and differentiation of stem cells from dental pulp tissue.

3.1 Introduction

Pulpitis remains a critical problem in the dental clinic. An estimated 24 million root canal treatments were performed in 2003, which accounted for approximately $8.2 billion in the US. [8]. Traditional endodontic therapy requires the complete removal of pulp, which leaves behind a weak tooth that is susceptible to fracture due to the loss of pulp vitality and a large amount of dentin and enamel [141]. Recent advances in tissue engineering have provided clinicians possible opportunities to use new types of endodontic therapy in which the regeneration of the damaged dental tissues might be achieved by combining scaffolds with target cells and growth factors. Instead of the complicated reconstruction of the entire dentin-pulp complex in a necrotic tooth, a clinically practical approach is to apply a scaffold on top of the remaining healthy pulp and use the potency of host cells and biological factors to regenerate new dentin[72]. In contrast to traditional pulp capping materials, implanted scaffolds integrate with dental tissues by providing a biomimetic micro-environment for cells to migrate to the affected tissue, grow, differentiate, and secrete new extracellular matrix (ECM) [102]. Scaffold materials are biodegradable and eventually replaced with newly formed tissues, transitioning from artificial materials to native tissues[102]. This approach provides better sealing of pulp tissues using a large volume of native dentin. Therefore, clinical complications, such as secondary caries and re-infection of pulp tissues, which are caused by current commercial pulp capping and restorative materials, are potentially minimized.

Human dental pulp stem cells are appropriate cells for dentin-pulp tissue regeneration. These stem cells have been isolated from pulp tissues of adult third molars. These progenitor cells migrate to different cell layers in the pulp and are capable of differentiating

into multiple cell lineages in response to different stimuli, specifically those associated with odontogenic differentiation [74, 142]. A combination of stem cells with suitable scaffolds and differentiation agents is required to stimulate odontogenic differentiation. However, knowledge of the suitable design of the scaffold for supporting dental tissue regeneration is limited. A gold standard for tissue engineering is that the scaffold should resemble the complexity of natural extracellular matrix (ECM) to provide a biomimetic artificial micro-environment for the growth of stem cells[143, 144]. In dentin ECM, a fibrous network of type I collagen is the major organic component that supports the deposition and hierarchical arrangement of hydroxyapatite crystals within and outside the fibrils, resulting in a high degree of mineralization [145, 146]. A scaffold that mimics the complexity of the dentin matrix will create a cellular environment that favors the odontogenic differentiation of stem cells. Cell attachment, growth, and differentiation are enhanced on collagenous matrices with a fibrillar structure supplemented with minerals similar to the dentin matrix[103, 147].

In Chapter 2, we studied the responses of primary osteoblast cells grown on an intrafibrous mineralized st-ELR scaffold and found that the mineralized scaffold promoted osteoblast proliferation and osteogenic differentiation compared to the non-mineralized scaffold. A mineralized electrospun ELR scaffold offers several advantages, including the flexibility of obtaining different scaffold morphologies, the presence of nano-hydroxyapatite (nHA), the mineral phase in bone and dentin, and mechanical properties that are similar to the native hard tissues. Because osteoblasts and odontoblasts are closely related cell lines and are responsible for the formation of mineralized tissues [67], we hypothesized that mineralized st-ELR scaffolds would exert similar effects on promoting the odontogenic

differentiation of hDPSCs as the primary osteoblast cells. Here, the in vitro response of hDPSCs interacting with st-ELR scaffolds was investigated.

3.2 Materials and Methods

3.2.1 Fabrication of electrospun st-ELR films

The fabrication of electrospun st-ELR fibers and subsequent biomimetic mineralization treatment are described in Chapter 2. Briefly, a 25% (w/v %) st-ELR polymer solution was electrospun into non-woven fibers and deposited on polished titanium discs (diameter=9 mm) to obtain fibrous films with a thickness of approximately 4 μm. The diameter of the st-ELR fibers ranged from 300 to 800 nm. Fibers were crosslinked overnight using a mixture of hexamethylene diisocyanate (HMDI) and acetone (1:9 v/v). After thorough washing, samples were mineralized using the polymer-induced liquid precursor (PILP) process for 7 days. Scanning electron microscopy (SEM, JEOL6500, Japan) was performed to analyze changes in the morphology of the st-ELR fibers before and after mineralization.

3.2.2 Stem cell culture

Human dental pulp stem cells were kindly donated by Dr. Kim Mansky (Dept. of Diagnostic and Biological Sciences, School of Dentistry, University of Minnesota, USA). The stem cells were isolated from third molars of dental patients. Cells were recovered from liquid nitrogen and cultured in α-MEM (SH3056801, GE Healthcare Life Sciences) supplemented with 10% fetal bovine serum (FBS, Thermo Fisher Scientific), 1% penicillin/streptomycin (P/S) (Thermo Fisher Scientific), and 1% L-glutamate (Thermo Fisher Scientific). Tissue culture plates were coated with a 0.1% gelatin solution before

cell culture to facilitate cellular attachment. Cells were passaged 3 times before being used in subsequent experiments.

3.2.3 Stem cell proliferation

Four groups of samples were tested in this study: mineralized st-ELR (Min st-ELR), nonmineralized st-ELR (Unmin st-ELR), a titanium disc control (Ti), and a tissue culture plate control (TCP). All samples (N=4 per group) were autoclaved and placed in a 24-well plate. One milliliter of culture medium was added to each well. After 2 hrs of soaking, hDPSCs were seeded in each well at a density of 2000 cells/well. Cells were cultured in an incubator (37 °, 5% CO_2) for 6 days and the media were replaced every 3 days. After 1, 3, and 6 days, the cells attached to the sample surfaces were rinsed with Hank's buffered salt solution (HBSS) 3 times, fixed with 4% paraformaldehyde (PFA) for 40 min in an ice bath and stained with 2 μg/mL DAPI for 10 min. After thorough rinsing, stained cells were visualized using fluorescence microscopy (Eclipse E800, Nikon, Japan). The number of stained nuclei was in each field (at 20X) was counted to assess proliferation of cells on each type of samples. Images of 16 fields from each group were captured.

3.2.4 Stem cell differentiation

Sterile samples (N=4 per group) were placed in a 48-well plate and incubated α-MEM for 2 hrs. hDPSCs were seeded in each well at a density of $1x10^5$ cells/well, followed by the addition of 1 mL of α-MEM. Cells were cultured for 2 days to allow cellular attachment. Thereafter, α-MEM was replaced with 0.5 mL of odontogenic differentiation medium (α-MEM supplemented with 12.5 mM β-glycerol phosphate, 6.25 mg/mL L-ascorbic acid and 0.1 nM dextramethasone). Cells were allowed to differentiate for 3 weeks. Within each

week of culture, the differentiation medium was refreshed on day 4, and the medium was collected at day 7 for further ELISAs. The production of differentiation-related protein biomarkers was determined on days 7, 14, and 21 of culture. Values were normalized to the total protein content, which was assessed using the Bio-Rad ^{DCTM} protein assay kit (Bio-Rad, Hercules, CA).

ALP activity: Cells growing on the sample surfaces were rinsed with HBSS buffer and lysed by adding 50 μL of lysis buffer to collect the cell supernatant for the alkaline phosphatase activity test. The detailed procedure is described in Chapter 2.

ELISA of dentin matrix protein 1 (DMP$_1$): The differentiation media were collected after 7, 14, and 21 days of cell culture. The levels of DMP$_1$ in the culture media were determined using human DMP$_1$ ELISA kits (Raybiotech, Norcross, GA, USA) according to the manufacturer's protocol. Briefly, 100 μL of media were added to a DMP$_1$ antibody-coated 96-well micro-plate for overnight incubation with gentle shaking at 4 ℃. The media were then removed and the micro-plate was washed 4 times with washing buffer. One hundred microliters of a secondary antibody (anti-DMP$_1$) solution were added to each well and incubated for 1 hr at room temperature. The micro-plate was washed again and treated with 100 μL of a streptavidin solution for 45 min. Then, 25 μL of stop solution were added to each well and the absorbance of the plate was immediately read at 450 nm with a Bio-reader (BioTek, Winooski, VT, and U.S.A). The absorbance values were converted into concentrations (pg/mL) using the standard curve for DMP$_1$.

Immunofluorescence staining: Osteocalcin (OCN) expression was analyzed using immunofluorescence staining. Briefly, before and after differentiation for 7 days, stem cells

were detached from the scaffolds and allowed to reattach to 12-well plates (pretreated with 0.1% gelatin). After 24 hrs, all samples were fixed with 4% paraformaldehyde for 40 min and then treated with 0.4% Triton X-100/phosphate-buffered saline for 10 min. Cells were incubated with phosphate-buffered saline containing 4% BSA (Sigma) for 1 hr to block unspecific reactions. Then, all samples were treated with a primary OCN antibody (1:100) overnight at 4 ℃ and then incubated with the secondary antibody (1:100) for 30 min at RT in the dark. Samples were washed and subjected to fluorescence microscopy to visualize the OCN staining.

3.2.5 Statistical analysis

One-way ANOVA and a post hoc test was used to analyze the statistical significance of differences (p-value<0.05) among different groups.

3.3 Results

3.3.1 SEM analysis of unmineralized and mineralized st-ELR fibers

Morphological changes in the st-ELR fibers before and after mineralization are shown in Figure 3.1. Before mineralization, the crosslinked electrospun st-ELR fibers exhibited a smooth surface (Fig. 3.1A). After 7 days of mineralization using the PILP process, the fiber surface showed a homogenous coating of needle-like mineral structures (Fig. 3.1B). As reported in Chapter 2, we confirmed that these minerals were composed of nano-scale hydroxyapatite. In addition, hydroxyapatite crystals were hierarchically arranged in the interstitial spaces within the ELR fibers, resulting in a high degree of both intra- and extra-fibrous mineralization. Intrafibrous mineralization also significantly increased the mechanical stiffness of the st-ELR films (Chapter 2).
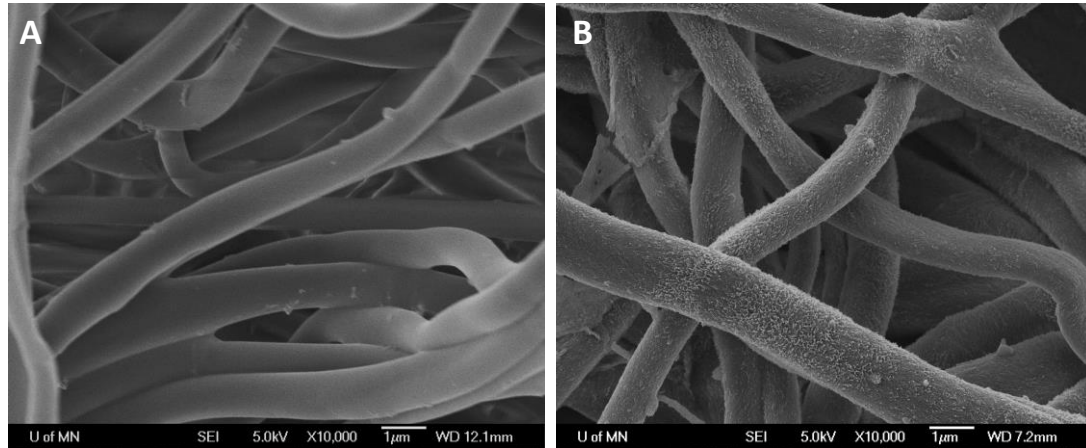
Figure 3.1 **Morphology of st-ELR fibers before mineralization (A) and after 7 days of mineralization (B).** St-ELR fibers showed a smooth surface before mineralization. After mineralization, the surface exhibited a rougher morphology with what appears to be a homogenous coating of needle-like minerals. The mineralization of the fibers noticeably increased the diameter of the fibers.

3.3.2 Proliferation of hDPSCs

Figure 3.2 shows the results for the proliferation of hDPSCs. hDPSCs continuously proliferated over time in all tested groups. The cells proliferated faster on control Ti and TCP samples than on the st-ELR samples. After one day of culture, no significant differences were observed among groups. After 3 days, Ti and TCP showed the highest number of cells, while surfaces with st-ELR fibers exhibited lower proliferation of stem cells. However, significantly higher cell counts were observed on mineralized st-ELR film surfaces than on the unmineralized st-ELR surfaces (p-value<0.05). Cell numbers in all groups increased significantly after 6 days of culture. The mineralized st-ELR group

showed relatively but not statistically significantly fewer cell numbers than the control groups. In contrast, unmineralized st-ELR samples exhibited the significantly lowest number of proliferating cells among all four groups after 6 days of culture (p-value <0.05). Thus, the mineralization of st-ELR supported the proliferation of human dental pulp stem cells. Stem cell proliferation was enhanced on the mineralized st-ELR scaffold compared to the unmineralized and thus less stiff st-ELR scaffold.
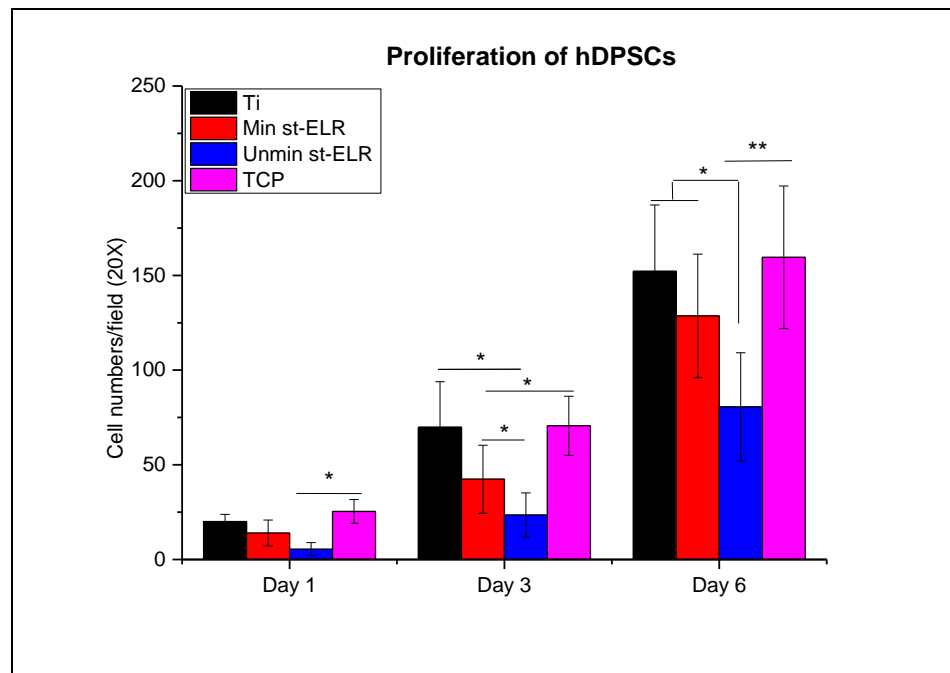
Figure 3.2 **Proliferation of hDPSCs.** Cell numbers continuously increased with culture time in all groups. Control Ti and TCP groups exhibited greater numbers of proliferating cells than the st-ELR groups after 3 days of culture. After 6 days, significantly greater numbers of proliferating cells were observed on mineralized st-ELR than on the Unmin st-ELR. * p-value <0.05, ** p-value <0.01.

3.3.3 Odontogenic differentiation of hDPSCs

ALP activity

ALP is a biomarker of early osteogenic and odontogenic differentiation. The ALP activity of hDPSCs cultured on all materials is shown in Figure 3.3. On day 7 of culture, the four groups exhibited similar levels of ALP activity. ALP activity peaked on day 14 in all groups, except Unmin st-ELR. The peak ALP activity of hDPSCs in the Ti and Min st-ELR groups was significantly greater than the Unmin st-ELR and TCP groups (p-value<0.05). Notably, this difference might be attributed to the fact that cells cultured on both Unmin st-ELR and TCP exhibited almost unnoticeable increases in ALP activity over the 21 days of culture. The ALP activity of cells decreased in all groups after 21 days of culture, with no significant differences among groups.
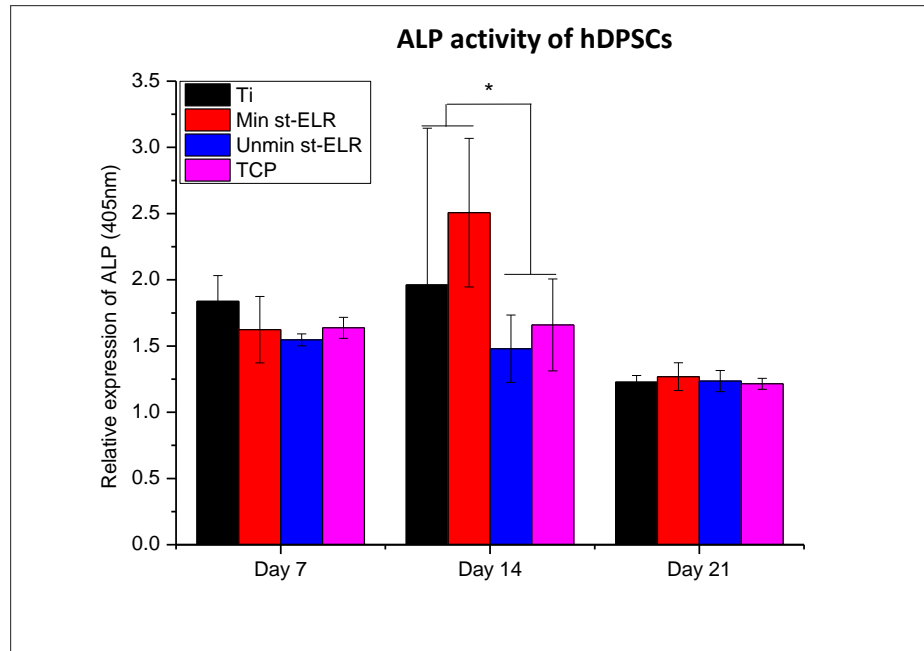
Figure 3. 3 **ALP activity of hDPSCs after 7, 14 and 21 days of culture.** On day 7 of culture, statistically significant differences were not observed among the four groups. The ALP activity of hDPSCs peaked on day 14 in the Ti and Min st-ELR groups, with significantly higher values than those in the Unmin st-ELR and TCP groups. Statistically significant differences in ALP activity were not observed between groups on day 21 of culture. * p-value<0.05.

DMP$_1$ production

The production of DMP$_1$ after 7, 14 and 21 days of culture is shown in Figure 3.4. On day 7, hDPSCs cultured on the Ti surface produced the greatest amount of DMP$_1$ among the four tested groups (p-value<0.05). A significant increase in DMP$_1$ levels was observed in

all groups after 14 days of culture in odontogenic differentiation media. Cells cultured on mineralized st-ELR surfaces exhibited similar levels of DMP_1 production as those of cells cultured on Ti surfaces, which were noticeably greater than those in cells cultured on unmineralized st-ELR and TCP surfaces. However, these differences were not statistically significant (the p-value for the comparison between mineralized and unmineralized st-ELRs is 0.0625). The level of DMP_1 decreased significantly in all groups after 21 days of culture, and the TCP group displayed the highest DMP_1 production.
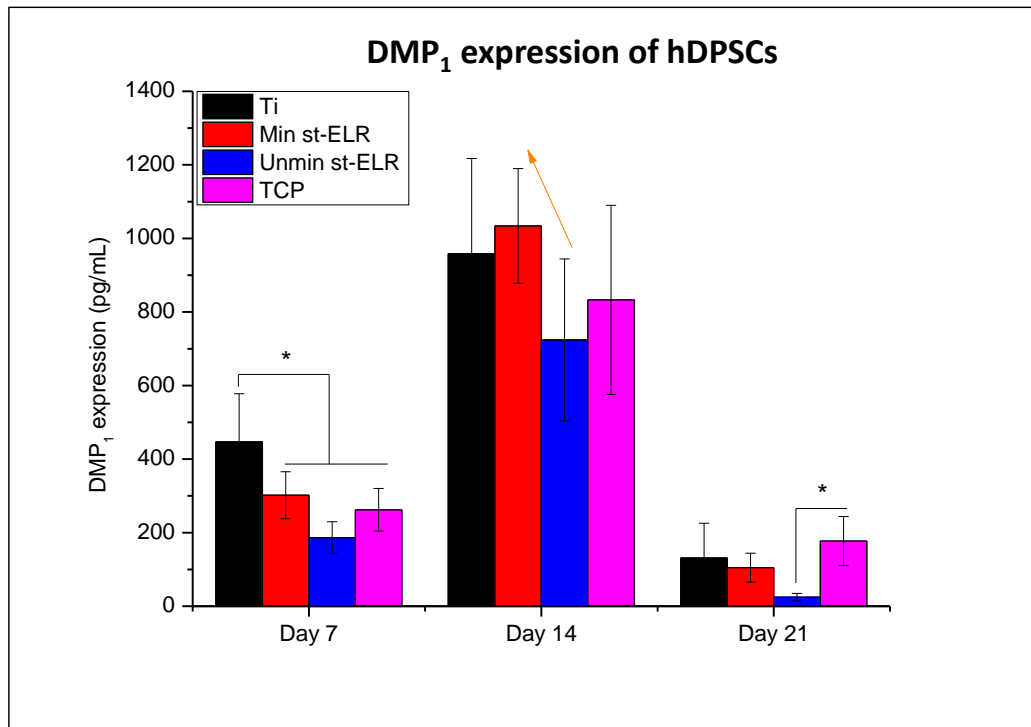
Figure 3.4 **DMP_1 production after 7, 14, and 21 days of culture.** On day 7, hDPSCs grown on Ti surfaces showed the highest level of DMP_1 production among all four groups. DMP_1 production increased markedly after 14 days of culture on Min st-ELR and Ti surfaces, as noticeably higher levels were observed than in cells cultured on Unmin st-ELR and TCP surfaces. However, the p-value for the comparison between Min st-ELR and

Unmin st-ELR was 0.0625. DMP$_1$ production decreased in all groups after 21 days of culture.

Immunofluorescence staining:

Immunofluorescence staining of differentiated hDPSCs after 7 days of differentiation showed a homogeneous distribution of positive staining for OCN (red) within cells compared to the undifferentiated stem cells, which showed no obvious OCN expression. Thus, hDPSCs might also differentiate into osteoblast-like cells.
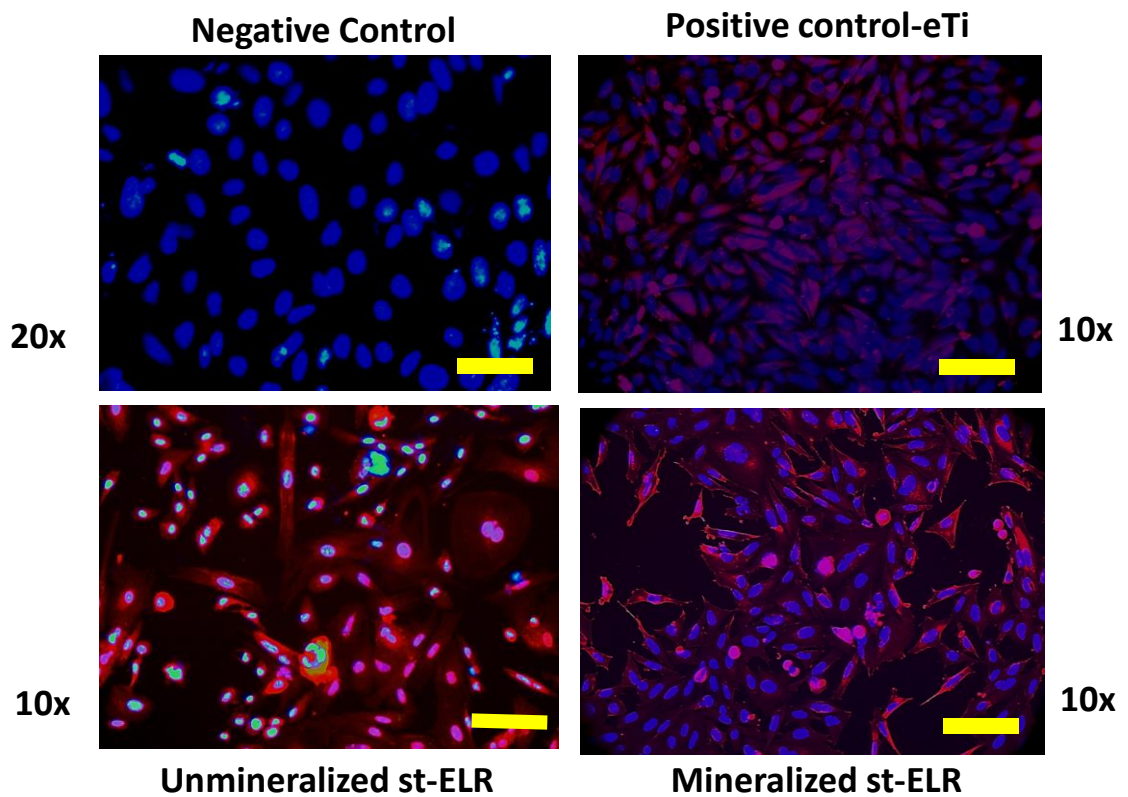
Figure 3.5 **Immunofluorescence staining of hDPSCs.** Images of OCN staining in positive control, unmineralized st-ELR and mineralized st-ELR groups after 7 days of

differentiation are shown. The undifferentiated hDPSCs did not express OCN. Blue: nucleus, red: OCN protein.

3.4 Discussion

As the global prevalence of dental caries and pulpitis is increasing, t an effective therapy that regenerates lost dental tissues must be developed and is urgently needed. Emerging evidence describing the interactions between engineered scaffolds, stem cells, and growth factors has provided significant insights into the development of better approaches for improving dental tissue regeneration. However, the regeneration of the whole pulp tissue remains a difficult problem. Since only a notably small apical foramen is available in each root canal to allow access of blood vessels and drainage of lymph and waste to the apical connective tissue, the growth of stem cells in the scaffolds is constrained when they are placed in the narrow pulp cavity. Thus, strategies inducing the restoration of the lost dental tissues by stimulating the regenerative potential of the remaining healthy pulp cells seems a more practical approach from the clinical perspective than whole pulp regeneration. The idea is to remove the coronal infected pulp tissues via partial pulpitis and place a sterile dental scaffold on top of the remaining healthy pulp in the root canals. The remaining pulp tissues will maintain the blood supply by providing the necessary nutrients and growth factors to support the further migration, proliferation, and differentiation of stem cells within the dental scaffold. This strategy would enable the generation of new dentin tissue. Although this technique is highly dependent on the selection of pulpitis cases, only partial pulpitis with good conditions are acceptable, animal studies have already shown its feasibility [72, 148].

In this study, we aimed to use mineralized st-ELR scaffolds as pulp capping materials for stimulating the odontogenic differentiation of hDPSCs and induce the regeneration of dentin tissues. A nano-fibrous scaffold of st-ELR was successfully electrospun, and the intrafibrous region was mineralized with nHA. The homogenous distribution of minerals on st-ELR fibers was observed under SEM. hDPSCs were then seeded in the mineralized and unmineralized st-ELR scaffolds to investigate cell-scaffold interactions. The mineralized st-ELR fibrous scaffold supported hDPSCs growth and proliferation. Mineralized st-ELR scaffolds exhibited similar proliferation levels as the two controls (Ti and TCP groups). Those cell proliferation values were significantly higher than cells cultured on unmineralized st-ELR scaffolds. These data indicate the good cytocompatibility and close interaction of the nanofibers with hDPSCs.

Furthermore, the mineralized st-ELR scaffold induced the differentiation of greater numbers of hDPSCs than the unmineralized control, as assessed by higher ALP activity and DMP1 expression in hDPSCs. ALP activity is an early biomarker of osteo/odontogenic differentiation, and its expression indicates the formation of hard tissues, such as bone and dentin. DMP_1 is a specific later biomarker of odontoblasts, which was used to determine the odontoblastic differentiation of hDPSCs. OCN is expressed by both the odontoblasts and osteoblasts at the later period of mineralized tissue formation. The mineralized st-ELR showed similar levels of ALP activity on day 7 and significantly higher ALP activity after 14 days than the Ti and TCP control groups. Lower DMP_1 production was observed in mineralized st-ELR than Ti control on day 7, but the value increased substantially and was greater than the other three groups after 14 days of differentiation. Based on these data, the

mineralization of st-ELR scaffolds supported the proliferation and odontogenic differentiation of hDPSCs and enhanced these responses compared to unmineralized scaffolds with the same chemical composition and structure. The decrease in ALP activity and DMP_1 levels observed after 21 days might indicate the low viability of stem cells after 21 days (Fig. 3.5). Interestingly, all stem cells expressed OCN after differentiation (Fig. 3.5), indicating that the stem cells had potential to differentiate into osteoblast cells. This conclusion is reasonable, as the differentiation medium recipe we used was designed for osteogenic differentiation. To date, all differentiation media used for hDPSCs are based on the recipe of osteogenic differentiation medium. The recipe for the differentiation medium recipe must be optimized to achieve a more specific odontogenic differentiation of hDPSCs for dental tissue regeneration. In addition, stem cells behave quite differently in vitro and in vivo. In the present study, although the odontoblastic differentiation of hDPSCs was enhanced by the mineralized st-ELR scaffold in vitro, the formation of dentin-like tissue only appeared to be achieved when the scaffolds were transplanted in vivo in the presence of tooth germ conditioned medium [71, 149]. Therefore, subsequent in vivo studies are required before the approach proceeds to clinical applications.

The promising bioactivity of the mineralized st-ELR scaffold toward hDPSCs is likely attributed to the combination of the fibrous structure and the presence of the minerals inside and outside the fibers. We used an electrospinning technique to fabricate a fibrous st-ELR scaffold that resembles the collagenous dentin matrix. The electrospun scaffolds exhibited well-distributed macro-porosity with excellent interconnectivity. This feature is advantageous for promoting cellular migration and the subsequent invasion of newly formed tissue into the scaffold. Electrospun scaffolds provide a cell-favorable matrix that

is capable of increasing the activities of diverse types of cells, such as osteoblasts [42], fibroblasts [150], and dental pulp stem cells[73]. Another factor is the intrafibrous mineralization of the st-ELR scaffold. We focused on the intrafibrous mineralization of the scaffold because it is the type of mineralization that is found in native dentin. The induction of the intrafibrous mineralization of the electrospun scaffold allowed us to achieve a scaffold that resembles the fibrous structure and mineral deposition, as well as its morphology. A scaffold with mechanical properties that closely resemble natural dentin was obtained. The chemistry of the minerals is also a relevant factor, as nano-crystals of hydroxyapatite are osteogenic/odontogenic conductive materials that produce an artificial environment that closely resembles the mineralized ECM in bone and dentin [151]. Furthermore, intrafibrous mineralization significantly increased the elastic modulus and hardness of the st-ELR scaffolds (Chapter 2), providing a favorable rigid matrix for the osteogenic/odontogenic differentiation of stem cells [74].

Based on the results from this study, the mineralization of an electrospun nano-fibrous st-ELR scaffold supports the proliferation and differentiation of hDPSCs. The mineralized eletrospun ELR scaffold represents a potential dental pulp capping biomaterial for stimulating dentin regeneration. While traditional pulp capping materials fail to yield complete regeneration of dentin, st-ELR fibrous scaffolds could serve as a template for the dentin matrix to stimulate the migration, proliferation, and differentiation of stem cells within pulp tissue, therefore inducing the bulk regeneration of dentin.

3.5 Conclusions

Electrospun st-ELR scaffolds are a promising artificial ECM for dentin regeneration applications when combined with dental pulp stem cells. The fibrous structure and

intrafibrous mineralization support the growth and odontogenic differentiation of dental pulp stem cells. Thus, mineralized st-ELR scaffolds have great potential for application in regenerative endodontics.

Chapter 4: Site-specific Functionalization of Cys-GL13K Peptide to Produce Antimicrobial Substrates against Relevant Oral Bacteria

Abstract

Modification of dental devices and biomaterials with antimicrobial agents is critical for reducing the risk of bacterial infection. We reported a bioconjugation technique to tether a cysteine-modified antimicrobial peptide, GL13K (Cys-GL13K), on a titanium surface to produce an anti-infective coating against common dental bacteria associated with biofilm formation and dental diseases: *S. mutans*, *S. gordonii* and *E. faecalis*. This technique utilizes thiol-maleimide coupling to provide a covalent, site-specific, noncleavable linkage between the peptide and the surface. The peptide conformation, physical/chemical properties of tethered peptides and antimicrobial ability of the coating against the aforementioned bacteria as well as the biocompatibility of Cys-GL13K-coated surfaces toward human dental pulp stem cells (hDPSCs) were evaluated. The soluble form of Cys-GL13K showed irreversible peptide conformational changes in response to a pH change and lower antimicrobial ability against bacterial growth than GL13K peptides. Cys-GL13K peptides were then tethered on a titanium (Ti) surface. XPS, ATR-FTIR and fluorescently labeled peptide visualization revealed that a homogenous, stable coating of peptides was obtained. Compared with controls, a tethered Cys-GL13K coating exerted antimicrobial effects against *S. mutans*, *S. gordonii* and *E. faecalis* by showing significant reduction in CFUs and ATP activity as well as having a notable impact on biofilm formation. Tethered Cys-GL13K also showed good cytocompatibility with hDPSCs. Overall, these results demonstrated that a site-specific thiol-maleimide coupling method is an efficient route to functionalize biomaterials with Cys-GL13K peptides to obtain antimicrobial activity for preventing bacterial infection.

4.1 Introduction

Postoperative infection is a significant problem for all medical devices and scaffolds surgically implanted in the oral cavity because the human mouth contains more than 700 species of bacteria that can colonize all soft and hard surfaces to eventually form a biofilm[77, 152]. These bacteria maintain microbial homeostasis under normal conditions. However, a significant increase in pathogen bacteria occurs once this homeostasis breaks down, leading to various dental diseases such as caries, pulpitis, periodontitis and peri-implantitis[77, 152]. This considerable compromise of host defense due to foreign implanted materials, tissue mobility, and the special morphology of biomaterials (porous, rough surfaces, etc.) may facilitate the colonization of and biofilm formation by opportunistic microbes[153]. Indeed, bacterial infection is considered the most common reason for the failure of medical implants. Additionally, the infected sites are difficult to treat and clean because biomaterials are always placed within tissues. Surgical removal of the infected implanted materials is often required eventually, placing additional costs of care and a heavy burden on the patients.

Streptococcus gordonii (*S. gordonii*), *Streptococcus mutans* (*S. mutans*) and *Enterococcus faecalis* (*E. faecalis*) are critical opportunistic pathogens in the oral cavity. *S. gordonii* is a primary colonizer in the initial stage of biofilm formation[154]; *S. mutans* is a key pathogen for dental caries infection[155], and *E. faecalis* is a major bacterium associated with failure after endodontic treatment[156, 157]. Targeting these bacteria can result in promising control of oral biofilm formation and the subsequent related dental diseases, particularly the prevention of peri-implantitis, caries and pulpitis. In addition to regular oral hygiene cleaning, abundant effort has been made to control oral bacterial infection using

antimicrobial agents to inhibit biofilm formation on tooth/restoration/implant surfaces[152, 158]. Conventional antibiotics have been used in oral biofilm control; however, they may raise problems because of their toxicity to host tissues and the emergence of resistant bacteria species, which may result in severer infections[159, 160].

Cationic antimicrobial peptides (AMPs), which are produced by a wide variety of organisms[161], provide an alternative approach to overcoming the above challenges. AMPs are involved in the primary innate immune reaction and have broad spectrum activity against both gram-positive and gram-negative bacteria[90, 162]. GL13K, a 13-amino-acid AMP, is derived from the human parotid secretory protein (PSP) and is effective against several oral bacteria such as *Pseudomonas aeruginosa*[100]*, Escherichia coli*[3]*, S. gordonii*[98]and *S. mutans*[101]. GL13K activity is retained under various conditions such as in salted solution or human saliva[163]. This antimicrobial peptide also exhibits good biocompatibility with low red blood cell lysis in cytotoxicity tests[100]. The mechanism of the antimicrobial activity of GL13K is complex, and evidence suggests that the peptide interacts with and accumulates on the bacterial membrane, eventually acquiring a predominantly β-sheet configuration that triggers disruption of the bacterial membrane via formation of carpet-like tunnels[164].

Several studies have demonstrated that tethered peptides can be used to obtain antimicrobial solid surfaces that are effective against a broad spectrum of bacteria[163, 165, 166], which suggests that these coatings are good candidates for preventing infection of medical devices. In our previous studies, we immobilized GL13K peptides using silanes and obtained surfaces that significantly reduced the biofilm growth of gram-negative and

73

gram-positive oral bacteria (*Porphyromonas gingivalis*). and *S. gordonii*[98, 99]. GL13K peptides were anchored to titanium surfaces with covalent bonding between silane molecules and the free amines of the positively charged lysines in the sequence of the GL13K peptide as well as at its N-terminus. The mobility of the immobilized peptide was limited by the multiple anchoring points between the peptide and the silanized surface. However, physical and biochemical interactions between the peptides on the functionalized surface and targeted bacteria were sufficient to kill bacteria, with evident disruption of their membrane and wall. The detailed mechanism for the antimicrobial activity of the coatings has not been determined, but the combination of a surface net positive charge and high hydrophobicity with the β-sheet structural conformation of the peptides on the surface proved to be critical for the GL13K coating to exert its antimicrobial effects[90, 167].

The bioconjugation method used in studies by Chen et al.[98] and Holmberg et al.[99] led to the coated implant surface exhibiting a significant antimicrobial effect (Fig. 4.1). However, this technique poses drawbacks when applied to functionalizing various substrates, especially polymeric biomaterials, with bioactive peptides. First, the net positive charge of the tethered peptides is reduced, as some of the positively charged groups, i.e., free amines, are consumed to form the covalent bond with the silane molecules. This change may alter the biofunction of the bioactive molecules because net positive charges are important for the antimicrobial ability of AMPs[90]. Second, the reaction is not site specific, i.e., control over the specific amino acid(s) that will react with the surface is not possible. Multiple lysine residues in the GL13K amino acid sequence as well as at the N-terminus of the peptide compete to react with the silane end group. The lack of control over the conjugation site may also affect the final conformation of the tethered peptides, which

is also known to have a significant effect on their antimicrobial properties[90]. Third, this technique cannot be used for the functionalization of polymers, which hinders its application for tissue engineering scaffolds.

Here, we used the alternative, fast, biocompatible and highly efficient maleimide-thiol coupling route to functionalize an analog of GL13K on solid surfaces. The GL13K analog contains a cysteine residue at the N-terminus of the peptide (Cys-GL13K).

The metal-free reaction between maleimide and thiol has been proven to be a practical and attractive bioconjugation method. First, the reaction is very specific under mild, near-physiological conditions (pH 7.0- 8.0), which facilitates the site-specific conjugation and retention of other functional groups of the peptide such as lysines. In addition, this reaction is fast, generates products that are easy to process and offers high yield in the absence of metal catalysts such as Cu or Br, thus reducing potential toxicity to the tissues[168, 169]. Lastly, the obtained covalent bond is very stable. Bioconjugate links are less vulnerable to hydrolysis in an *in vivo*, reducing environment. This bioconjugation method has been applied to tether thiolated DNA probe oligonucleotides to silicon nitride surfaces to capture target biomolecules from solutions[170]. Similarly, Rezania et al. modified solid surfaces with RGD peptides and demonstrated that tethered RGD retained its function in promoting cell attachment[171]. Bioconjugation has also been adapted for the conjugation of biomolecules to polymers such as polyethylene glycol (PEG), collagen and elastin-like polymers[172-174].

In this study, we adapted thiol-maleimide coupling for covalent grafting of Cys-GL13K to titanium surfaces to obtain an antimicrobial coating. This method keeps all positively

75

charged lysine residues available to retain biofunction and secondary structure, enables site-specific conjugation[175] and facilities further functionalization of implants or polymeric scaffolds with these antimicrobial peptides as well as a diverse set of bioactive molecules such as growth factors, DNA and mRNA. Here, the stability and antimicrobial activity against *S. gordonii*, *S. mutans* and *E. faecalis* were analyzed to evaluate the biofunctionality of the immobilized Cys-GL13K peptide.

4.2 Materials and Methods

4.2.1 Materials

GL13K, Cys-GL13K and a peptide with a random sequence of Cys-GL13K (Cys-GL13K-R1) (Table 4.1) were purchased from APeptide (Shanghai, China) at >98% purity. The compound (3-aminopropyl) triethoxysilane (APTES) was purchased from Sigma-Aldrich (St. Louis, MO, USA.). Sulfosuccinimidyl 4-(N-maleimidomethyl) cyclohexane-1-carboxylate (sulfo-SMCC), tris (2-carboxyethyl) phosphine (TCEP), penicillin/streptomycin (P/S), fetal bovine serum (FBS) and Hank's balanced salt solution (HBBS) were purchased from Thermo Fisher Scientific (Minneapolis, MN, USA.). Brain heart infusion (BHI), Todd-Hewitt broth (THB) powders and other bacterial culture-related agars were purchased from BD Biosciences (San Jose, CA, USA). Human dental pulp stem cells (hDPSCs) were graciously donated by the Dr. Kim Mansky's laboratory (School of Dentistry, University of Minnesota, USA.).

The bacterial strains *S. mutans* (ATCC 700610), *S. gordonii* (ML-5) and *E. faecalis* (V583) were used in the experiment. BHI media was used for the growth of *S. mutans,* and THB media was used for the culturing of *S. gordonii* and *E. faecalis* in all experiments. All

bacterial culture experiments were carried out in an anaerobic chamber (80% N_2, 10% CO_2, and 10% H_2) at 37 °C.

Peptide	Sequence
GL13K	GKIIKLKASLKLL-CO(NH2)
Cys-GL13K	CGKIIKLKASLKLL-CO(NH2)
Cys-GL13K-R1	CIGIKLLKSKLKAL-CO(NH2)

Table 4.1 **Sequences of peptides.**

4.2.2 Circular dichroism (CD)

Peptide conformations were investigated by CD. GL13K was dissolved in sodium phosphate buffer solution (SBS, pH 7.4) at a concentration of 0.5 mg/mL (0.0032 mM). Cys-GL13K and Cys-GL13K-R1 were reduced using TCEP solution (pH 7.0) for 30 min and then dissolved in SBS at the same concentration as the GL13K solution. A JASCO J-815 spectropolarimeter was used to record the spectra of different peptides at different pH values using a quartz cell with a 0.1 cm path length. To analyze the change in peptide conformation with pH, we initially recorded CD spectra at pH 7.4, and then the pH of the same peptide solution was adjusted to 9.5 and back to 7.4 using NaOH and HCl. The spectra of the peptide solutions at the different pH values were recorded in the 190-260 nm wavelength range.

To study the secondary structures of immobilized Cys-GL13K and Cys-GL13K-R1, two 8x25x0.5 mm quartz slides (SPI, US) were modified with maleimide and then bioconjugated with Cys-GL13K and Cys-GL13K-R1 following the same procedure used for the immobilization of the peptides on titanium surfaces (described below). The slide was inserted into a 1 cm quartz cell for CD analysis. CD data are shown as the mean residue ellipticity and analyzed using a set of software programs (CDSSTR, CONTINLL and SELCON3) in CD Pro Analysis to determine the percentage of the different secondary structure components.

4.2.3 Minimal inhibitory concentration (MIC)

Prior to the MIC test, Cys-GL13K, Cys-GL13K-R1, and GL13K peptides were dissolved in 0.01% acetic acid solution at a density of 10 mg/mL and kept at 4 °C. *S. mutans, S. gordonii* and *E. faecalis* were diluted 1:2000 from their overnight culture before being subjected to the MIC test. Peptide solutions were added to a 96 well polypropylene plate (no. 4917; Thermo Fisher Scientific, Waltham, MA) with a serial dilutions to reach concentrations of 512 μg/mL, 256 μg/mL, 128 μg/mL, 64 μg/mL, 32 μg/mL, 16 μg/mL, 8 μg/mL, 4 μg/mL, 2 μg/mL, and 1 μg/mL. One hundred microliters of bacterial solution was pipetted into each well, and the plate was kept in the anaerobic chamber overnight with gentle shaking. All MIC tests were performed in triplicate.

4.2.3 Peptide coating on titanium surfaces

A schematic description of the complete peptide coating procedure is shown in Figure 4.2. Polished commercial pure titanium grade II (McMaster, USA) disks with a 9 mm diameter

were etched in a 5 M NaOH solution at 60 ˚C overnight (eTi). The samples were thoroughly

cleaned and silanized with a 5% APTES solution (dissolved in 95% ethanol) in a 60 ℃

incubator for 2 hrs. After silanization, the samples were thoroughly rinsed with distilled

water, acetone, and isopropyl alcohol and then immersed in 0.5 mg/mL sulfo-SMCC

solution (dissolved in sodium phosphate buffer, pH 7.2) for 1 hr at room temperature to

complete maleimide modification. The Cys-GL13K and Cys-GL13K-R1 were coated on

etched titanium surfaces separately by immersing the maleimide-modified eTi samples in

two 0.5 mM peptide solutions (pH 7.2) for 30 min, respectively. The samples were then

washed using distilled water, acetone and isopropyl alcohol with 5 min of sonication. All

the samples were dried under N$_2$ gas and stored in a -25 ℃ freezer before being used.
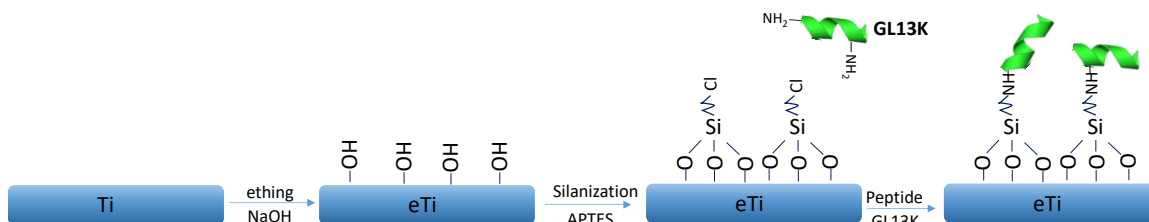
Figure 4.1 **Schematics of the GL13K peptide coating procedure based on silane**

chemistry in Chen et al. studies. Note: The amines are used as the conjugation linkers.
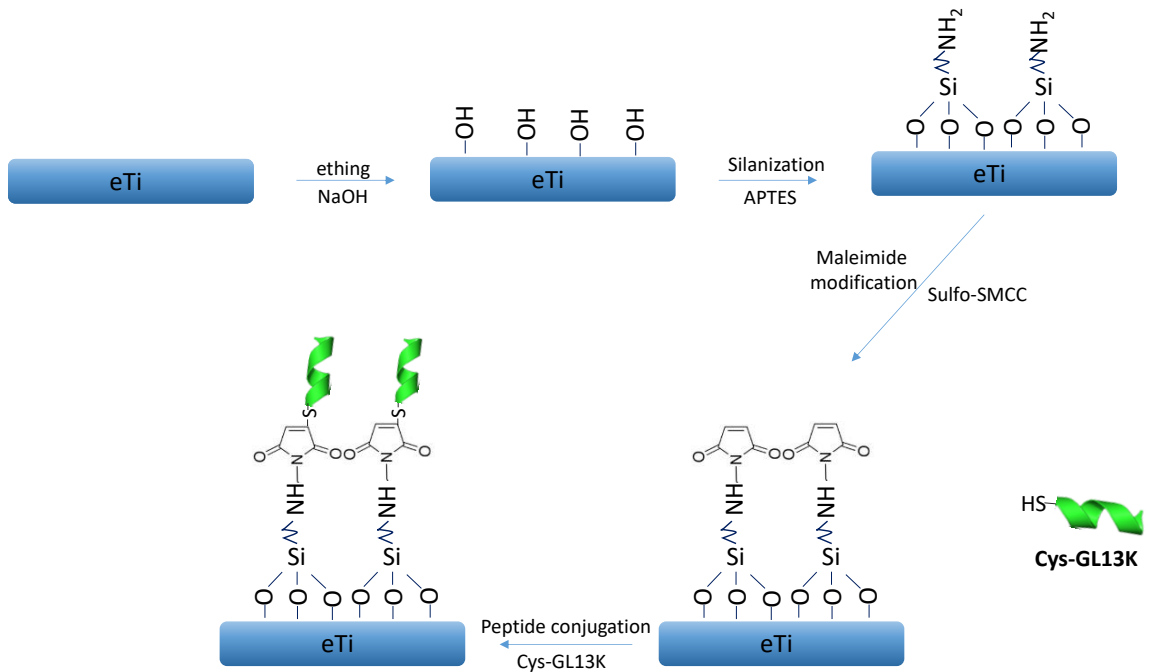
Figure 4.2 **Schematics of the Cys-GL13K peptide coating procedure.**

4.2.4 Characterization of peptide coating

Attenuated total reflectance Fourier transform infrared spectroscopy (ATR-FTIR, Nicolet Magna-IR 750) was used to determine the molecular groups present on the peptide-immobilized surfaces. Sixty-four scans were collected for each sample, and the spectra were analyzed using OMNIC software (Nicolet Instruments Corp.).

X-ray photoelectron spectroscopy (XPS, Physical Electronics Model 555, Al Kα X-ray, 1 mm spot size, 35 ° take-off angle) was performed to investigate the surface chemical composition after each step of the treatment.

To analyze the surface hydrophilicity/hydrophobicity, we determined the water contact angles (DM-CE1, Kyowa Interface Science, Japan) on the surfaces after each step of the treatment using the sessile drop method (2 μL drops) and the appropriate software, FAMAS (Kyowa Interface Science, Niiza-City, Japan).

Visual assessment of fluorescently labeled peptides on the modified surfaces was used to determine the stability of the peptide conjugation. Fluorescent GL13K-FAM was modified with thiols using Traut's reagent (ThermoFisher Scientific) according to the manufacturer's protocol. Briefly, GL13K-FAM was dissolved in SBS buffer (pH 7.2, containing 5 mM EDTA) at a concentration of 10 mg/mL. Traut's reagent was dissolved in water at a concentration of 2 mg/mL (14 mM). Then, 200 μL of GL13K-FAM was added to 7 mL of Traut's reagent solution with gentle mixing. Thiol moieties were linked to the amines on GL13K-FAM during the reaction. After 2 hrs of reaction at room temperature, the solution was purified twice using Zeba™ Spin Desalting Columns (ThermoFisher Scientific) and lyophilized. The powder of thiol-modified GL13K-FAM was collected and dissolved in SBS at a 10 mg/mL concentration. The peptides were coated on maleimide-modified eTi (experimental group) and eTi (control group) samples following the same protocol as that used for Cys-GL13K modification. Fluorescence signals on the surface were visualized under a fluorescence microscope (Eclipse E800, Nikon, Japan) after rinsing, 5 min of sonication, and 30 min of sonication using distilled water.

4.2.5 Bacterial culture

First, eTi, maleimide-modified eTi, and Cys-GL13K-, Cys-GL13K-R1- and chitosan-coated eTi disks were loaded into a 24 well plate. Samples were immersed in 70% ethanol solution for 30 min and further disinfected under UV light for 40 min before experiments with bacteria were performed. Overnight inoculum of *S. mutans* was diluted to an OD value of 0.6 and then further diluted 25-fold using BHI media. One milliliter of *S. mutans* solution was added to each well. For the *S. gordonii* and *E. faecalis* experiments, the inocula were diluted 1:2000 using THB media. One milliliter of bacterial solution was added to each sample. The plates were placed in the anaerobic chamber for overnight culturing with gentle shaking.

4.2.6 Antimicrobial activity of immobilized peptides

Bacterial viability was determined by counting colony forming units (CFUs) of *S. mutans*, *S. gordonii* and *E. faecalis* on agar plates. Mitis-salivarius sucrose bacitracin (MSSB) agar plates were used for the plating of *S. mutans,* while THB agar plates were used for *S. gordonii* and *E. faecalis*. Briefly, after overnight culture, all the samples were gently washed 3 times with 0.9% NaCl. The biofilm grown on the different tested surfaces was collected in 1 mL of 0.9% NaCl solution by sonicating the samples for 10 min. The solution was serially diluted 10-, 100-, 1000-, 10000- and 100000-fold. Ten microliters of each dilution was plated on MSSB agar plates (for *S. mutans*) and Todd-Hewitt agar plates (for *S. gordonii* and *E. faecalis*) and incubated at 37 ℃ in the anaerobic chamber. The number of CFUs was counted after 48 hrs of incubation. An ATP assay was used to determine the bacterial metabolic activity. A total of 100 μL of the collected bacterial solution was mixed

with 100 μL of the BacTiter-Glo Microbial Cell Viability kit (Promega, Madison, WI, USA) in a solid white 96 well plate (Corning 3789, Fisher Scientific. Waltham, MA, USA.) and incubated for 15 min to obtain full cell lysis at room temperature. The bioluminescence was measured with a microplate luminometer (BioTek, Winooski, VT, and USA).

To further analyze the effects of the immobilized peptides on the viability of the biofilms, a BacLight Bacterial Viability Kit (Invitrogen, Grand Island, NY, USA) was used to stain the alive and dead bacterial cells. The biofilms on the tested surfaces were gently rinsed with 0.9% NaCl three times. The staining solution was made by adding 30 μL of green dye and red dye into 1 mL of sterile water. Then, 200 μL of the mixed solution was added to each sample. After 20 min of incubation at room temperature, samples were rinsed gently and immediately transferred to a fluorescence microscope for visualization.

4.2.6 Cytotoxicity test

hDPSCs were seeded on eTi, maleimide-modified eTi, and Cys-GL13K-R1-, Cys-GL13K- and chitosan-coated eTi surfaces at a density of 5000 cells/well in 24 well plates. α-MEM (HyClone SH30568, GE healthcare, Little Chalfont, UK) supplemented with 10% FBS, 1% P/S and 1% L-glutamine was used as the culture medium. The medium was changed every three days. After 1, 3 and 6 days of culture, the cells attached on the tested surfaces were rinsed with HBBS buffer, fixed with 4% paraformaldehyde (PFA) for 20 min and then stained with 0.2 μg/mL DAPI for 10 min. Proliferation analysis of each sample was recorded by counting the stained nuclei of stem cells using a fluorescence microscope.

4.2.7 Statistical analysis

All experiments were conducted, and at least 4 samples per group were tested. Statistically significant differences in CFUs, ATP activity and stem cell proliferation between groups ($p\text{-value} < 0.05$) were analyzed using one-way ANOVA with Tukey's multiple comparison post hoc test.

4.3 Results

4.3.1 CD analysis

Figure 4.3 and Figure 4.4 show the CD spectra of the peptide secondary structure at different pH values for the unmodified GL13K (Fig. 4.3A and Fig. 4.4A&a) and cysteine-modified peptide (Cys-GL13K, Fig. 4.3B and Fig. 4.4 B&b), as well as for the random sequence of Cys-GL13K peptide (Cys-GL13K-R1, Fig. 4.3C and Fig. 4.4C&c), in solution. At neutral pH, GL13K peptides preferred random coil conformations. When the pH increased to 10.5, these peptides showed a notable transformation into a β-sheet configuration (Fig. 4.3A and Fig. 4.4A&a). These conformational changes reverted when the pH was repeatedly cycled between high and low values (Fig. 4.3A). However, the Cys-GL13K peptide exhibited a different conformational state than the GL13K peptide, and the responses of these peptides to repeated pH cycling also differed (Fig. 4.3B). The initial secondary structure showed a higher β-sheet contribution at neutral pH for Cys-GL13K peptides than for GL13K peptides (Fig. 4.4a&b). Unlike GL13K, when the pH increased to 10.5, most of the Cys-GL13K peptides transformed into an α-helix conformation (Fig. 4.4B & b). In addition, the Cys-GL13K peptides did not reconfigure significantly to a β-sheet conformation when the pH was brought back to neutral pH (Fig. 4.3B). The Cys-GL13K-R1 peptide was prevalently a random coil at pH 7.4 and an α-helix at pH 10.5 (Fig.

4.3C and Fig. 4.4C&c). However, the peptide conformation was reversed by changing the pH value. CD analysis of tethered Cys-GL13K and Cys-GL13K-R1 is shown in Figure 2D. Tethered Cys-GL13K and Cys-GL13K-R1 showed a mixture of α-helix and β-sheet conformations but was dominated by α-helix.
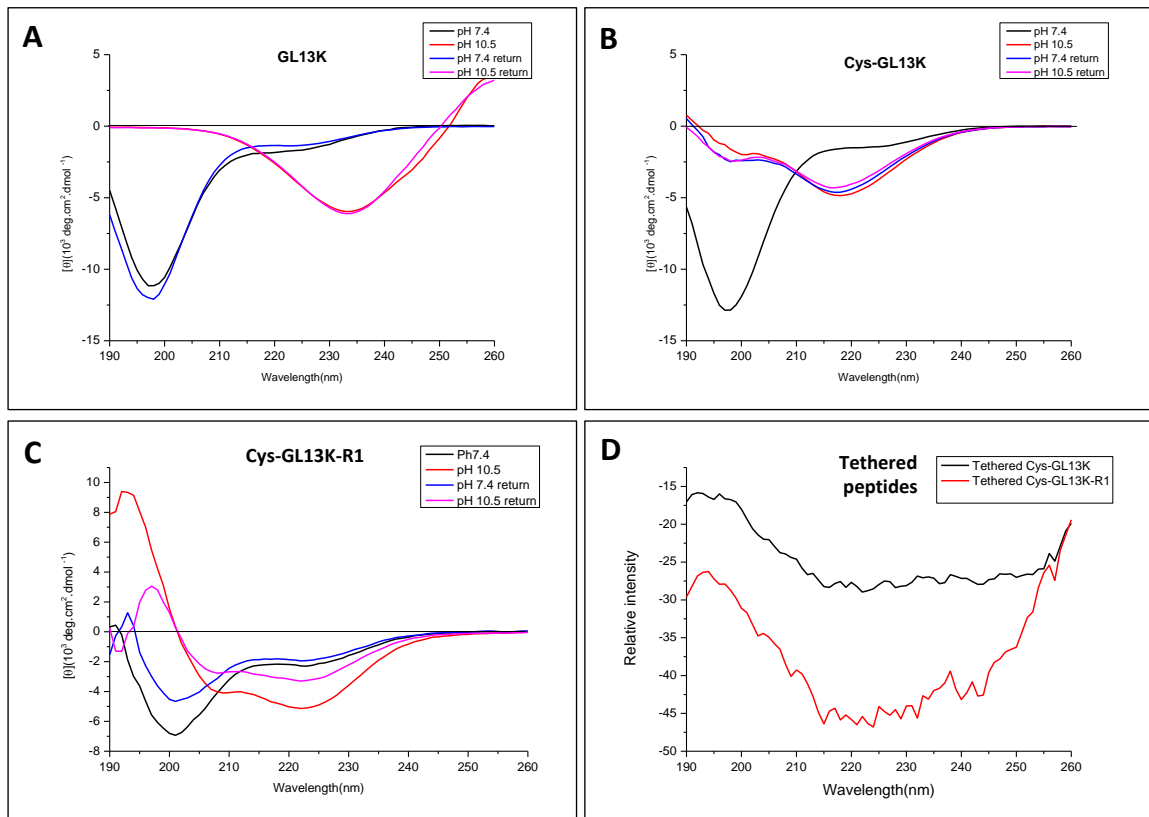
Figure 4.3 **CD analysis of soluble and tethered peptides. A, B, C:** CD spectra of GL13K (A), Cys-GL13K (B), and Cys-GL13K-R1(C) in solution. **D:** CD analysis of Cys-GL13K and Cys-GL13K-R1 tethered on glass slides.

a GL13K	pH7.4	pH10.5	pH7.4 return	pH10.5 return
α-helix	0.028	0.393	0.066	0.469
β-sheet	0.161	0.581	0.161	0.28
unorder	0.811	0.026	0.773	0.251

b Cys-GL13K	PH7.4	pH 10.5	pH7.4 return	pH 10.5 return
α-helix	0.11	0.74	0.491	0.427
β-sheet	0.3395	0.141	0.223	0.264
unorder	0.494	0.119	0.286	0.309

c Cys-GL13K-R1	PH7.4	pH 10.5	pH7.4 return	pH 10.5 return
α-helix	0.11	0.69	0.191	0.431
β-sheet	0.183	0.167	0.244	0.290
unorder	0.707	0.143	0.565	0.279

Figure 4.4 **Peptide secondary structure components.** Quantification of the proportions of peptide secondary structure components: GL13K (A&a), Cys-GL13K (B&b) and Cys-GL13K (C&c).

4.3.2 MIC test

The MIC results for the three peptides (GL13K, Cys-GL13K, and control Cys-GL13K-R1) are shown in Table 4.2. The GL13K peptide exhibited a MIC at 64 μg/mL against both *S. mutans* and *S. gordonii*. However, when GL13K was modified with the cysteine residue, no significant antimicrobial effect was observed. Bacterial cultures treated with 512 μg/mL, 256 μg/mL and 128 μg/mL Cys-GL13K showed disperse colonies instead of aggregated bacteria mass in the bottom of the well plate. This result might indicate that Cys-GL13K inhibited the aggregation of bacteria, although its soluble form did not possess bactericidal ability. Cys-GL13K-R1 showed no antimicrobial or antiaggregation effect against both *S.*

mutans and *S. gordonii* in solution. All three peptides showed no antimicrobial effect against *E. faecalis.*

	GL13K	Cys-GL13K	Cys-GL13KR
S. mutans	64μg/mL	-	-
S. gordonii	64μg/mL	-	-
E. faecalis	-	-	-

Table 4. 2 **MIC of GL13K, Cys-GL13K and Cys-GL13K-R1 against *S. mutans*, *S. gordonii* and *E. faecalis*.** The MIC of GL13K against *S. mutans* and *S. gordonii* is 64 μg/mL. Cys-GL13K and Cys-GL13KR did not show an antimicrobial effect in liquid solution; however, Cys-GL13K inhibited the aggregation of biofilm when the peptide concentration was ≥128 µg/mL. All three peptides showed no antimicrobial effect against *E. faecalis*.

4.3.3 Surface characterization

ATR-FTIR analysis of the Cys-GL13K-immobilized surface is shown in Figure 4.5A. No specific peaks were exhibited by the eTi surface. After peptide immobilization, characteristic bands for amides were detected at 1435 cm^{-1} and 1567 cm^{-1}, indicating the presence of amide groups in tethered peptides. The spectra also showed a small peak for maleimide at 1771 cm^{-1}, which was attributed to unreacted maleimide moieties on the surface.

XPS spectra for the surfaces at each step of the immobilization process are shown in Figure 4.5B. The eTi surface showed a strong Ti 2p peak. When the surface was silanized, a C 1s peak from the silane molecules appeared. A small N peak from the terminal amine group of these silane molecules was also detected. The modification with maleimide significantly decreased the signal of Ti 2p, suggesting that the Ti surface was covered with a thick layer of organic molecules. Immobilization of Cys-GL13K on the maleimide-modified surface led to the emergence of a strong N 1s peak and a marked increase in the C 1s signal. We attribute the emergence of a Na peak from these surfaces to precipitated salts from the buffer. These data indicated that Cys-GL13K peptides were present on the eTi surface prepared using the maleimide-thiol route. The Cys-GL13K peptide coating also resulted in a significant increase in surface hydrophobicity, as indicated by contact angles that increased from approximately 20 ℃ (prior to peptide immobilization) to near 60 ℃ (after the surface with modified Cys-GL13K) (Fig. 4.5C). Surfaces modified with Cys-GL13K-R1 showed similar hydrophobicity to those modified with Cys-GL13K (Fig. 4.5C). Visualization of the surfaces modified with fluorescently labeled peptides demonstrated that Cys-GL13K molecules were strongly retained on the titanium surfaces when the maleimide-thiol coupling was used (Fig. 4.5D & E). The fluorescently labeled thiolated peptides were homogeneously coated on the maleimide-modified eTi surface. Strong fluorescent signals were retained on this surface after 5 min and 30 min of sonication in distilled water, indicating the stable covalent anchoring of the peptides (Fig. 4.5D & Fig. 4.5E, 1st row). In the control group in which the peptides had been physically adsorbed, most of the fluorescent signal disappeared after sonication (Fig. 4.5E, 2nd row).
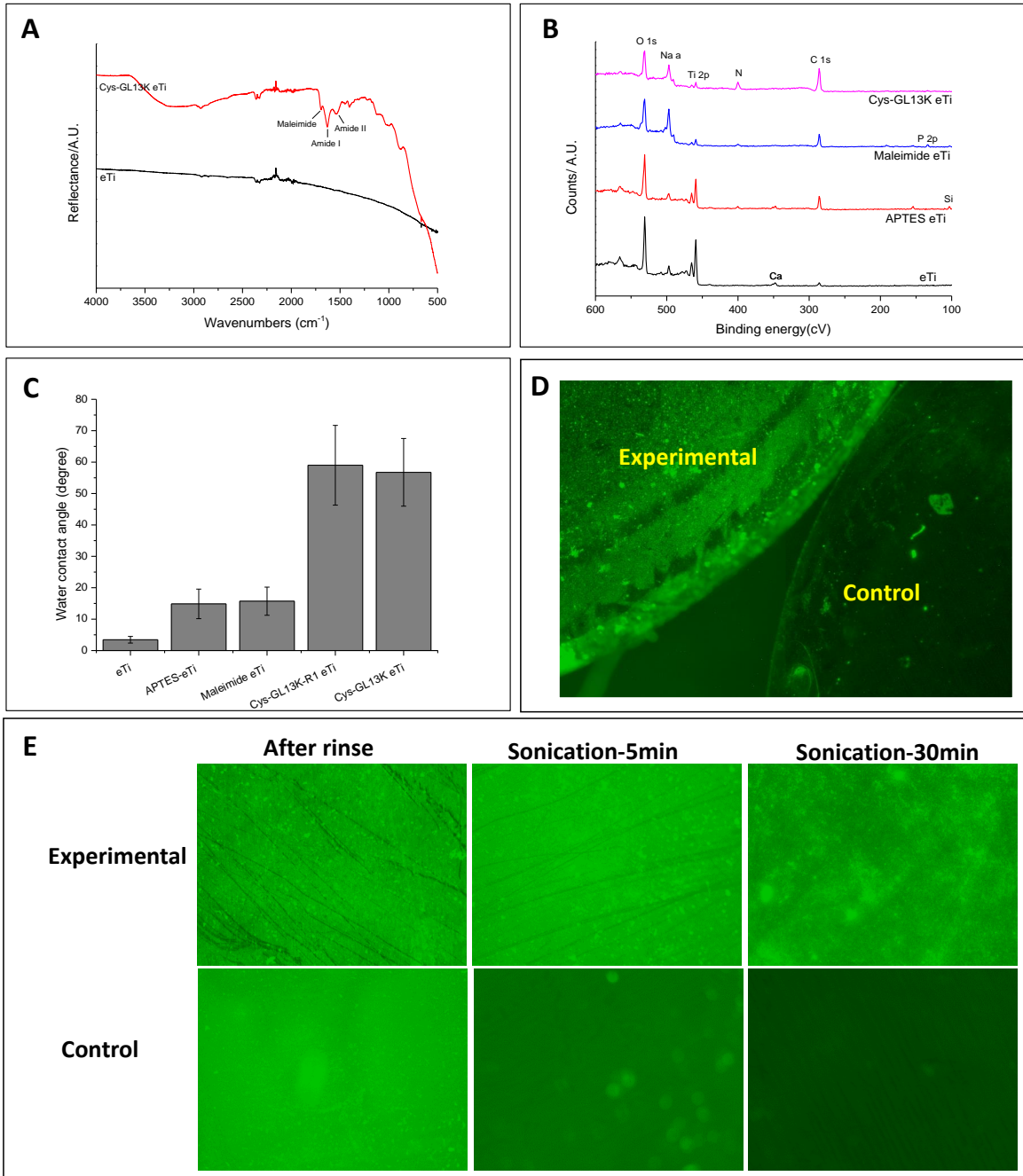
Figure 4.5 **Surface characterization of Cys-GL13K conjugates. A:** ATR-FTIR spectra

of eTi surfaces before and after immobilization of Cys-GL13K peptides. **B:** XPS survey

spectra and **C:** water contact angles of modified eTi surfaces after each step of the Cys-

GL13K immobilization process. **D:** Side-by-side visualization of surfaces coated with

fluorescently labeled GL13K peptides that were physisorbed (Control) or immobilized using the maleimide-thiol route after 30 min of sonication in distilled water. **E:** Surfaces with immobilized (1st row) or physisorbed (control, 2nd row) fluorescently labeled peptides.

4.3.4 Antimicrobial activity of immobilized peptides

The antimicrobial effects of immobilized Cys-GL13K against *S. mutans*, *S. gordonii* and *E. faecalis* were evaluated by analyzing the CFUs, ATP activity and visualization of live and dead cells. As shown in Figure 4.6A, a thick biofilm of *S. mutans* was formed on the eTi, APTES eTi, maleimide eTi and Cys-GL13K-R1-treated Ti surfaces. Large numbers of bacteria were found alive on these sample surfaces, while most bacteria were dead on Cys-GL13K-coated eTi surfaces. Consistent with these results, statistically significant reductions (p-value<0.01) were observed in the CFUs (Fig. 4.6B) and ATP activity (Fig. 4.6C) of *S. mutans* on the Cys-GL13K coating compared with those of *S. mutans* on all other surfaces. The results were similar to that of the positive control using chitosan as the antimicrobial agent. The Cys-GL13K-R1 coating also decreased the ATP activity of *S. mutans* (p-value<0.05).

The antimicrobial activity of the different surfaces against *S. gordonii* was similar to that obtained against *S. mutans* (Fig. 4.7). Cys-GL13K coatings on the eTi surface led to a significant reduction in bacterial growth and metabolic activity (Fig. 4.7B &C). A higher proportion of bacteria cells were dead on Cys-GL13K-coated surfaces than on all other surfaces (Fig. 4.7A) except for the positive control (chitosan-coated surfaces). Interestingly, compared with surfaces that had not been coated with peptides, the surface with Cys-GL13K-R1 exhibited a certain inhibitory effect by showing a significant decrease in the

CFUs and ATP activity of *S. gordonii* (Fig. 4.7B & C, p-value<0.05). However, Cys-GL13K-coated surfaces had a significantly higher antimicrobial effect than Cys-GL13K-R1-coated surfaces.

Decreased CFUs and ATP activity of *E. faecalis* on peptide-coated surfaces were also observed (Fig. 4.8B & C). However, the viability images showed few dead bacteria on the Cys-GL13K and Cys-GL13K-R1 coatings compared with the control groups (Fig. 4.8A). The eTi, APTES-, and maleimide-treated surfaces showed thick biofilm formation, while many fewer bacteria were observed on the two peptide-coated surfaces (Fig. 4.8A).
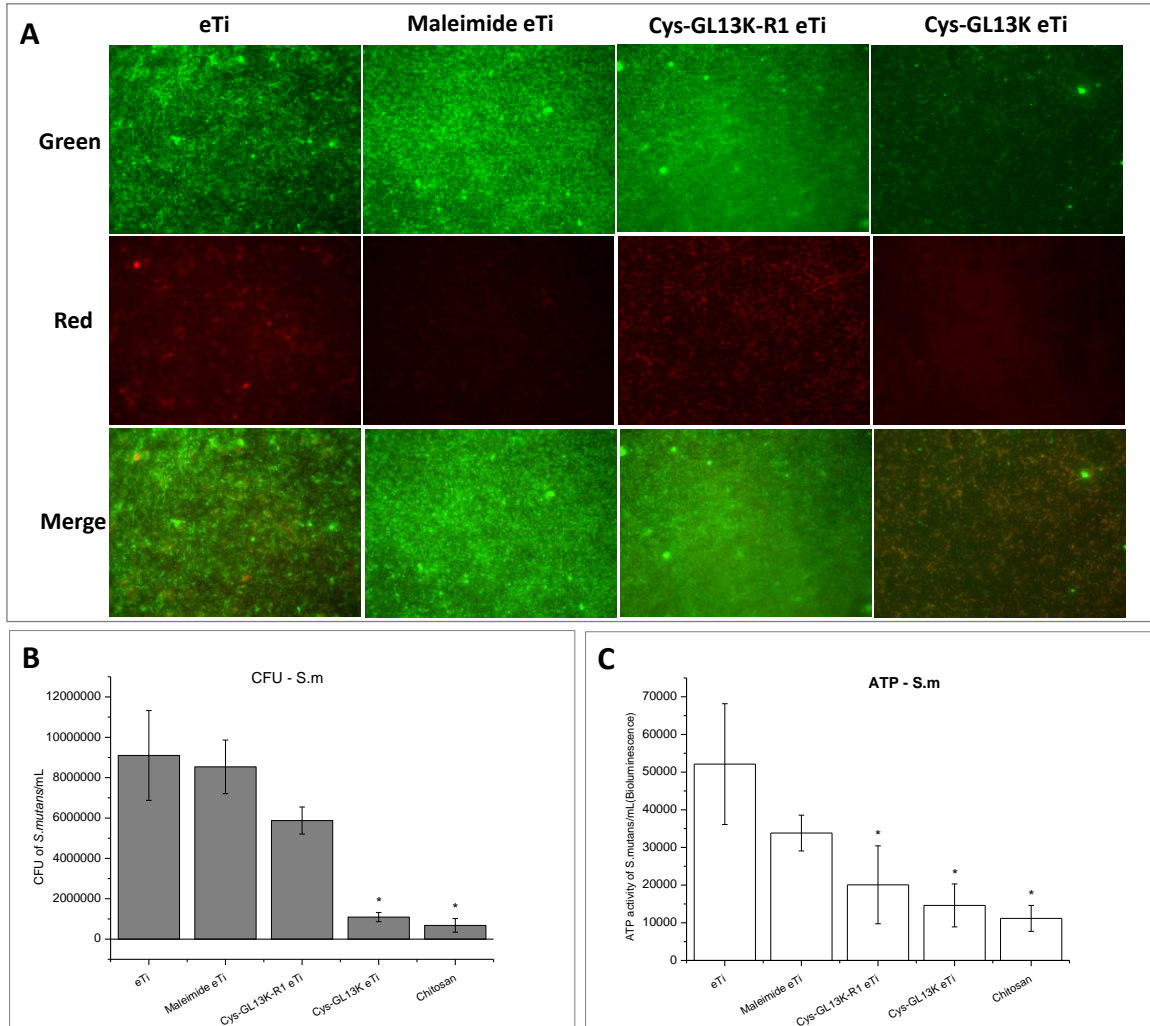
Figure 4.6 **Antimicrobial test with *S. mutans*. A:** Live and dead assay (green: alive cells, red: dead cells); **B:** CFUs; **C:** ATP activity. * P-value<0.05.
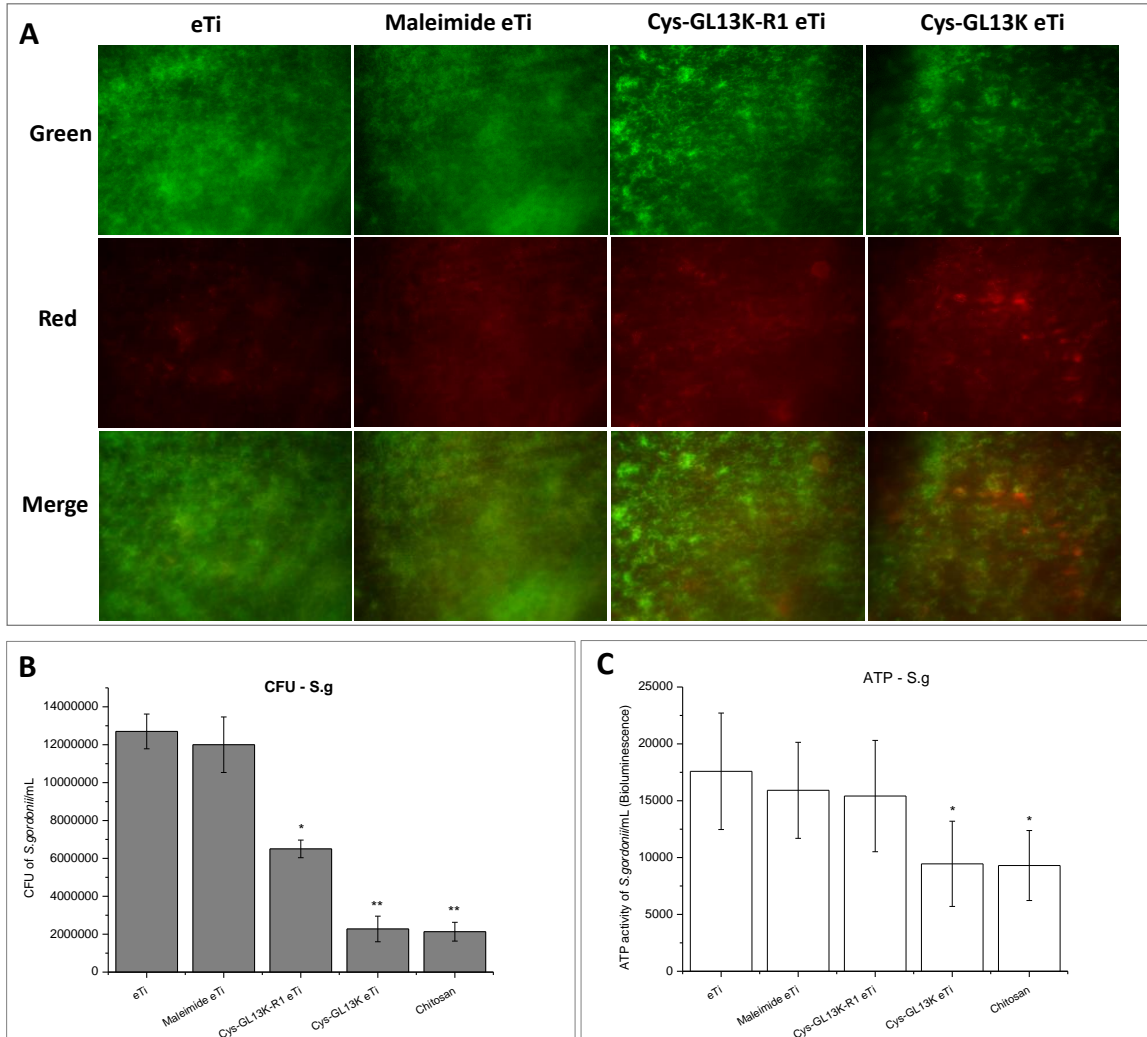
Figure 4.7 **Antimicrobial test with *S. gordonii*. A:** Live and dead assay (green: live cells, red: dead cells); **B:** CFUs; **C:** ATP activity. *: p-value<0.05, **: p-value<0.01.
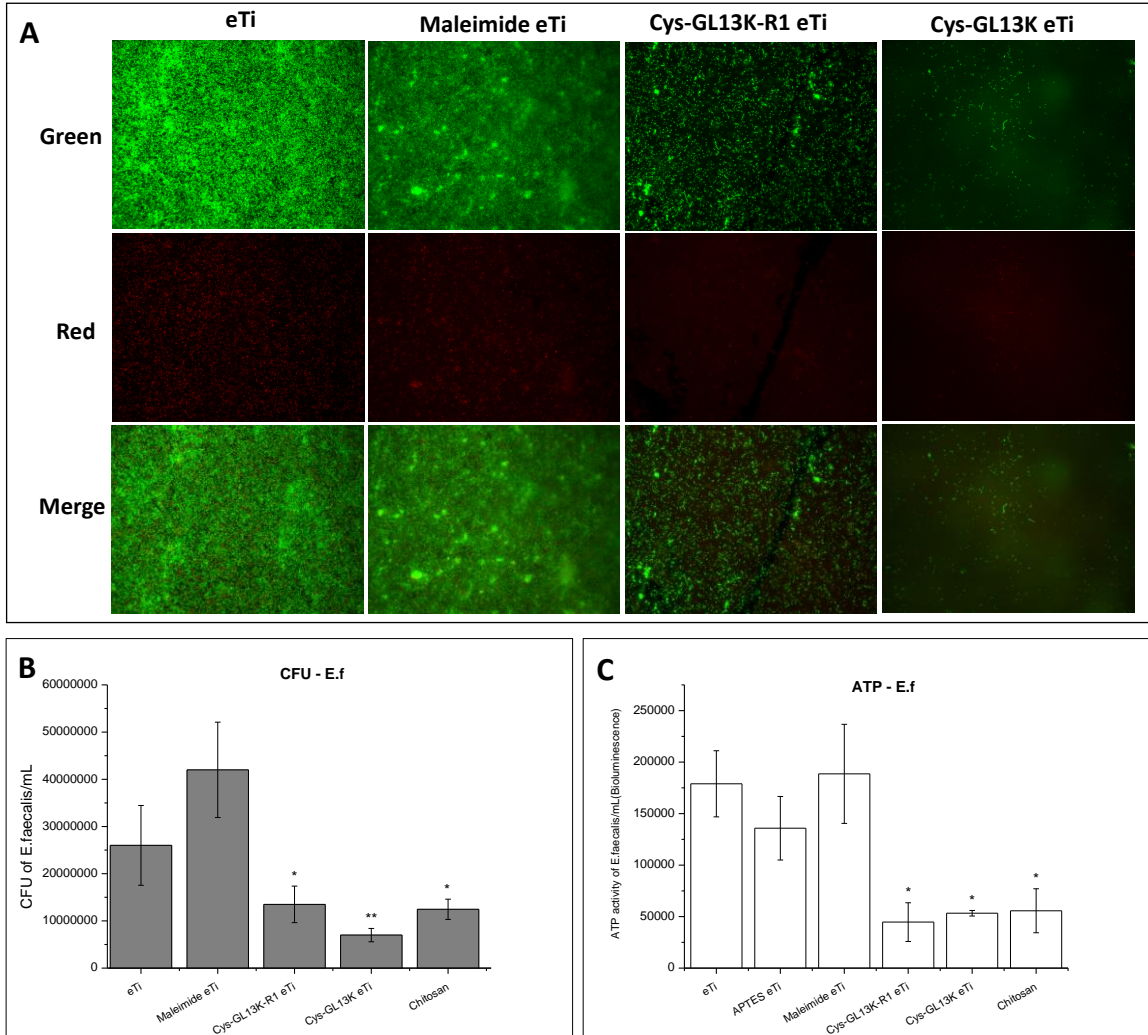
Figure 4.8 **Antimicrobial test with *E. faecalis*. A:** Live and dead assay (green: live cells, red: dead cells); **B:** CFUs*;* **C:** ATP activity. *: p-value<0.05, **: p-value<0.01.

4.3.5 hDPSC cytotoxicity of immobilized peptides

To test the biocompatibility of surfaces with immobilized peptides, we assessed the proliferation of hDPSCs on the different tested surfaces after 1, 3 and 6 days in culture. Figure 4.8 shows the continuous growth of cells over time on all surfaces tested (Fig. 4.9A),

with no significant differences between them after 1, 3 and 6 days of culture (Fig. 4.9B).

These data demonstrated that Cys-GL13K coatings were not cytotoxic to hDPSCs *in vitro*.
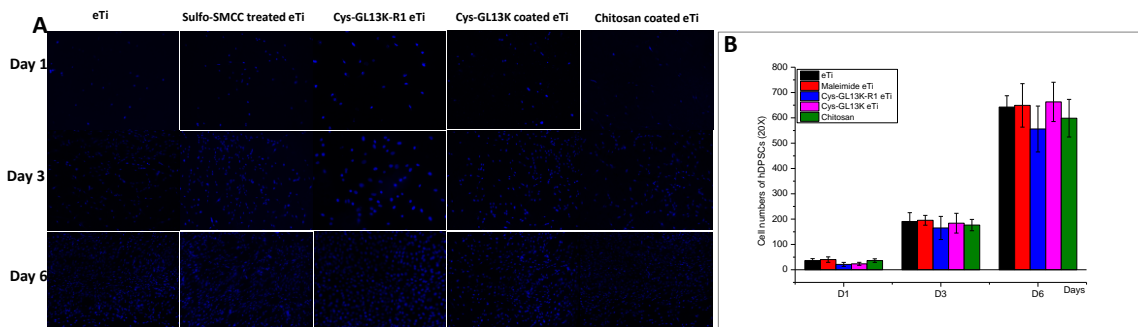
Figure 4.9 **Proliferation of hDPSCs on eTi surfaces after different treatments. A:** Stem cell nuclei on different surfaces after 1, 3 and 6 days of culture. 40X. **B:** Cell numbers/field of different samples after 1, 3 and 6 days.

4.4 Discussion

It has been previously demonstrated that tethered GL13K peptides exert strong antimicrobial effects[98, 99]. In this study, we focused on the application of an alternative site-specific bioconjugation technique to tether peptides to a titanium surface while retaining their antimicrobial effect, secondary structure and biocompatibility with hDPSCs. The bioconjugation method studied here is based on thiol-maleimide coupling, i.e., a rapid, specific, safe and easy approach to conjugate biomolecules to natural and synthetic substrates. ATR, XPS, hydrophobicity testing and visualization of fluorescently labeled peptides on the treated surfaces before and after sonication demonstrated that the Cys-GL13K peptides were homogeneously immobilized on the Ti surface (Fig. 4.4). The stability of the fluorescent peptide signal after several periods of sonication in water

suggested that the tethered peptides have strong resistance to removal when sheared in water-based fluids.

As the conjugation method used for Cys-GL13K in this study is different from the technique used in previous studies in our laboratory, a notably lower surface hydrophobicity was observed for the immobilized Cys-GL13K peptides[98, 99]. The water contact angle on Cys-GL13K immobilized surfaces was near 60 °, while the GL13K-coated Ti surfaces had water contact angle values higher than 110 °[98]. As shown in Figure 4.1, the lysine residues provided the sites for conjugation when GL13K peptides were immobilized using silane chemistry. Lysines are positively charged and hydrophilic amino acids and are in the GL13K peptide sequence. Their tendency to react with the negatively charged chlorine end groups of the silane molecules locates the lysine residues near the titanium surface, and thus, the hydrophobic residues are exposed at the solid-air interface. As a result, a highly hydrophobic GL13K-coated surface was obtained[90, 164]. However, in this study (see Fig. 4.2), the cysteine is located at the N-terminus of the peptides, which enables their site-specific conjugation and therefore provides a less spatially restricted positioning of their hydrophilic lysine residues. CD analysis of tethered Cys-GL13K and Cys-GL13K-R1 peptides revealed the presence of both α-helix and β-sheet conformations. GL13K tethered through silane chemistry displayed a predominant β-sheet conformation, which results in a highly hydrophobic surface[176]. The low proportion of β-sheet structure may also contribute to the Cys-GL13K coating being less hydrophobic than the coatings with GL13K peptides in our previous work.

Cys-GL13K peptides tethered on eTi surfaces exerted strong antimicrobial effects (as assessed by the MIC tests) against *S. mutans*, *S. gordonii* and *E. faecalis*, despite their low activity in solution. GL13K is a small peptide with only 13 amino acids. A minor change to the peptide structure (sequence, residues, charges, etc.) may have significant effects on its bioactivity. As shown from the CD analysis, the addition of cysteine resulted in notable changes in the peptide conformation in solution. Compared to GL13K, Cys-GL13K peptides showed a higher proportion of β-sheet conformation at pH 7.4 and a higher proportion of α-helix conformation when the pH increased to result in alkaline conditions. Some AMPs such as LL-37 have antimicrobial activity that depends on them achieving an α-helix configuration[177, 178], but GL13K is effective in a β-sheet configuration, according to its interactions with and potential disruption of model bacteria membranes[164]. The limited proportion of β-sheets in Cys-GL13K peptides in solution might contribute to their low antimicrobial activity.

Conversely, the significant antimicrobial effect of immobilized Cys-GL13K demonstrated that the tethered peptides do not retain the properties of their soluble analogs. The limited mobility and specific arrangement of the immobilized GL13K peptides compared with the solubilized peptides might notably contribute to the different effectiveness against the strains of bacteria investigated here. Chen et al. found that GL13K peptides immobilized on solid surfaces through silane chemistry retained a β-sheet conformation, which might assist bacterial membrane disruption[176]. However, tethered Cys-GL13K showed both α-helix and β-sheet structures (Fig. 4.3D). Its antimicrobial effect suggests that the β-sheet conformation is not the only key determinant of its biofunction. Peptide sequence, net charge, and hydrophobicity/amphipathicity supplement the secondary conformation as

specific properties that determine the antimicrobial effects of peptides[167, 179]. In addition to these properties, the antimicrobial effects of tethered peptides can be influenced by the bioconjugation site, the linker, the spacer and the sequences of the free ends of peptides[97]. Placing cationic residues near the linker as well as placing hydrophobic residues close to the N-terminus enhances the antimicrobial effect of tethered AMPs[97]. In our study, most of the cationic lysine residues in the immobilized peptides are close to the linker site, and hydrophobic glycine and leucine residues are proximal to the N-terminus. Thus, tethered Cys-GL13K peptides can adopt an optimal configuration when interacting with bacteria and therefore exert antimicrobial effects.

The tethered Cys-GL13K peptide showed direct bactericidal ability against *S. mutans* and *S. gordonii*, as shown in the viability studies. In another preliminary study, we compared the antimicrobial ability of GL13K tethered using silane chemistry and that of Cys-GL13K tethered using the thiol-maleimide coupling technique against *S. mutans* (unpublished data). Both tethered peptides led to significantly fewer bacterial CFUs after overnight culture than eTi and silanized eTi groups. No significant difference between antimicrobial ability of the two tethered peptides was observed (unpublished data). For antimicrobial tests against *S. gordonii*, Chen et al. reported an approximately 93% reduction in bacteria on GL13K peptides tethered using silane chemistry (Fig. 4.10A)[176]. In this study, we obtained an approximately 82% reduction in *S. gordonii* on the Cys-GL13K-coated surface (Fig. 4.10B), which is slightly lower than that of the aforementioned study. However, both the immobilized GL13K and Cys-GL13K exerted similar antimicrobial effects as the positive control chitosan in two studies, indicating the promising antimicrobial ability of the tethered Cys-GL13K. The difference between GL13K and Cys-GL13K coatings might

be attributed to their properties as well as the individual operational differences in the experiment. Direct comparison of two peptide coatings should be performed to determine their efficiency. Based on their similarities in killing *S. mutans*, it is highly possible that tethered GL13K and Cys-GL13K use two different methods to show similar antimicrobial effects against *S. gordonii*. These data demonstrated that the thiol-maleimide coupling technique enabled tethered Cys-GL13K to retain the antimicrobial ability of the GL13K peptide. With its advantages of site-specific conjugation, few side-effects and wide application, the thiol-maleimide coupling technique provides an even more attractive approach than silane chemistry for applying antimicrobial peptides to the modification of dental devices and scaffolds, as reported previously.
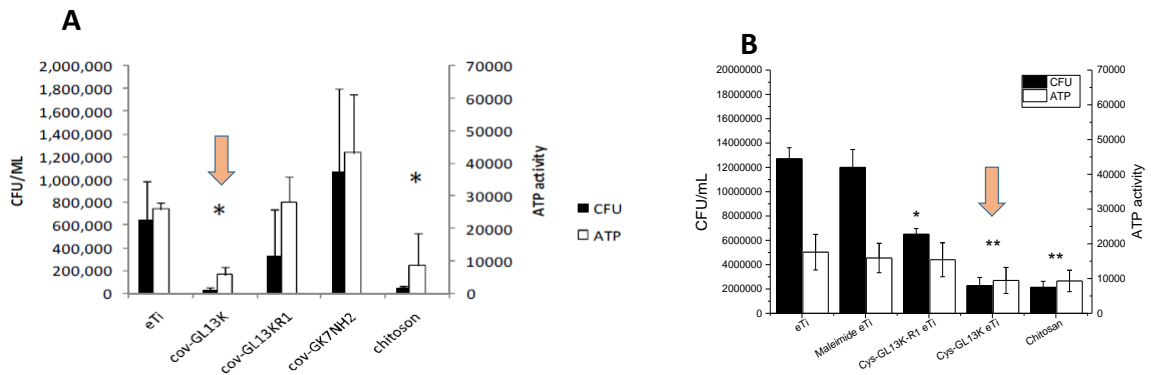
Figure 4.10 **Comparison of the antimicrobial ability of tethered GL13K and Cys-GL13K peptides against *S. gordonii***. A: CFUs and ATP activity of *S. gordonii* on GL13K tethered using silane chemistry in a study of Chen et al.[176]. **B**: CFUs and ATP activity of *S. gordonii* on surfaces coated with Cys-GL13K using thiol-maleimide coupling in this study. Note: Arrows indicate the groups with peptide coating.

However, compared with their direct bactericidal effect against *S. mutans* and *S. gordonii*, both Cys-GL13K and Cys-GL13K-R1 coatings exerted inhibitory effects on the biofilm formation of *E. faecalis* in addition to bactericidal ability. Instead of direct interactions with the bacterial membrane to cause bacterial disruption, tethered AMPs may create an unfavorable surface for bacterial colonization or interrupt some key steps in the biofilm formation of *E. faecalis* such as the production of peptidoglycan, gelatinase and determinant species[181]. It is likely that tethered Cys-GL13K acts similarly to some antibiotics in inhibiting the synthesis of peptidoglycan, a critical component for cell wall and biofilm formation. The peptides have good affinity for the cells and might inhibit the further incorporation of some peptides such as the MurNAc-pentapeptide into the cell wall[182]. This change can impact the communication between different bacteria, weaken the cell wall and therefore inhibit the establishment of mature biofilms. However, little is known about the detailed mechanism, and further investigation is required to understand the differences in antimicrobial abilities against various bacterial species. *E. faecalis* is the critical pathogen related to root canal infection and is found in 30-90% of endodontically treated canals[183]. It is a tough bacterium that can survive in extreme conditions and is resistant to most antimicrobial agents[180], frustrating endodontic therapy. To date, antimicrobial ability of tethered GL13K against *E. faecalis* has not been reported. We observed the inhibitory effect of immobilized Cys-GL13K on *E. faecalis* for the first time. This result will bring new insight into the control of endodontic infection and the application of biomaterials in root canals.

Cys-GL13K coatings were cytocompatible with hDPSCs. Cell proliferation successfully progressed on the surfaces with immobilized peptides at the same rates as noncoated

titanium surfaces. These results prove the specific biofunctional bactericidal effects of the peptide coatings against nonmammalian cells and opens the potential application of this method to obtaining effective antimicrobial biomedical implants, devices, and scaffolds.

4.5 Conclusion

We presented a reliable bioconjugation method to homogeneously functionalize a titanium surface with antimicrobial Cys-GL13K peptides using thiol-maleimide coupling. The tethered Cys-GL13K peptide was mechanically stable, cytocompatible with hDPSCs and strongly antimicrobial against the common oral bacteria *S. mutans, S. gordonii* and *E. faecalis,* which are associated with pathological infections in the mouth. The Cys-GL13K coating was bactericidal against *S. mutans* and *S. gordonii* and showed an inhibitory effect on the biofilm formation of *E. faecalis*.

Chapter 5: Functionalization of st-ELR Matrix with the Cys-GL13K Antimicrobial Peptide

Abstract

Bacterial infection of implanted biomaterials is a major cause for the *in vivo* failure of prosthetics in contact with living tissues. The present study aimed to functionalize a dental scaffold with antimicrobial ability for dentin regeneration. Elastin-like recombinamers that contained a statherin-derived peptide (st-ELR) were electrospun to obtain a nanofibrous scaffold or coated on titanium surfaces. Cys-GL13K, an analog of the antimicrobial peptide GL13K, was conjugated on both electrospun st-ELR fibers and immobilized st-ELR films using thiol-maleimide coupling. Properties of modified st-ELR matrices, their antimicrobial ability against *S. mutans* and *S. gordonii* and their cytocompatibility with human dental pulp stem cells (hDPSCs) were analyzed using a series of surface characterization techniques and in vitro biological techniques. Modification of Cys-GL13K on crosslinked st-ELR fibrous scaffolds did not show significant inhibitory effects on bacterial growth. For immobilized st-ELR films on titanium surfaces, XPS, water contact angles, circular dichroism and visualization of fluorescent-labeled peptides before and after mechanical challenge revealed that Cys-GL13K peptides were covalently conjugated to the st-ELR film. Modification of Cys-GL13K and its randomized version, Cys-GL13K-R1, on st-ELR film led to significant reduction of bacterial colony-forming units and ATP activity for both *S. mutans* and *S. gordonii*. Furthermore, antimicrobial peptide-functionalized st-ELR films were cytocompatible with hDPSCs. Thus, Cys-GL13K functionalization offers st-ELR matrices good antimicrobial properties for preventing potential oral bacterial infection and excellent cellular interactions for their potential applications in dental tissue regeneration.

5.1 Introduction

Tissue engineering has attracted high interest in dentistry with the aim of regenerating lost dental tissues, such as pulp-dentin complex[184, 185], periodontal ligament[186] and alveolar bone[187]. In the field of regenerative endodontics, an approach to restore dentin and pulp tissues is to use the remaining dental pulp in combination with a biocompatible scaffold as the pulp capping biomaterial after pulptomy in partial pulpitis cases[21]. However, the long-term prognosis of tissue regeneration is not always predictable. A serious problem is postoperative infection, which has been considered a critical problem for causing the failure of biomedical devices or scaffolds in contact with tissues [76, 188]. Although the control of sterility during operation and antibiotic prophylaxis have been well standardized in the clinic, the implanted materials are still prone to bacterial infection as the oral cavity is inhabited by an abundant, highly diverse microflora[78]. The infection of implanted scaffolds is mediated by contamination during the procedure, remaining bacteria in the root canal and dentin tubules or invading bacteria from the outside oral flora. It is extremely difficult to treat the infection within the pulp cavity, especially for the established biofilm[189]. Failure of regenerative therapy due to reinfection results in the need for complex revision therapy and eventual root canal therapy in most cases. Therefore, preventing and treating bacterial infection associated with implanted scaffolds to facilitate their long-term clinical success is strongly needed.

Many efforts have been made to prevent the incidence of infection for implanted scaffolds[189]. In addition to the systemic administration of antibiotics, a common method is to supplement commercial antibiotics within the scaffold matrix and allow the scaffold to serve as a local drug delivery system to gradually release antibiotics[190]. Commercial

antibiotics, such as doxycycline, vancomycin and silver particles, have been blended into scaffolds, but limited effects have been achieved [191-194]. However, the rapid emergence of antibiotic-resistant bacteria, potential host-tissue damage, and short life-duration of drugs limit the use of many antibiotics, driving researchers to search for effective alternative antimicrobial strategies to improve performance of implanted biomaterials.

Antimicrobial peptides (AMPs), a family of small cationic, amphiphilic peptides secreted by most native tissues, possess active antimicrobial effects against a wide range of microbiomes while showing lower bacterial resistance and cytotoxicity when compared to commercial antibiotics[90, 195]. AMPs play a critical role in the human immune system[196] by fighting bacterial infection though bacterial membrane depolarization and disruption[91, 179]. GL13K is a short AMP derived from the parotid secretory protein. GL13K is active against many different oral bacteria, such as *S. mutans, S. gordonii* [98], and Lactobacillis. In addition, once tethered to solid surfaces using silane chemistry, the GL13K peptide retains strong antimicrobial ability toward *S. mutans, S. gordonii* [98] and P. gingivalis [99], indicating its potential application in the functionalization of dental implants for preventing peri-implantitis. However, the GL13K immobilization technique used in the above studies cannot be used for functionalizing GL13K on polymeric scaffolds, which limits its further application in tissue regeneration. Previously, we modified GL13K by adding a cysteine in its N-terminus (Cys-GL13K) and then tethered Cys-GL13K peptides to titanium surfaces using thiol-maleimide coupling (Chapter 4). A homogenous coating of peptides was achieved in addition to a strong antibacterial ability against *S. mutans, S. gordonii* and *E. faecalis*. This technique ensured that all the positively charged

lysine residues on the peptides were available for peptide-bacteria interactions and enabled further functionalization of peptides on different surfaces and biomaterials.

Functionalization of dental scaffolds with antimicrobial ability provides a promising approach for preventing potential infection of the pulp cavity. In Chapters 2 and 3, we presented an elastin-like recombinamer containing a statherin-derived peptide (st-ELR) with potential to enhance the regenerative functionality of dentin by mimicking mineralization of type I collagen (Chapter 2) and facilitating appropriate responses of dental pulp stem cells (Chapter 3). This tri-block copolymer has good biocompatibility and a similar biodegradation rate to natural elastin, is easy to fabricate and induces intrafibrous mineralization [60](Chapter 2). These properties make st-ELR an excellent scaffold for replacement and/or regeneration of the dentin matrix. The present study aimed to modify the st-ELR polymeric scaffold with the Cys-GL13K antimicrobial peptide using thiol-maleimide coupling to prevent oral bacterial growth. The hypothesis that the st-ELR matrix functionalized with antimicrobial peptides inhibits bacterial growth and is cytocompatible was tested. Here, this study reported the method for conjugating peptides to the polymer and analysis of the antibacterial effect of the modified polymer on two oral pathogens, namely, *S. mutans* and *S. gordonii*, as well as its cytocompatibility with hDPSCs.

5.2 Materials and Methods

5.2.1 Part I: Antimicrobial functionalization of st-ELR fibrous scaffold

5.2.1.1: Fabrication of st-ELR fibrous scaffold

Fabrication of electrospun st-ELR fibers on 9 mm titanium disc surfaces was presented in Chapter 2. Schematics of fiber cross-linking and antimicrobial peptide bioconjugation are

shown in Figure 5.1. Crosslinking of st-ELR molecules was performed to improve stability of the fibrous scaffolds. Samples were immersed in a mixture of hexamethylene diisocyanate (HMDI; Sigma-Aldrich):acetone (1:9 ratio) for 6, 12 and 16 hr in three experiments. The samples were thoroughly washed using acetone and distilled water, and they were then lyophilized. Sulfosuccinimidyl 4-(N-maleimidomethyl) cyclohexane-1-carboxylate (Sulfo-SMCC; ThermoFisher Scientific) was prepared in sodium phosphate buffer (SBS, pH 7.2) at a concentration of 0.5 mg/mL. Cross-linked st-ELR fibrous scaffolds were placed in freshly prepared sulfo-SMCC solution for 2 hr at room temperature (RT) while gently shaking. The objective of this step was to modify the remaining free amines on st-ELR fibers with maleimide moieties. Cys-GL13K peptide [sequence: CGKIIKKLKASLKLL-CO(NH2), purchased from Apeptide (Shanghai, China)] was dissolved in 2.9 mg/mL Tris (2-carboxyethyl) phosphine (TECP; pH 7.0, Thermo Fisher Scientific) the night before at a concentration of 10 mg/mL. Five samples of maleimide-modified st-ELR scaffolds were placed in a round tissue culture plate (diameter of 5 cm) followed by addition of 3 mL of SBS (pH 7.2) and 30 μL of Cys-GL13K stock solution. After 2 hr of reaction, all samples were washed with SBS in an ultrasonic bath for 5 min to remove any unreacted peptides. Samples were lyophilized and stored at 4 ℃ before antimicrobial assessment.
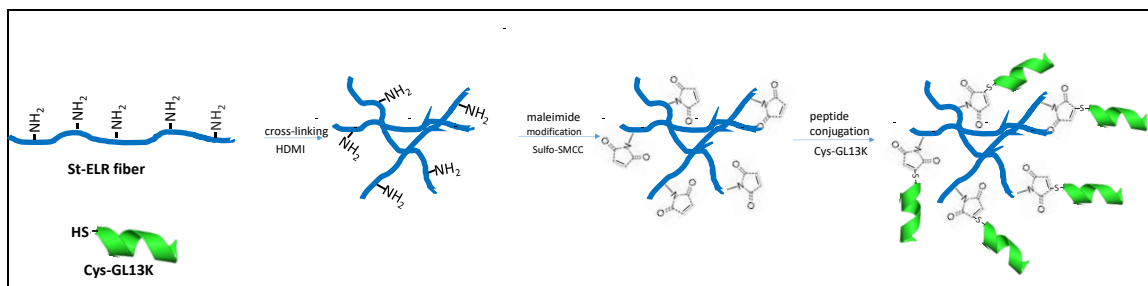
Figure 5.1 **Schematics of crosslinking st-ELR electrospun fibers and modification with Cys-GL13K.**

5.2.1.2 Antimicrobial test against *S. mutans* and *S. gordonii*

Bacteria culture

The following four groups of samples were subjected to antimicrobial tests: eTi, cross-linked st-ELR fibers (st-ELR), maleimide-modified st-ELR fibers (st-ELR+Maleimide), and Cys-GL13K-conjugated st-ELR fibers (st-ELR+Cys) (N=4 per group). All the samples were loaded in a 24 well plate, soaked with 70% ethanol for 40 min, and disinfected under UV light for 20 min. Two bacteria strains, namely, *S. mutans* (ATCC 700610) and *S. gordonii* (ML-5), were inoculated overnight using BHI and THB media, respectively. The inoculums were diluted 100 times before being used. BHI or THB media (1 mL) was added to each well followed by the addition of 20 μL of diluted bacterial inoculums. The plates were incubated in an anaerobic chamber for 24 hr. Experiments were performed in triplicate.

CFU and ATP assay

Colony-forming units (CFUs) were used to evaluate bacterial growth and metabolic activity. After overnight culture, samples were gently rinsed with 0.9% sterile NaCl solution. Samples were then transferred into 10 mL centrifuge tubes, which contained 1 mL of NaCl solution, and subjected to sonication for 10 min to detach the biofilm from the sample surfaces. A series of 10 to 10,000-fold dilutions were made using 0.9% NaCl solution. Each diluted solution (10 μL) was plated on Mitis-salivarius sucrose bacitracin (MSSB) agar plates and Todd–Hewitt broth (THB) agar plates for *S. mutans* and *S. gordonii*, respectively. Plates were incubated in an anaerobic chamber for 48 hr, and the colonies formed on each of the agar plates were counted. For the ATP assay, 100 μL of undiluted bacteria solution was added into a solid white 96 well plate (Coning 3789, Fisher Scientific) followed by the addition of 100 μL of ATP assay reagent (BacTiter-Glo Microbial Cell Viability kit, Promega, Madison, WI, USA). After 15 min of incubation at RT, the bioluminescence of each sample was analyzed using a microplate luminometer (BioTek, Winooski, VT, USA).

5.2.2 Part II：Functionalization of uncrosslinked st-ELR film with Cys-GL13K

5.2.2.1: Immobilization of st-ELR molecules on Ti surface

The st-ELR electrospun fibers were crosslinked using HMDI. However, the cross-linker consumes the lysine residues of st-ELR, which may result in a low concentration of free amino acids for further modification with Cys-GL13K peptides. To avoid the influence of the cross-linker and to maximize the available lysine residues, a layer of st-ELR molecules was coated on a titanium surface, which modified the membrane with Cys-GL13K without the involvement of any cross-linkers.

Covalent bonding of st-ELR membranes on titanium surfaces was achieved following a previously described protocol[125] (Fig. 5.2). Briefly, Ti discs (9 mm diameter) were polished and cleaned using distilled water and acetone, and they were then dried under N_2 gas. Discs were subjected to etching using a 5 M NaOH solution at 60 ℃ overnight to activate the surface. A silanization solution consisting of 13.6% (3-chloropropyl)triethoxysilane (CPTES; Sigma), 6.8% DIEA (Sigma) and 79.5% pentane (Sigma) was used to silanize the etched Ti surface in a N_2 environment for 1 hr at room temperature. Specimens were subsequently cleaned three times using ethanol, isopropanol, deionized water, and acetone. After being dried under N_2 gas, samples were immersed in st-ELR solution (1 mg/mL in sodium carbonate buffer, pH 9.5) and gently shaken overnight to covalently immobilize st-ELR molecules on Ti surfaces. Samples were then washed thoroughly with brief sonication.

5.2.2.2 Modification of st-ELR molecules with Cys-GL13K peptides

St-ELR-coated Ti samples were immersed in freshly prepared Sulfo-SMCC solution (0.5 mg/mL in SBS, pH 7.2) for at least 30 min at room temperature. As shown in Figure 5.2, sulfo-SMCC reacted with free amines in the lysine residues of st-ELR molecules and linked the maleimide moieties to the polymer backbone. After maleimide modification, all samples were washed thoroughly using SBS and then placed in a tissue culture plate followed by the addition of 5 mL of sodium phosphate buffer (pH 7.4). Reduced Cys-GL13K stock solution (40 μL; 10 mg/mL) was added into the plate. Thiols on cysteine residues specifically bound to the maleimide moieties of the st-ELR membrane and led to the covalent conjugation of Cys-GL13K [CGKIIKKLKASLKLL-CO(NH2)] to the

polymer backbone. After 2 hr of reaction at room temperature, samples were washed, dried under N$_2$, and stored at 4 ℃ before being processed. Cys-GL13K-R1 (CIGIKLLKSKLKAL-CO(NH2)), a randomized sequence of Cys-GL13K used as a control peptide, was conjugated to st-ELR membranes on Ti surfaces following the same methods described before.
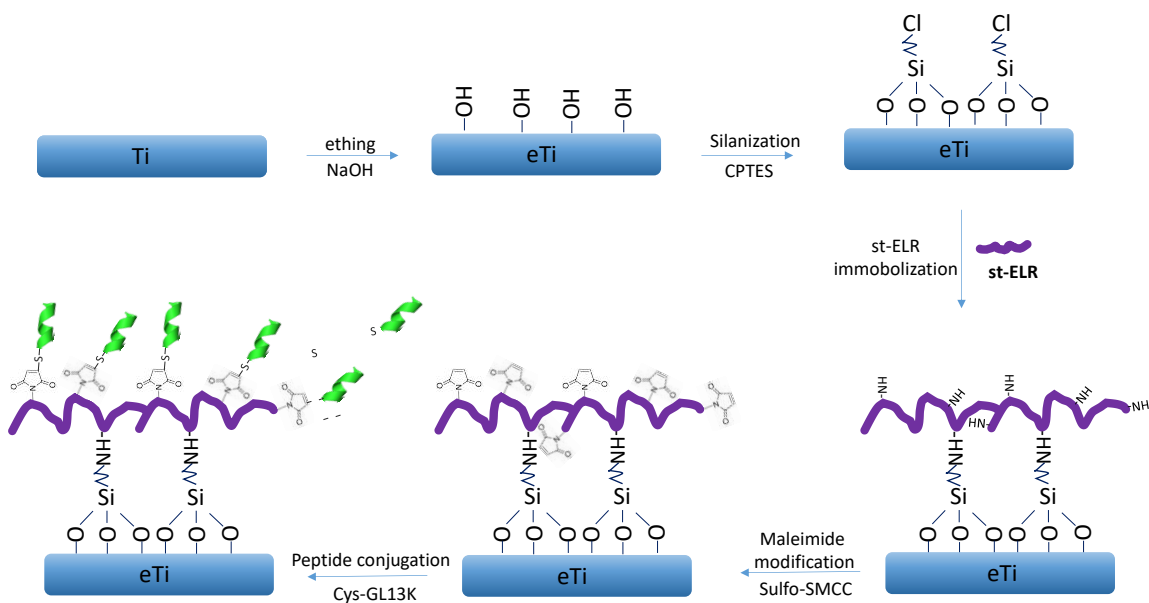
Figure 5.2 **Schematics of st-ELR immobilization on Ti surfaces and bioconjugation of Cys-GL13K to st-ELR membranes**.

5.2.2.3 Surface characterization

XPS analysis

X-ray photoelectron spectroscopy (XPS; SSX-100, Al Kα X-ray, 1 mm spot size, 35 °take-off angle) was used to analyze the elemental chemical composition of the sample surfaces.

All samples were thoroughly cleaned with distilled water and acetone followed by drying under N_2 gas before being subjected to XPS analysis. Survey scans of etched Ti, st-ELR-coated eTi, maleimide-modified st-ELR membrane and Cys-GL13K-conjugated st-ELR membrane were taken at 1 eV step-size with a binding energy ranging between 0 and 1000 EV. Four scans were performed for each sample. XPS spectra were analyzed using ESCA 2005 software.

Water contact angles

Dynamic water contact angles were measured (DM-CE1, Kyowa Interface Science, Japan), and image analysis software (FAMAS, Kyowa Interface Science, Japan) was used to determine changes in wettability as a result of the different molecules attached to them. Samples were washed and dried in the desiccator overnight before measurement. Sessile drops of distilled water (2 μL in volume) were deposited on the tested surfaces, and the contact angles were recorded every other second for 40 s.

Fluorescent-labeled peptide visualization

Fluorescent peptides were prepared as described in Chapter 4. Peptide solution (30 μL; 10 mg/mL) was added to two small plates that contained 3 mL of SBS buffer. Maleimide-modified and unmodified (negative control) st-ELR membranes were separately placed into one of the plates. Visualization of the fluorescent signal of the membranes was performed using a fluorescence microscope (Eclipse E800, Nikon, Tokyo, Japan) after the initial rinse and after 5 and 30 min of sonication in water.

5.2.2.4 Antimicrobial test against *S. mutans* and *S. gordonii*

The following five groups of samples were subjected to antimicrobial tests: eTi, eTi with st-ELR coating (st-ELR), maleimide-modified st-ELR membrane (st-ELR+Maleimide), Cys-GL13K-R1-conjugated st-ELR membrane (st-ELR+Cys-R1), and Cys-GL13K-conjugated st-ELR membrane (st-ELR+Cys) (N=4 per group). All samples were placed in 24 well plates. Disinfection of samples and bacteria seeding were conducted following the methodology described in section 5.2.1.2.

After overnight culture, CFU, live/dead, and ATP assays were performed to evaluate bacterial growth and metabolic activity. The CFU and ATP assays described in paragraph 5.1.2 (Part I study) were adapted. For the live/dead assay, bacterial viability was analyzed using a BacLight Bacterial Viability Kit (Invitrogen, Grand Island, NY, USA). Briefly, the biofilms on tested samples were gently rinsed three times with 0.9% sterile NaCl solution followed by fluorescent staining using the live/dead dyes at RT (30 μL of green and red dyes in 1 mL of sterile H$_2$O). After 20 min of incubation, biofilms were rinsed gently and immediately visualized by fluorescence microscopy.

5.2.2.4 Cytotoxicity test

Human dental pulp stem cells were seeded on eTi, unmodified st-ELR membrane, maleimide-modified st-ELR membrane, and Cys-GL13K-R1-modified st-ELR membrane and Cys-GL13K-modified st-ELR membrane at a density of 5000 cells/well in 24 well plates. The cell proliferation test was performed as described in Chapter 4.

5.2.2.5 Statistical analysis

All experiments were conducted in triplicate with four samples in each group. Statistically significant differences between groups (p-value<0.05) for CFU, ATP activity, and stem

cell proliferation were analyzed using one-way ANOVA with Tukey's multiple comparison post hoc test.

5.3 Results

5.3.1 Part I: Antimicrobial activity of st-ELR fibrous scaffold functionalized with Cys-GL13K peptides

The CFU and ATP activity results for *S. mutans* and *S. gordonii* on the different st-ELR fibrous scaffolds are presented in Figure 5.3. The cross-linked, maleimide-modified, and Cys-GL13K-functionalized st-ELR fibrous scaffolds did not show statistically significant differences in CFU (Fig. 5.3A & C) and ATP activity (Fig. 5.3B & D) for both *S. mutans* and *S. gordonii* (p-value>0.05). Antimicrobial tests of the crosslinked st-ELR scaffolds with different crosslinking time periods (6, 12, and 16 hr) were conducted, and no statistically differences were observed among the groups.
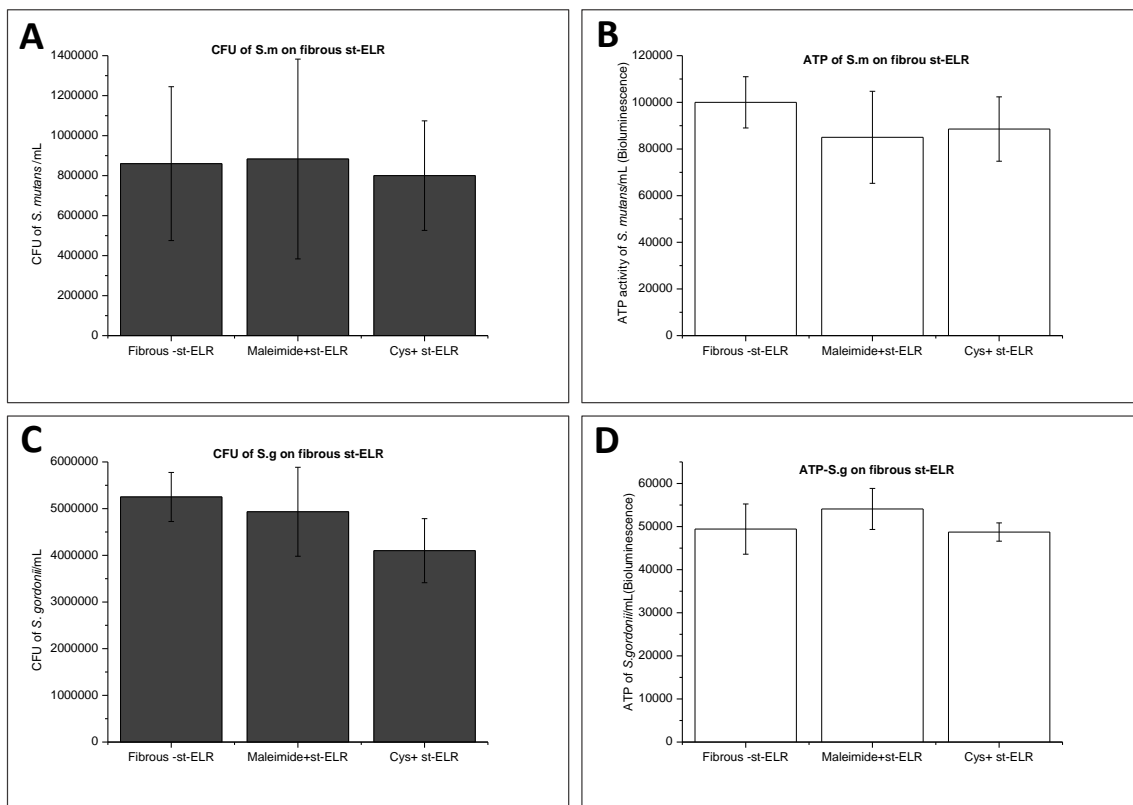
Figure 5.3 **CFU and ATP assay for *S. mutans* (A & B) and *S. gordonii* (C & D) on fibrous st-ELR scaffolds with different treatments.** The scaffolds were crosslinked for 12 hr.

5.3.2 Part II: Functionalization of uncrosslinked st-ELR film with Cys-GL13K

5.3.2.1: XPS

Figure 5.4 shows the XPS spectra of the surfaces at different steps of the manufacturing process. The etched Ti surface showed intense peaks of Ti 2p and O1s. When st-ELR molecules were immobilized on the eTi surface, spectra exhibited strong signals of N1s and C1s as well as decreased signals of Ti 2p and O 1s. Physical absorbed st-ELR

molecules on eTi surface were vastly removed after being washed and sonicated using washing buffer. The N1s and C1s signals on the spectra indicated the presence of covalently bound st-ELR molecules on the titanium surfaces. When st-ELR membranes were treated with Sulfo-SMCC, the free amines on the lysine residues of st-ELR were consumed in the reaction, resulting in a decrease of C1s and O1s signals on the spectrum for the maleimide-modified st-ELR surface. Re-emergence of strong peaks of C1s and O1s was observed after Cys-GL13K functionalization. This high intensity of C1s and O1s signals can be attributed to the abundant additional amino acids present after the Cys-GL13K peptides were successfully conjugated to the st-ELR membrane.
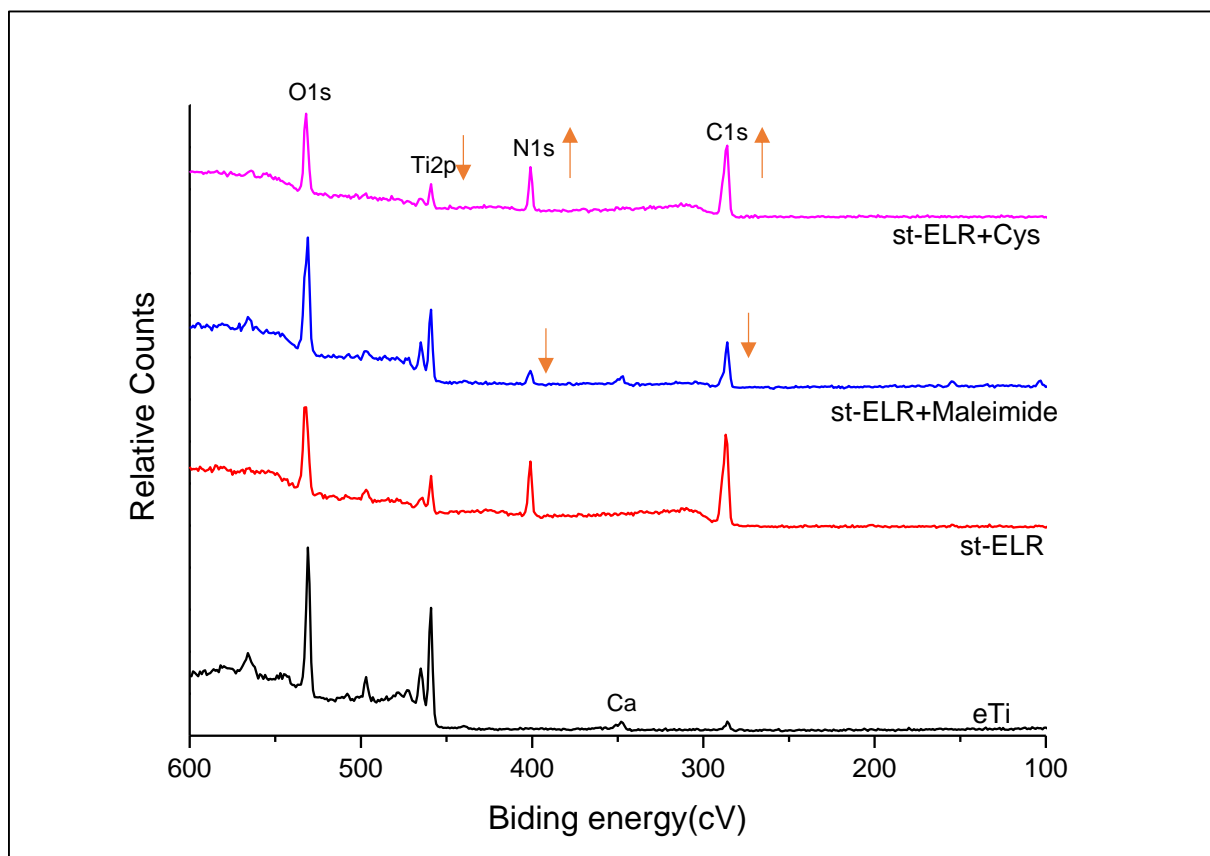
Figure 5.4 **XPS spectra of eTi surface after the different steps of surface and molecular modifications.** st-ELR immobilization showed significant increases in N1s and C1s peaks. These two peaks decreased when the membrane was modified with maleimide. After Cys-GL13K conjugation, markedly increased N1s and C1s peaks were observed. **Note:** arrows indicate the change of N1s and C1s intensities after different steps of modification.

5.3.2.2 Dynamic water contact angles

Surface properties participate in the regulation of many matrix-cell interactions. In the study, wettability of the functionalized surfaces was analyzed via dynamic contact angle analysis. As shown in Figure 5.5, the eTi surface exhibited high hydrophilicity by showing constant low water contact angles (<10 °). After subsequent st-ELR coating and peptide modification, initial water contact angles were greater than 100 °. The contact angle decreased gradually with time and reached a stable value after approximately 20 s. The final stable contact angles for the st-ELR membrane were near 30 °. Modification with maleimide decreased the hydrophilicity of the st-ELR membrane and increased the contact angle up to 90 °. The conjugation of st-ELR membranes with Cys-GL13K and Cys-GL13K-R1 resulted in final values at approximately 50 ° and 70 ° after 40 s, respectively, with hydrophobicity between maleimide-modified surfaces and nonmodified st-ELR membranes.
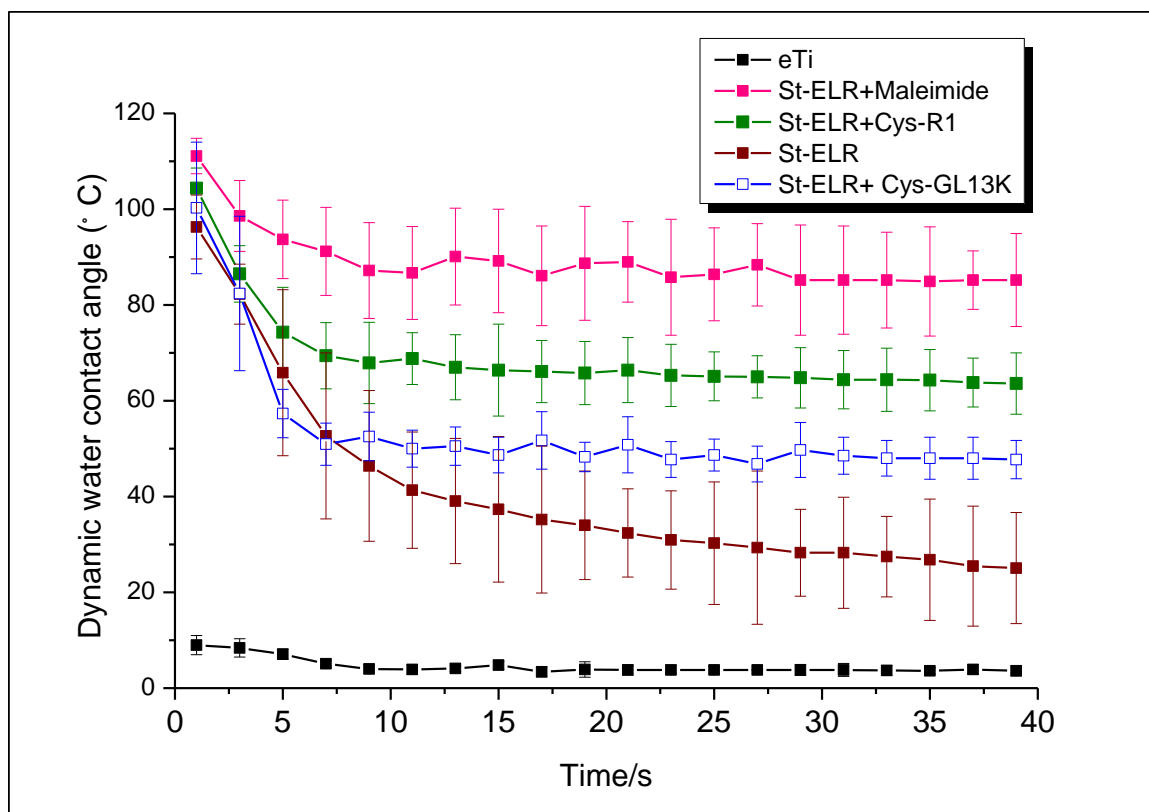
Figure 5.5 **Dynamic water contact angle analysis after different steps of modification.**
The etched surface showed high hydrophilicity ($<10°$). Surfaces with tethered st-ELRs showed a continuous and notable drop in values of water contact angle over time. The final contact angles of st-ELR, maleimide-modified st-ELR, Cys-GL13K-R1-modified st-ELR, and Cys-GL13K-modified st-ELR membranes after 40 s were approximately 30 °C, 90 °C, 70 °C, and 50 °C, respectively.

3.2.3 Visualization of Fluorescent-labeled peptides on modified ELR membranes

118

Visualization of membranes with conjugated fluorescent-labeled thiol-modified peptides confirmed their homogeneous and stable conjugation to st-ELR molecules. As shown in Figure 5.6, both the experimental and negative control groups exhibited strong fluorescent signals after rinsing. However, after sonication for 5 and 30 min, most of the physically absorbed peptides on the control surfaces were removed, while significant signal and amount of peptide molecules remained high and homogeneous on the maleimide-treated ELR membranes.
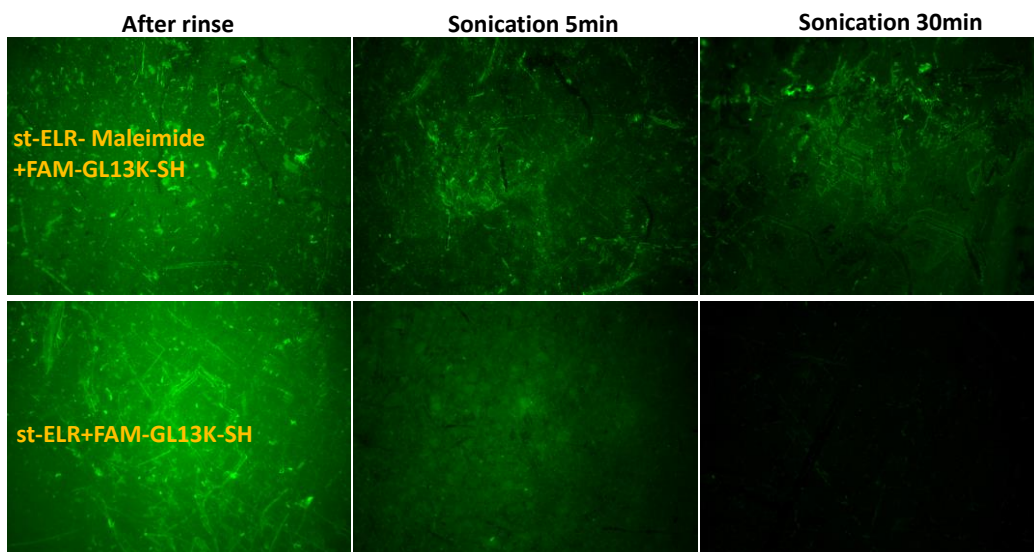
Figure 5.6 **Fluorescence signal analysis.** 1st row: Experimental group; 2nd row: Control group. FAM-GL13K-SH peptides were physically absorbed on st-ELR membrane. After rinsing, strong fluorescence signals were retained on both groups. Surfaces with ELR films conjugated with thiol-modified GL13K peptides (experimental group) showed a homogenous distribution of fluorescence signal, which was retained on the surface after sonication for 5 and 30 min in water. In the control group, however, most of the

fluorescence signal and therefore, the ELR molecules were washed away after sonicating for 30 min.

3.2.4: Antimicrobial test

The analysis of antimicrobial activity of the membranes against *S. mutans* is shown in Figure 5.7. Both Cys-GL13K- and Cys-GL13K-R1-modified st-ELR membranes showed a large amount of dead *S. mutans* on the surfaces compared to the etched Ti, st-ELR, and maleimide-treated st-ELR groups (Fig. 5.7A). Consistent with the live/dead results, the CFU analysis indicated that the Cys-GL13K-modified st-ELR group exhibited an approximate 40% reduction of biofilm growth (p-value<0.05; comparison with all control groups, except Cys-Gl13K-R1), while the Cys-GL13K-R1 modification led to 30% reduction of *S. mutans* growth compared to the st-ELR group (Fig. 5.7B). The ATP assay was used to analyze the biofilm metabolic activity, and it demonstrated that both ELR membranes conjugated with Cys-GL13K and Cys-GL13K-R1 provoked a significant reduction in bacterial ATP activity (p-value <0.05) (Fig. 5.7C). It is worth noting that the maleimide-modified st-ELR membranes also showed a significant decrease in ATP activity although there was no reduction in CFU.
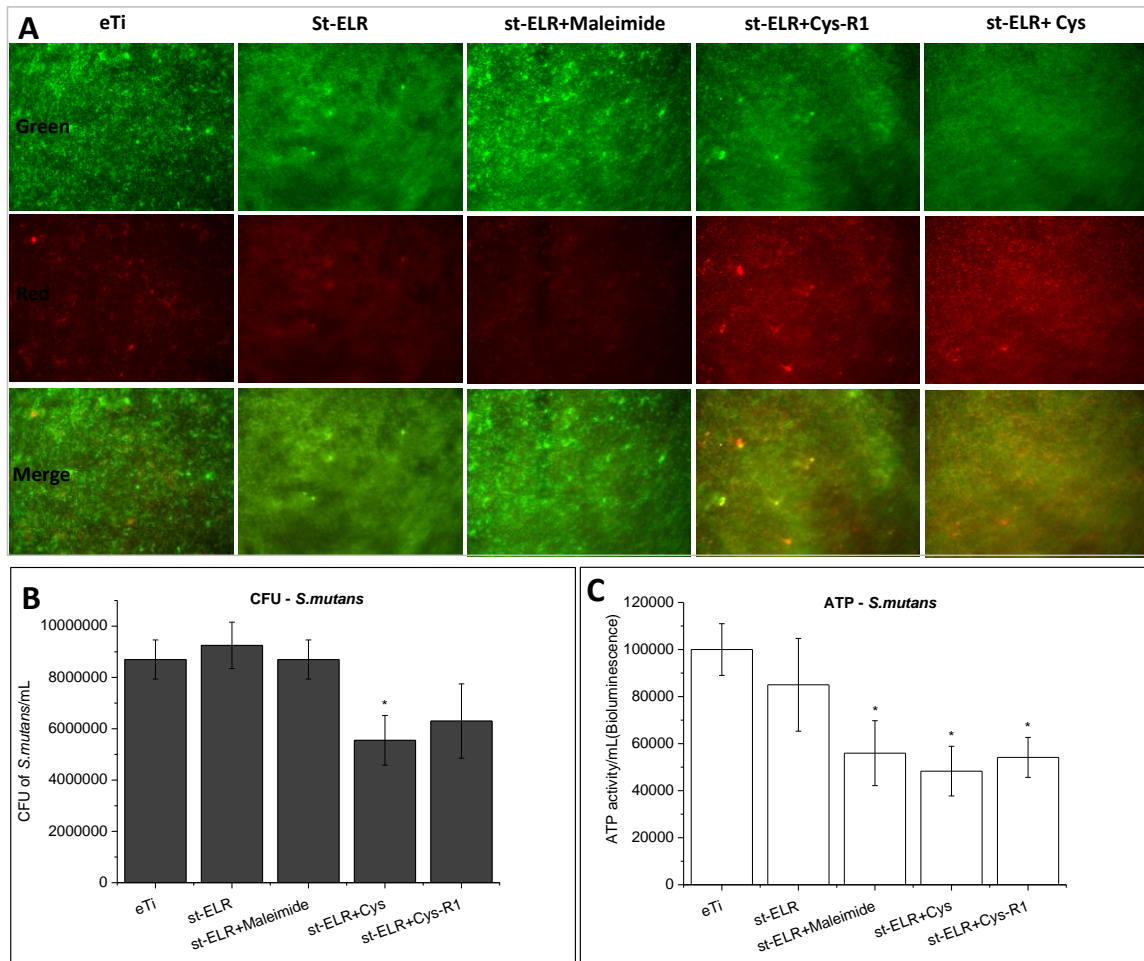
Figure 5.7 **Antimicrobial test of the different surfaces against *S. mutans*. A: Live/dead assay, B: CFU results, C: ATP activity.** Cys-GL13K-modified st-ELR membrane showed significant reduction of *S. mutans* CFU (p-value<0.05). Maleimide-modified st-ELR, Cys-GL13K-R1-modified st-ELR, and Cys-GL13K-modified st-ELR membranes all showed decreased bacterial metabolic activity. In the live/dead assay, large amounts of dead bacteria were found on Cys-GL13K-R1- and Cys-GL13K-modified st-ELR samples. **Note:** Green denotes live bacteria; red denotes dead bacteria.

Antimicrobial tests with *S. gordonii* showed similar results to ones obtained with *S. mutans*. The most notable difference was that the live/dead assay of *S. gordonii* showed bacterial death only on the Cys-GL13K-modified st-ELR surface (Fig. 5.8A). The Cys-GL13K modification also led to a significant decrease of CFU and ATP activity of *S. gordonii* (P-value <0.05) (Fig. 5.8 B & C) with respect to control groups without peptides. The Cys-GL13K-R1-modified st-ELR surface also showed significantly reduced CFU and ATP values with respect to control groups.

The aforementioned data, along with the results obtained with *S. mutans,* demonstrated that the modification of the st-ELR membrane with Cys-GL13K produces a bactericidal conjugated membrane that can prevent the biofilm growth of both *S. mutans* and *S. gordonii*.
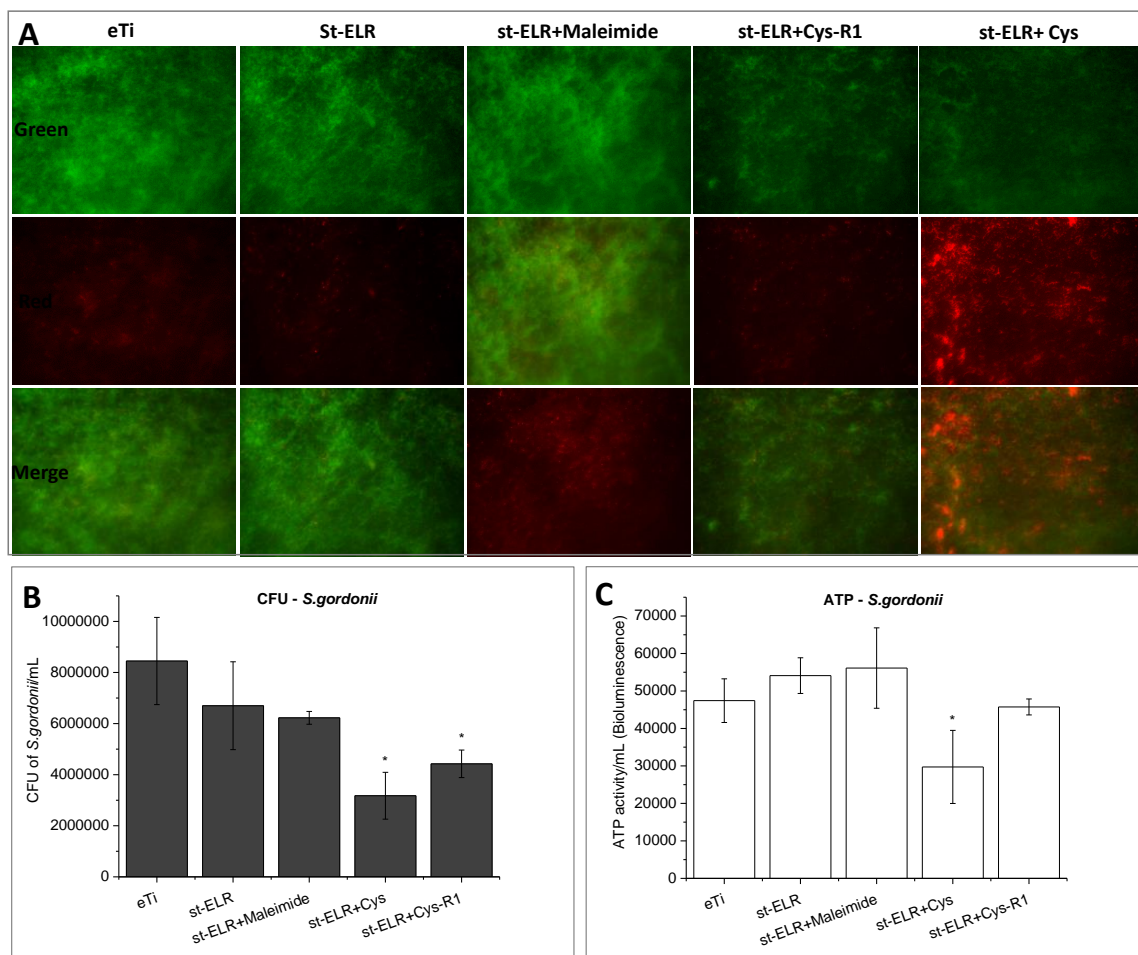
Figure 5.8 **Antimicrobial test of the different surfaces against *S. gordonii*. A: Live/dead assay, B: CFU results, C: ATP activity.** Cys-GL13K-modified st-ELR membrane showed significant reduction of CFU and ATP activity of *S. gordonii* (p-value<0.05). Cys-GL13K-R1-modified st-ELR and Cys-GL13K-modified st-ELR membranes also decreased the ATP activity of *S. gordonii*. In the live/dead assay, a large number of dead bacteria was found on Cys-GL13K-modified st-ELR samples. **Note:** Green denotes live bacteria; red denotes dead bacteria.

3.2.5 Cytocompatibility with hDPSCs

The results of hDPSC proliferation on peptide-modified st-ELR membranes are shown in Figure 5.9. Cell numbers increased gradually over time in all five tested groups. After 1 day of culture, stem cells successfully attached to all surfaces. Between days 1 and 3 of culture, the number of cells increased significantly, and large numbers of cells were observed in all groups after 6 days. No significant differences among groups were observed at any time point, which indicated similar and good cytocompatibility of the peptide-modified st-ELR membranes with or without conjugated peptides.
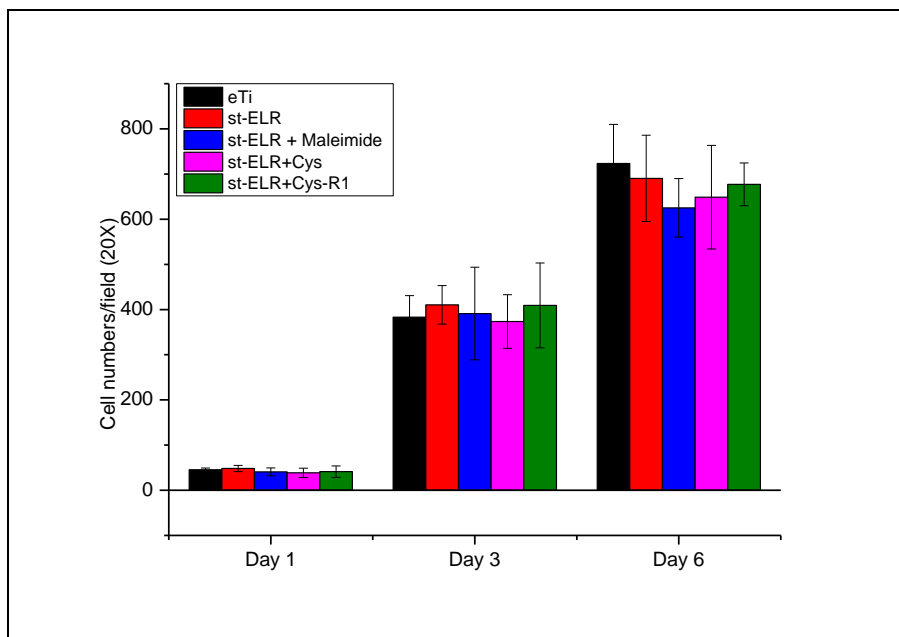
Figure 5.9 **Cell counts of hDPSCs/field on different samples after 1, 3 and 6 days of culture.** Proliferation of stem cells increased gradually overtime, and all groups showed similar cell counts after 1, 3 and 6 days.

5.4 Discussion

In part I of the study, the CFU and ATP analyses suggested that the incorporation of Cys-GL13K peptides on the fibrous st-ELR scaffold does not provide the scaffold with antimicrobial activity against *S. mutans* and *S. gordonii* (Fig. 5.3). Low amounts of conjugated Cys-GL13K peptides on st-ELR scaffolds can be the major cause for their limited antimicrobial effect after functionalization. The final concentration of conjugated Cys-GL13K is determined by the concentration of available lysine residues on the cross-linked st-ELR fibers. In the present study, lysine residues were partially consumed while cross-linking the electrospun st-ELR fibers using HDMI. The remaining free amines reacted to conjugate the Cys-GL13K peptides. Presumably, the cross-linking reaction significantly decreased the available lysine residues, resulting in the low amounts of free amines available for the Cys-GL13K conjugation. The st-ELR fibers were crosslinked for different time periods (6, 12, and 16 hr) in attempt to retain more free amines for the subsequent conjugation. However, no differences among the various groups were observed in antimicrobial ability because the uncrosslinked fibers were dissolved in solution and the stabilized crosslinked fibers failed to provide enough free amines. Further studies should be conducted to investigate the concentration of free amines that are unreacted after cross-linking st-ELR molecules.

In part II of the study, Cys-GL13K peptides were modified on st-ELR membranes. XPS analysis, fluorescence signal test, and dynamic water contact angle analysis confirmed the successful conjugation of peptides on st-ELR (Figs. 5.4 & 5.5). Different values of water contact angles were observed on different surfaces (Fig. 5.5). The following several factors may contribute to the dynamic response of water contact angles on the modified and

unmodified st-ELR membranes: 1) nanoporous structure of st-ELR structure on eTi; 2) rearrangement of st-ELR molecules after immobilization; and 3) physical-chemical properties of maleimide moieties and tethered peptides. The immobilization of st-ELR polypeptide chains resulted in a nanoporous matrix of polymer on the eTi surface. When coated on the eTi surface, st-ELR molecules underwent self-assembly as st-ELR is a thermal sensitive recombinamer that shows temperature driven β spiral conformation. The increase in temperature led to the interaction between the polar and nonpolar residues within st-ELR, which drove the nonpolar segments (VPGIG and VPGAG) to aggregate together, therefore resulting in nanoporous structures[134]. The self-assembly of st-ELR molecules might also contribute to the separation in distribution of hydrophobic and hydrophilic residues in the matrix. As shown in Supplemental Figure 1, 82.5% of the st-ELR molecule secondary structure was a random coil at 4 ℃. When the temperature increased to 37 ℃, the random coil percentage decreased to 52.8%, while the st-ELR β-spiral structural proportion increased to 34.6%. At 50 ℃, approximately 40% of the st-ELR conformation turned into β-spiral. This self-assembly of the molecules in the polymer membrane resulted in an increased exposure of hydrophilic segments of st-ELR on the outer surface of the matrix (Fig. 5B), thereby explaining the continuous decrease of water contact angle of st-ELR membrane over time.

The interaction between the positive-charged lysine residues of st-ELR molecules and the CPTES-modified eTi surface further separated the hydrophilic and hydrophobic segments of st-ELR. The hydrophilic segments (VPGKG) of ELR chains tend to interact with the activated negatively charged eTi surfaces during the immobilization process of st-ELR and are located close to the eTi surface. In contrast, hydrophobic residues (VPGIG and VPGAG)

are then located away from the polar groups of the eTi surfaces and thus close to the outer surface of matrix. When the water droplets contact the outer layer of this porous matrix, they find the hydrophobic residues of the attached molecules, and the initial water contact angle is consequently high. Because the ELRs have many residues free to move, the polymer molecules reconfigure once the water is in contact with them and in the process exposes increasing amounts of hydrophilic residues (VPGKG) at the polymer-water interface until equilibrium is reached. The final contact angle is dependent on the overall proportion of hydrophilic and hydrophobic groups in the st-ELR.

The dynamic water contact angle of the st-ELR membrane was changed by the subsequent modification. Modification of the remaining lysine residues with maleimide caused the increase of surface hydrophobicity. Maleimide moieties have low wettability, which led to an increased final water contact angle on the maleimide-modified membrane (Fig. 5.5). The addition of Cys-GL13K or Cys-GL13K-R1 peptides introduced new hydrophilic amino acids to the coated matrix and consequently, lowered the final contact angle compared to the maleimide-modified membrane (Fig. 5A). The difference in final water contact angles between Cys-GL13K and Cys-GL13K-R1 may be attributed to the specific configuration of each peptide after conjugation. The distinct interactions between the neighboring peptides in each of the two molecules may cause the contact angles to vary.

In the subsequent analysis of antimicrobial ability, the specificity of the sequence in Cys-GL13K to kill and/or prevent attachment of bacteria was compromised when conjugated to the st-ELR polymers compared to this peptide being directly tethered to a solid substrate as demonstrated in Chapter 4. In addition to the concentration of available lysine residues

on st-ELR as discussed previously, a hydrophobic-hydrophilic interaction may exist between the peptides and st-ELR because both of them are amphiphilic biomolecules. The hydrophobic segments of st-ELR might interact with the hydrophobic parts of Cys-GL13K and embed the peptides within the matrix, which may affect the peptide conformation and hinder their subsequent contact with bacteria. Further studies need to be conducted to verify these facts. In the present study, the st-ELR scaffold is expected to be applied in the pulpal cavity where a much lower microbe load is expected in comparison to other oral areas (e.g., periodontal sockets or alveolar sockets) that have direct contact with the oral flora.

In the stem cell cytocompatibility test, all the groups exhibited a similar proliferation level of stem cells after 1, 3 and 6 days of culture (Fig. 5.9). These data indicate that Cys-GL13K-modified st-ELR membrane has good biocompatibility on dental pulp stem cells.

5.5 Conclusion

The st-ELR matrix was successfully functionalized with antimicrobial ability by conjugating Cys-GL13K peptides to the backbone of ELR molecules. A series of surface characterization tests demonstrated that the peptide modification was highly stable and homogenous. Further bacteria and stem cells studies revealed that modification of st-ELR membrane with Cys-GL13K peptides had antimicrobial ability against *S. mutans* and *S. gordonii* while retaining excellent cytocompatibility toward human dental pulp stem cells. The present study provided insight for the development of scaffolds with multiple functionalities. Growth factors, AMPs, and even DNA or mRNA can be functionalized on polymeric scaffolds to improve the scaffold-tissue interaction, vascularization and enervation, which would enable specific and varied therapeutic effects.

Chapter 6: Future Directions

6.1 Improving the stability of electrospun st-ELR scaffold

Although st-ELR undergoes self-assembly at high temperature, the polymer can easily be dissolved in water. To improve the stability of the fibrous scaffold, electrospun st-ELR fibers were crosslinked using HMDI prior to any subsequent treatments, such as mineralization and antimicrobial peptide functionalization. In Chapter 5, Cys-GL13K peptides were conjugated to the crosslinked st-ELR fibrous scaffold but failed to achieve good antimicrobial effects, which may have been due to large amounts of available lysine residues being consumed in the fiber crosslinking, thereby resulting in low concentration of free amines for the subsequent conjugation with Cys-GL13K. Therefore, improving the stability of fibrous st-ELR scaffolds while avoiding the use of crosslinkers that consume lysine residues is needed. Modification of the sequence of the elastin-like recombinamers is an alternative to address this issue. For instance, cysteine residues can be added into the sequence of ELR. Crosslinking of different ELR molecules is induced based on the formation of disulfide linkages between two different cysteines. Such modification could leave all the lysine residues available for further functionalization.

6.2 *In vivo* and/or *Ex vivo* study

The present studies were all conducted *in vitro*. The next step is to move forward to in vivo studies. Studies may be performed *ex vivo* to prove the biomimetic route of mineralization and recovery of functional properties of the affected dentin in extracted teeth. Mineralized st-ELR scaffolds can be placed on top of injury pulp in an animal model (e.g., rat and dog) to investigate their ability to stimulate regeneration of dentin-pulp-like tissue. For the in vivo test of antimicrobial scaffolds, the Cys-GL13K-functionalized st-ELR membrane will be implanted subcutaneously in an animal model. The defect side will be infected with

target oral pathogens, such as *S. mutans* and *E. faecalis*, and the antimicrobial effect will then be analyzed.

6.3 Modify st-ELR scaffolds with multiple bioactive molecules

St-ELR is a polymer with functional groups that can be modified with diverse bioactive molecules. The "thiol-maleimide" coupling technique adapted in the present study is also feasible for the functionalization of polymers and solid surfaces with other functional moieties, which would allow further functionalization of st-ELR with multifunctional molecules in the application of tissue engineering and drug delivery system. For instance, angiogenic factors such as vascular endothelial growth factor (VEGF) can be conjugated to ELR scaffolds to facilitate vascularization within the artificial matrix, which will shed light on solving the current challenge in restoring sufficient blood supply to support cellular growth. Modification of ELR scaffolds with growth factors such as bone morphogenetic protein 1 (BMP_1) and transforming growth factor (TGF) can improve the osteoconductivity of the scaffold, thereby stimulating the growth of targeted tissues. Some other biomolecules such as small sequences of DNA, mRNA, or therapeutic peptides can be linked to the scaffold and utilized in gene therapy or cancer treatment. Thus, development of the st-ELR scaffold and the bioconjugation method provides great and wide potential in tissue engineering.

Chapter 7: Bibliography

1. Marshall Jr GW: **Dentin: Microstructure and characterization**. *Quintessence International* 1993, **24**(9).
2. Goldberg M, Kulkarni AB, Young M, Boskey A: **Dentin: Structure, Composition and Mineralization: The role of dentin ECM in dentin formation and mineralization**. *Frontiers in bioscience (Elite edition)* 2011, **3**:711.
3. Sessle B: **Invited review: the neurobiology of facial and dental pain: present knowledge, future directions**. *Journal of Dental Research* 1987, **66**(5):962-981.
4. Pashley DH: **Dynamics of the pulpo-dentin complex**. *Critical Reviews in Oral Biology & Medicine* 1996, **7**(2):104-133.
5. Pashley DH, Carvalho R: **Dentine permeability and dentine adhesion**. *Journal of dentistry* 1997, **25**(5):355-372.
6. Bergenholtz G: **Evidence for bacterial causation of adverse pulpal responses in resin-based dental restorations**. *Critical Reviews in Oral Biology & Medicine* 2000, **11**(4):467-480.
7. Hahn C-L, Liewehr FR: **Relationships between caries bacteria, host responses, and clinical signs and symptoms of pulpitis**. *Journal of endodontics* 2007, **33**(3):213-219.
8. Kinra D: **Endodontic quality: at what cost**. *Dentistry today* 2011, **30**(7):14, 16-14, 16.
9. AAo E: **Endodontics: Colleagues for Excellence-Cracking the Cracked Tooth Code**. *Chicago, IL: American Association of Endodontists* 2008.
10. Ajay Sharma L, Sharma A, Dias GJ: **Advances in regeneration of dental pulp–a literature review**. *Journal of investigative and clinical dentistry,* 2015, **6**(2):,pp. 85-98.
11. FORD TRP, Torabinejad M, ABEDI HR, BAKLAND LK, KARIYAWASAM SP: **Using mineral trioxide aggregate as a pulp-capping material**. *The Journal of the American Dental Association* 1996, **127**(10):1491-1494.
12. Asgary S, Eghbal MJ, Parirokh M, Ghanavati F, Rahimi H: **A comparative study of histologic response to different pulp capping materials and a novel endodontic cement**. *Oral Surgery, Oral Medicine, Oral Pathology, Oral Radiology, and Endodontology* 2008, **106**(4):609-614.
13. Parirokh M, Torabinejad M: **Mineral trioxide aggregate: a comprehensive literature review—part III: clinical applications, drawbacks, and mechanism of action**. *Journal of endodontics* 2010, **36**(3):400-413.
14. Schuurs A, Gruythuysen R, Wesselink P: **Pulp capping with adhesive resin - based composite vs. calcium hydroxide: a review**. *Dental Traumatology* 2000, **16**(6):240-250.
15. de Souza CC, Duarte PT, De Souza P, Giro E, Hebling J: **Cytotoxic effects and pulpal response caused by a mineral trioxide aggregate formulation and calcium hydroxide**. *American journal of dentistry* 2008, **21**(4):255-261.
16. Sculean A, Nikolidakis D, Schwarz F: **Regeneration of periodontal tissues: combinations of barrier membranes and grafting materials–biological foundation and preclinical evidence: a systematic review**. *Journal of clinical periodontology* 2008, **35**(s8):106-116.
17. Iohara K, Nakashima M, Ito M, Ishikawa M, Nakasima A, Akamine A: **Dentin regeneration by dental pulp stem cell therapy with recombinant human bone morphogenetic protein 2**. *Journal of Dental Research* 2004, **83**(8):590-595.
18. Nakashima M, Akamine A: **The application of tissue engineering to regeneration of pulp and dentin in endodontics**. *Journal of endodontics* 2005, **31**(10):711-718.
19. Yen A-H, Yelick P: **Dental tissue regeneration–a mini-review**. *Gerontology* 2011, **57**(1):85-94.

20.   Zhang W, Yelick PC: **Vital pulp therapy—current progress of dental pulp regeneration and revascularization**. *International journal of dentistry* 2010, **2010**.
21.   Huang GT-J: **Dental pulp and dentin tissue engineering and regeneration–advancement and challenge**. *Frontiers in bioscience (Elite edition)* 2011, **3**:788.
22.   Griffith LG, Naughton G: **Tissue engineering--current challenges and expanding opportunities**. *Science* 2002, **295**(5557):1009-1014.
23.   Howard D, Buttery LD, Shakesheff KM, Roberts SJ: **Tissue engineering: strategies, stem cells and scaffolds**. *Journal of anatomy* 2008, **213**(1):66-72.
24.   Lind M: **Growth factors: Possible new clinical tools - A review**. *Acta Orthop Scand* 1996, **67**(4):407-417.
25.   Silva EA, Mooney DJ: **Synthetic extracellular matrices for tissue engineering and regeneration**. *Curr Top Dev Biol* 2004, **64**:181-205.
26.   Hutmacher DW: **Scaffolds in tissue engineering bone and cartilage**. *Biomaterials* 2000, **21**(24):2529-2543.
27.   Chang B-S, Hong K-S, Youn H-J, Ryu H-S, Chung S-S, Park K-W: **Osteoconduction at porous hydroxyapatite with various pore configurations**. *Biomaterials* 2000, **21**(12):1291-1298.
28.   Gauthier O, Bouler J-M, Aguado E, Pilet P, Daculsi G: **Macroporous biphasic calcium phosphate ceramics: influence of macropore diameter and macroporosity percentage on bone ingrowth**. *Biomaterials* 1998, **19**(1):133-139.
29.   Lu J, Flautre B, Anselme K, Hardouin P, Gallur A, Descamps M, Thierry B: **Role of interconnections in porous bioceramics on bone recolonization in vitro and in vivo**. *Journal of Materials Science: Materials in Medicine* 1999, **10**(2):111-120.
30.   Mastrogiacomo M, Scaglione S, Martinetti R, Dolcini L, Beltrame F, Cancedda R, Quarto R: **Role of scaffold internal structure on in vivo bone formation in macroporous calcium phosphate bioceramics**. *Biomaterials* 2006, **27**(17):3230-3237.
31.   Nam YS, Park TG: **Biodegradable polymeric microcellular foams by modified thermally induced phase separation method**. *Biomaterials* 1999, **20**(19):1783-1790.
32.   Thadavirul N, Pavasant P, Supaphol P: **Development of polycaprolactone porous scaffolds by combining solvent casting, particulate leaching, and polymer leaching techniques for bone tissue engineering**. *Journal of Biomedical Materials Research Part A* 2014, **102**(10):3379-3392.
33.   Mikos AG, Thorsen AJ, Czerwonka LA, Bao Y, Langer R, Winslow DN, Vacanti JP: **Preparation and characterization of poly (L-lactic acid) foams**. *Polymer* 1994, **35**(5):1068-1077.
34.   Yang S, Leong K-F, Du Z, Chua C-K: **The design of scaffolds for use in tissue engineering. Part I. Traditional factors**. *Tissue engineering* 2001, **7**(6):679-689.
35.   Xu C, Inai R, Kotaki M, Ramakrishna S: **Aligned biodegradable nanofibrous structure: a potential scaffold for blood vessel engineering**. *Biomaterials* 2004, **25**(5):877-886.
36.   Zhang L, Morsi Y, Wang Y, Li Y, Ramakrishna S: **Review scaffold design and stem cells for tooth regeneration**. *Japanese Dental Science Review* 2013, **49**(1):14-26.
37.   Kim HW, Lee HH, Knowles J: **Electrospinning biomedical nanocomposite fibers of hydroxyapatite/poly (lactic acid) for bone regeneration**. *Journal of Biomedical Materials Research Part A* 2006, **79**(3):643-649.
38.   Zhang Y, Ouyang H, Lim CT, Ramakrishna S, Huang ZM: **Electrospinning of gelatin fibers and gelatin/PCL composite fibrous scaffolds**. *Journal of Biomedical Materials Research Part B: Applied Biomaterials* 2005, **72**(1):156-165.

39. Song J-H, Kim H-E, Kim H-W: **Electrospun fibrous web of collagen–apatite precipitated nanocomposite for bone regeneration**. *Journal of Materials Science: Materials in Medicine* 2008, **19**(8):2925-2932.

40. Shin S-Y, Park H-N, Kim K-H, Lee M-H, Choi YS, Park Y-J, Lee Y-M, Ku Y, Rhyu I-C, Han S-B: **Biological evaluation of chitosan nanofiber membrane for guided bone regeneration**. *Journal of periodontology* 2005, **76**(10):1778-1784.

41. Murugan R, Ramakrishna S: **Nano-featured scaffolds for tissue engineering: a review of spinning methodologies**. *Tissue engineering* 2006, **12**(3):435-447.

42. Yoshimoto H, Shin YM, Terai H, Vacanti JP: **A biodegradable nanofiber scaffold by electrospinning and its potential for bone tissue engineering**. *Biomaterials* 2003, **24**(12):2077-2082.

43. Keogh MB, O'Brien FJ, Daly JS: **Substrate stiffness and contractile behaviour modulate the functional maturation of osteoblasts on a collagen–GAG scaffold**. *Acta biomaterialia* 2010, **6**(11):4305-4313.

44. Leipzig ND, Shoichet MS: **The effect of substrate stiffness on adult neural stem cell behavior**. *Biomaterials* 2009, **30**(36):6867-6878.

45. Balooch M, Habelitz S, Kinney JH, Marshall SJ, Marshall GW: **Mechanical properties of mineralized collagen fibrils as influenced by demineralization**. *J Struct Biol* 2008, **162**(3):404-410.

46. Siperko LM, Landis WJ: **Aspects of mineral structure in normally calcifying avian tendon**. *J Struct Biol* 2001, **135**(3):313-320.

47. Dubey DK, Tomar V: **Role of the nanoscale interfacial arrangement in mechanical strength of tropocollagen-hydroxyapatite-based hard biomaterials**. *Acta Biomaterialia* 2009, **5**(7):2704-2716.

48. Beniash E: **Biominerals—hierarchical nanocomposites: the example of bone**. *Wiley Interdisciplinary Reviews: Nanomedicine and Nanobiotechnology* 2011, **3**(1):47-69.

49. Roach H: **Why does bone matrix contain non-collagenous proteins? The possible roles of osteocalcin, osteonectin, osteopontin and bone sialoprotein in bone mineralisation and resorption**. *Cell biology international* 1994, **18**(6):617-628.

50. Qin C, Baba O, Butler W: **Post-translational modifications of sibling proteins and their roles in osteogenesis and dentinogenesis**. *Critical Reviews in Oral Biology & Medicine* 2004, **15**(3):126-136.

51. Traub W, Jodaikin A, Arad T, Veis A, Sabsay B: **Dentin phosphophoryn binding to collagen fibrils**. *Matrix* 1992, **12**(3):197-201.

52. Nudelman F, Pieterse K, George A, Bomans PH, Friedrich H, Brylka LJ, Hilbers PA, de With G, Sommerdijk NA: **The role of collagen in bone apatite formation in the presence of hydroxyapatite nucleation inhibitors**. *Nature materials* 2010, **9**(12):1004-1009.

53. Olszta MJ, Cheng XG, Jee SS, Kumar R, Kim YY, Kaufman MJ, Douglas EP, Gower LB: **Bone structure and formation: A new perspective**. *Mat Sci Eng R* 2007, **58**(3-5):77-116.

54. Thula TT, Rodriguez DE, Lee MH, Pendi L, Podschun J, Gower LB: **In vitro mineralization of dense collagen substrates: a biomimetic approach toward the development of bone-graft materials**. *Acta biomaterialia* 2011, **7**(8):3158-3169.

55. Jose MV, Thomas V, Johnson KT, Dean DR, Nyairo E: **Aligned PLGA/HA nanofibrous nanocomposite scaffolds for bone tissue engineering**. *Acta biomaterialia* 2009, **5**(1):305-315.

56.   Chen JL, Chu B, Hsiao BS: **Mineralization of hydroxyapatite in electrospun nanofibrous poly(L-lactic acid) scaffolds**. *Journal of Biomedical Materials Research Part A* 2006, **79A**(2):307-317.

57.   Gowda DC, Parker TM, Harris RD, Urry DW: **Synthesis, characterizations, and medical applications of bioelastic materials**. In: *Peptides.* Springer; 1994: 81-111.

58.   Rodriguez-Cabello JC, Martin L, Alonso M, Arias FJ, Testera AM: **"Recombinamers" as advanced materials for the post-oil age**. *Polymer* 2009, **50**(22):5159-5169.

59.   Prieto S, Shkilnyy A, Rumplasch C, Ribeiro A, Arias FJ, Rodríguez-Cabello JC, Taubert A: **Biomimetic calcium phosphate mineralization with multifunctional elastin-like recombinamers**. *Biomacromolecules* 2011, **12**(5):1480-1486.

60.   Herrero-Vanrell R, Rincon A, Alonso M, Reboto V, Molina-Martinez I, Rodriguez-Cabello J: **Self-assembled particles of an elastin-like polymer as vehicles for controlled drug release**. *Journal of Controlled Release* 2005, **102**(1):113-122.

61.   Reguera J, Fahmi A, Moriarty P, Girotti A, Rodríguez-Cabello JC: **Nanopore formation by self-assembly of the model genetically engineered elastin-like polymer [(VPGVG) 2 (VPGEG)(VPGVG) 2] 15**. *Journal of the American Chemical Society* 2004, **126**(41):13212-13213.

62.   Li YP, Chen X, Fok A, Rodriguez-Cabello JC, Aparicio C: **Biomimetic Mineralization of Recombinamer-Based Hydrogels toward Controlled Morphologies and High Mineral Density**. *Acs Appl Mater Inter* 2015, **7**(46):25784-25792.

63.   Tejeda-Montes E, Klymov A, Nejadnik MR, Alonso M, Rodriguez-Cabello JC, Walboomers XF, Mata A: **Mineralization and bone regeneration using a bioactive elastin-like recombinamer membrane**. *Biomaterials* 2014, **35**(29):8339-8347.

64.   Shah S, Kosoric J, Hector MP, Anderson P: **An in vitro scanning microradiography study of the reduction in hydroxyapatite demineralization rate by statherin-like peptides as a function of increasing N-terminal length**. *Eur J Oral Sci* 2011, **119**:13-18.

65.   Santos O, Kosoric J, Hector MP, Anderson P, Lindh L: **Adsorption behavior of statherin and a statherin peptide onto hydroxyapatite and silica surfaces by in situ ellipsometry**. *J Colloid Interf Sci* 2008, **318**(2):175-182.

66.   Raj PA, Johnsson M, Levine MJ, Nancollas GH: **Salivary Statherin - Dependence on Sequence, Charge, Hydrogen-Bonding Potency, and Helical Conformation for Adsorption to Hydroxyapatite and Inhibition of Mineralization**. *J Biol Chem* 1992, **267**(9):5968-5976.

67.   Gronthos S, Mankani M, Brahim J, Robey PG, Shi S: **Postnatal human dental pulp stem cells (DPSCs) in vitro and in vivo**. *Proceedings of the National Academy of Sciences* 2000, **97**(25):13625-13630.

68.   Murray PE, Lumley PJ, Ross HF, Smith AJ: **Tooth slice organ culture for cytotoxicity assessment of dental materials**. *Biomaterials* 2000, **21**(16):1711-1721.

69.   Murray PE, Garcia-Godoy F, Hargreaves KM: **Regenerative endodontics: a review of current status and a call for action**. *Journal of endodontics* 2007, **33**(4):377-390.

70.   Yang X, Yang F, Walboomers XF, Bian Z, Fan M, Jansen JA: **The performance of dental PCL/gelatin/nHA scaffolds pulp stem cells on nanofibrous**. *JOURNAL OF BIOMEDICAL MATERIALS RESEARCH PART A* 2010, **93**(1):247-257.

71.   Yu J, Deng Z, Shi J, Zhai H, Nie X, Zhuang H, Li Y, Jin Y: **Differentiation of dental pulp stem cells into regular-shaped dentin-pulp complex induced by tooth germ cell conditioned medium**. *Tissue engineering* 2006, **12**(11):3097-3105.

72. Almushayt A, Narayanan K, Zaki A, George A: **Dentin matrix protein 1 induces cytodifferentiation of dental pulp stem cells into odontoblasts**. *Gene therapy* 2006, **13**(7):611-620.

73. Wang J, Ma HY, Jin XB, Hu J, Liu XH, Ni LX, Ma PX: **The effect of scaffold architecture on odontogenic differentiation of human dental pulp stem cells**. *Biomaterials* 2011, **32**(31):7822-7830.

74. Engler AJ, Sen S, Sweeney HL, Discher DE: **Matrix elasticity directs stem cell lineage specification**. *Cell* 2006, **126**(4):677-689.

75. Zheng L, Yang F, Shen H, Hu X, Mochizuki C, Sato M, Wang S, Zhang Y: **The effect of composition of calcium phosphate composite scaffolds on the formation of tooth tissue from human dental pulp stem cells**. *Biomaterials* 2011, **32**(29):7053-7059.

76. Campoccia D, Montanaro L, Arciola CR: **The significance of infection related to orthopedic devices and issues of antibiotic resistance**. *Biomaterials* 2006, **27**(11):2331-2339.

77. Aas JA, Paster BJ, Stokes LN, Olsen I, Dewhirst FE: **Defining the normal bacterial flora of the oral cavity**. *J Clin Microbiol* 2005, **43**(11):5721-5732.

78. Zaura E, Keijser BJ, Huse SM, Crielaard W: **Defining the healthy**. *BMC microbiology* 2009, **9**(1):259.

79. Marsh P: **Are dental diseases examples of ecological catastrophes?** *Microbiology* 2003, **149**(2):279-294.

80. Tanzer JM, Livingston J, Thompson AM: **The microbiology of primary dental caries in humans**. *Journal of dental education* 2001, **65**(10):1028-1037.

81. Nyvad B, Kilian M: **Comparison of the initial streptococcal microflora on dental enamel in caries-active and in caries-inactive individuals**. *Caries research* 1990, **24**(4):267-272.

82. Kayaoglu G, Ørstavik D: **Virulence factors of Enterococcus faecalis: relationship to endodontic disease**. *Critical Reviews in Oral Biology & Medicine* 2004, **15**(5):308-320.

83. Love RM, Jenkinson HF: **Invasion of dentinal tubules by oral bacteria**. *Critical reviews in oral biology and medicine : an official publication of the American Association of Oral Biologists* 2002, **13**(2):171-183.

84. Trelles K, Arnabat J, Espana-Tost T: **Microleakage in Class V cavities with self-etching adhesive system and conventional rotatory or laser Er,Cr:YSGG**. *Laser therapy* 2012, **21**(4):255-268.

85. Silverman LD, Lukashova L, Herman OT, Lane JM, Boskey AL: **Release of gentamicin from a tricalcium phosphate bone implant**. *Journal of orthopaedic research* 2007, **25**(1):23-29.

86. Jiang B: **Multifunctional Biomaterial System for Drug Delivery and Scaffolding to Promote Neovascularization in Tissue Engineering**. 2013.

87. Song J-H: **What's new on the antimicrobial horizon?** *International Journal of Antimicrobial Agents* 2008, **32**:S207-S213.

88. Giuliani A, Pirri G, Bozzi A, Di Giulio A, Aschi M, Rinaldi A: **Antimicrobial peptides: natural templates for synthetic membrane-active compounds**. *Cellular and Molecular Life Sciences* 2008, **65**(16):2450-2460.

89. Hancock RE, Sahl H-G: **Antimicrobial and host-defense peptides as new anti-infective therapeutic strategies**. *Nature biotechnology* 2006, **24**(12):1551-1557.

90. Brogden KA: **Antimicrobial peptides: pore formers or metabolic inhibitors in bacteria?** *Nature Reviews Microbiology* 2005, **3**(3):238-250.

91.   Findlay B, Zhanel GG, Schweizer F: **Cationic Amphiphiles, a New Generation of Antimicrobials Inspired by the Natural Antimicrobial Peptide Scaffold**. *Antimicrob Agents Ch* 2010, **54**(10):4049-4058.

92.   Yang L, Harroun TA, Weiss TM, Ding L, Huang HW: **Barrel-stave model or toroidal model? A case study on melittin pores**. *Biophysical journal* 2001, **81**(3):1475-1485.

93.   Pouny Y, Rapaport D, Mor A, Nicolas P, Shai Y: **Interaction of antimicrobial dermaseptin and its fluorescently labeled analogs with phospholipid membranes**. *Biochemistry* 1992, **31**(49):12416-12423.

94.   Matsuzaki K, Murase O, Fujii N, Miyajima K: **An antimicrobial peptide, magainin 2, induced rapid flip-flop of phospholipids coupled with pore formation and peptide translocation**. *Biochemistry* 1996, **35**(35):11361-11368.

95.   Haynie SL, Crum GA, Doele BA: **Antimicrobial activities of amphiphilic peptides covalently bonded to a water-insoluble resin**. *Antimicrobial agents and chemotherapy* 1995, **39**(2):301-307.

96.   Onaizi SA, Leong SS: **Tethering antimicrobial peptides: current status and potential challenges**. *Biotechnology advances* 2011, **29**(1):67-74.

97.   Hilpert K, Elliott M, Jenssen H, Kindrachuk J, Fjell CD, Körner J, Winkler DF, Weaver LL, Henklein P, Ulrich AS: **Screening and characterization of surface-tethered cationic peptides for antimicrobial activity**. *Chemistry & biology* 2009, **16**(1):58-69.

98.   Chen X, Hirt H, Li YP, Gorr SU, Aparicio C: **Antimicrobial GL13K Peptide Coatings Killed and Ruptured the Wall of Streptococcus gordonii and Prevented Formation and Growth of Biofilms**. *Plos One* 2014, **9**(11).

99.   Holmberg KV, Abdolhosseini M, Li YP, Chen X, Gorr SU, Aparicio C: **Bio-inspired stable antimicrobial peptide coatings for dental applications**. *Acta Biomaterialia* 2013, **9**(9):8224-8231.

100.   Hirt H, Gorr S-U: **Antimicrobial peptide GL13K is effective in reducing biofilms of Pseudomonas aeruginosa**. *Antimicrobial agents and chemotherapy* 2013, **57**(10):4903-4910.

101.   Schnitt RA: **Antimicrobial Effects of GL13K Peptide Coatings on S. mutans and L. casei**. UNIVERSITY OF MINNESOTA; 2015.

102.   Holzwarth JM, Ma PX: **Biomimetic nanofibrous scaffolds for bone tissue engineering**. *Biomaterials* 2011, **32**(36):9622-9629.

103.   Elsdale T, Bard J: **Collagen substrata for studies on cell behavior**. *The Journal of cell biology* 1972, **54**(3):626-637.

104.   Landis WJ, Hodgens KJ, Arena J, Song MJ, McEwen BF: **Structural relations between collagen and mineral in bone as determined by high voltage electron microscopic tomography**. *Microsc Res Techniq* 1996, **33**(2):192-202.

105.   Fratzl P, Groschner M, Vogl G, Plenk H, Eschberger J, Fratzl-Zelman N, Koller K, Klaushofer K: **Mineral crystals in calcified tissues: a comparative study by SAXS**. *J Bone Miner Res* 1992, **7**(3):329-334.

106.   Jee SS, Kasinath RK, DiMasi E, Kim YY, Gower L: **Oriented hydroxyapatite in turkey tendon mineralized via the polymer-induced liquid-precursor (PILP) process**. *Crystengcomm* 2011, **13**(6):2077-2083.

107.   Li YP, Thula TT, Jee S, Perkins SL, Aparicio C, Douglas EP, Gower LB: **Biomimetic Mineralization of Woven Bone-Like Nanocomposites: Role of Collagen Cross-Links**. *Biomacromolecules* 2012, **13**(1):49-59.

108. El‑Backly RM, Massoud AG, El‑Badry AM, Sherif RA, Marei MK: **Regeneration of dentine/pulp‑like tissue using a dental pulp stem cell/poly (lactic‑co‑glycolic) acid scaffold construct in New Zealand white rabbits**. *Australian Endodontic Journal* 2008, **34**(2):52-67.

109. Young CS, Terada S, Vacanti JP, Honda M, Bartlett JD, Yelick PC: **Tissue engineering of complex tooth structures on biodegradable polymer scaffolds**. *Journal of Dental Research* 2002, **81**(10):695-700.

110. Ma Z, Kotaki M, Ramakrishna S: **Electrospun cellulose nanofiber as affinity membrane**. *Journal of membrane science* 2005, **265**(1):115-123.

111. Matthews JA, Wnek GE, Simpson DG, Bowlin GL: **Electrospinning of collagen nanofibers**. *Biomacromolecules* 2002, **3**(2):232-238.

112. Buttafoco L, Kolkman N, Engbers-Buijtenhuijs P, Poot A, Dijkstra P, Vermes I, Feijen J: **Electrospinning of collagen and elastin for tissue engineering applications**. *Biomaterials* 2006, **27**(5):724-734.

113. Shin SY, Park HN, Kim KH, Lee MH, Choi YS, Park YJ, Lee YM, Ku Y, Rhyu IC, Han SB *et al*: **Biological evaluation of chitosan nanofiber membrane for guided bone regeneration**. *J Periodontol* 2005, **76**(10):1778-1784.

114. Khatiwala CB, Peyton SR, Putnam AJ: **Intrinsic mechanical properties of the extracellular matrix affect the behavior of pre-osteoblastic MC3T3-E1 cells**. *Am J Physiol Cell Physiol* 2006, **290**(6):C1640-1650.

115. Guo Y, Zhang CQ, Zeng QC, Li RX, Liu L, Hao QX, Shi CH, Zhang XZ, Yan YX: **Mechanical strain promotes osteoblast ECM formation and improves its osteoinductive potential**. *Biomed Eng Online* 2012, **11**:80.

116. Parekh SH, Chatterjee K, Lin-Gibson S, Moore NM, Cicerone MT, Young MF, Simon CG: **Modulus-driven differentiation of marrow stromal cells in 3D scaffolds that is independent of myosin-based cytoskeletal tension**. *Biomaterials* 2011, **32**(9):2256-2264.

117. Bertassoni LE, Habelitz S, Kinney J, Marshall SJ, Marshall Jr GW: **Biomechanical perspective on the remineralization of dentin**. *Caries research* 2009, **43**(1):70-77.

118. Kinney J, Habelitz S, Marshall S, Marshall G: **The importance of intrafibrillar mineralization of collagen on the mechanical properties of dentin**. *Journal of dental research* 2003, **82**(12):957-961.

119. Wutticharoenmongkol P, Pavasant P, Supaphol P: **Osteoblastic phenotype expression of MC3T3-E1 cultured on electrospun polycaprolactone fiber mats filled with hydroxyapatite nanoparticles**. *Biomacromolecules* 2007, **8**(8):2602-2610.

120. Kim HW, Kim HE: **Nanofiber generation of hydroxyapatite and fluor‑hydroxyapatite bioceramics**. *Journal of Biomedical Materials Research Part B: Applied Biomaterials* 2006, **77**(2):323-328.

121. Rodriguez K, Renneckar S, Gatenholm P: **Biomimetic Calcium Phosphate Crystal Mineralization on Electrospun Cellulose-Based Scaffolds**. *Acs Appl Mater Inter* 2011, **3**(3):681-689.

122. MacEwan SR, Chilkoti A: **Elastin‑like polypeptides: Biomedical applications of tunable biopolymers**. *Peptide Science* 2010, **94**(1):60-77.

123. Salvagni E, Berguig G, Engel E, Rodriguez-Cabello JC, Coullerez G, Textor M, Planell JA, Gil FJ, Aparicio C: **A bioactive elastin-like recombinamer reduces unspecific protein adsorption and enhances cell response on titanium surfaces**. *Colloids Surf B Biointerfaces* 2014, **114**:225-233.

124. de Torre IG, Santos M, Quintanilla L, Testera A, Alonso M, Cabello JCR: **Elastin-like recombinamer catalyst-free click gels: Characterization of poroelastic and intrinsic viscoelastic properties**. *Acta biomaterialia* 2014, **10**(6):2495-2505.

125. Li Y, Chen X, Ribeiro AJ, Jensen ED, Holmberg KV, Rodriguez‑Cabello JC, Aparicio C: **Hybrid Nanotopographical Surfaces Obtained by Biomimetic Mineralization of Statherin‑Inspired Elastin‑Like Recombinamers**. *Advanced healthcare materials* 2014, **3**(10):1638-1647.

126. Girotti A, Reguera J, Rodríguez-Cabello JC, Arias FJ, Alonso M, Testera AM: **Design and bioproduction of a recombinant multi (bio) functional elastin-like protein polymer containing cell adhesion sequences for tissue engineering purposes**. *Journal of Materials Science: Materials in Medicine* 2004, **15**(4):479-484.

127. Jee SS, Culver L, Li Y, Douglas EP, Gower LB: **Biomimetic mineralization of collagen via an enzyme-aided PILP process**. *Journal of Crystal Growth* 2010, **312**(8):1249-1256.

128. Li Y, Aparicio C: **Discerning the subfibrillar structure of mineralized collagen fibrils: A model for the ultrastructure of bone**. *PloS one* 2013, **8**(9):e76782.

129. Oliver WC, Pharr GM: **An Improved Technique for Determining Hardness and Elastic-Modulus Using Load and Displacement Sensing Indentation Experiments**. *J Mater Res* 1992, **7**(6):1564-1583.

130. Kirkham J, Brookes SJ, Shore RC, Bonass WA, Robinson C: **The effect of glycosylaminoglycans on the mineralization of sheep periodontal ligament in vitro**. *Connect Tissue Res* 1995, **33**(1-3):23-29.

131. Veis A: **Mineralization in organic matrix frameworks**. *Rev Mineral Geochem* 2003, **54**:249-289.

132. Gower LB: **Biomimetic model systems for investigating the amorphous precursor pathway and its role in biomineralization**. *Chemical reviews* 2008, **108**(11):4551-4627.

133. Liu Y, Kim Y-K, Dai L, Li N, Khan SO, Pashley DH, Tay FR: **Hierarchical and non-hierarchical mineralisation of collagen**. *Biomaterials* 2011, **32**(5):1291-1300.

134. Yeo GC, Aghaei-Ghareh-Bolagh B, Brackenreg EP, Hiob MA, Lee P, Weiss AS: **Fabricated Elastin**. *Advanced Healthcare Materials* 2015, **4**(16):2530-2556.

135. Cantaert B, Beniash E, Meldrum FC: **The role of poly(aspartic acid) in the precipitation of calcium phosphate in confinement**. *J Mater Chem B* 2013, **1**(48):6586-6595.

136. Piez KA, Miller A: **The structure of collagen fibrils**. *J Supramol Struct* 1974, **2**(2-4):121-137.

137. Orgel JPRO, Irving TC, Miller A, Wess TJ: **Microfibrillar structure of type I collagen in situ**. *P Natl Acad Sci USA* 2006, **103**(24):9001-9005.

138. Zhang X, Nakagawa R, Chan KHK, Kotaki M: **Mechanical property enhancement of polylactide nanofibers through optimization of molecular weight, electrospinning conditions, and stereocomplexation**. *Macromolecules* 2012, **45**(13):5494-5500.

139. Even-Ram S, Artym V, Yamada KM: **Matrix control of stem cell fate**. *Cell* 2006, **126**(4):645-647.

140. Wang J, Ma H, Jin X, Hu J, Liu X, Ni L, Ma PX: **The effect of scaffold architecture on odontogenic differentiation of human dental pulp stem cells**. *Biomaterials* 2011, **32**(31):7822-7830.

141. Sedgley CM, Messer HH: **Are endodontically treated teeth more brittle?** *Journal of Endodontics* 1992, **18**(7):332-335.

142. d'Aquino R, De Rosa A, Laino G, Caruso F, Guida L, Rullo R, Checchi V, Laino L, Tirino V, Papaccio G: **Human Dental Pulp Stem Cells: From Biology to Clinical Applications**. *J Exp Zool Part B* 2009, **312B**(5):408-415.

143. Ravindran S, Gao Q, Kotecha M, Magin RL, Karol S, Bedran-Russo A, George A: **Biomimetic extracellular matrix-incorporated scaffold induces osteogenic gene expression in human marrow stromal cells**. *Tissue Engineering Part A* 2011, **18**(3-4):295-309.

144. Teo WE, He W, Ramakrishna S: **Electrospun scaffold tailored for tissue‐specific extracellular matrix**. *Biotechnology journal* 2006, **1**(9):918-929.

145. Gajjeraman S, Narayanan K, Hao JJ, Qin CL, George A: **Matrix macromolecules in hard tissues control the nucleation and hierarchical assembly of hydroxyapatite**. *J Biol Chem* 2007, **282**(2):1193-1204.

146. Landis WJ, Hodgens KJ, Song MJ, Arena J, Kiyonaga S, Marko M, Owen C, McEwen BF: **Mineralization of collagen may occur on fibril surfaces: Evidence from conventional and high-voltage electron microscopy and three-dimensional imaging**. *J Struct Biol* 1996, **117**(1):24-35.

147. Grinnell F, Bennett MH: **Ultrastructural studies of cell--collagen interactions**. *Methods in enzymology* 1982, **82**:535.

148. Nakashima M, Iohara K: **Pulp Regeneration by Harnessing Dental Pulp Stem Cells**; 2014.

149. Gronthos S, Brahim J, Li W, Fisher L, Cherman N, Boyde A, DenBesten P, Robey PG, Shi S: **Stem cell properties of human dental pulp stem cells**. *Journal of Dental Research* 2002, **81**(8):531-535.

150. Zhong SP, Teo WE, Zhu X, Beuerman RW, Ramakrishna S, Yung LYL: **An aligned nanofibrous collagen scaffold by electrospinning and its effects on in vitro fibroblast culture**. *Journal of Biomedical Materials Research Part A* 2006, **79A**(3):456-463.

151. Itoh S, Kikuchi M, Takakuda K, Koyama Y, Matsumoto HN, Ichinose S, Tanaka J, Kawauchi T, Shinomiya K: **The biocompatibility and osteoconductive activity of a novel hydroxyapatite/collagen composite biomaterial, and its function as a carrier of rhBMP-2**. *J Biomed Mater Res* 2001, **54**(3):445-453.

152. Marsh PD: **Controlling the oral biofilm with antimicrobials**. *Journal of Dentistry* 2010, **38**:S11-S15.

153. Kuijer R, Jansen EJ, Emans PJ, Bulstra SK, Riesle J, Pieper J, Grainger DW, Busscher HJ: **Assessing infection risk in implanted tissue-engineered devices**. *Biomaterials* 2007, **28**(34):5148-5154.

154. Cook G, Costerton J, Lamont R: **Biofilm formation by Porphyromonas gingivalis and Streptococcus gordonii**. *Journal of periodontal research* 1998, **33**(6):323-327.

155. Hamada S, Slade HD: **Biology, immunology, and cariogenicity of Streptococcus mutans**. *Microbiological reviews* 1980, **44**(2):331.

156. Gomes BP, Pinheiro ET, Sousa EL, Jacinto RC, Zaia AA, Ferraz CCR, de Souza-Filho FJ: **Enterococcus faecalis in dental root canals detected by culture and by polymerase chain reaction analysis**. *Oral Surgery, Oral Medicine, Oral Pathology, Oral Radiology, and Endodontology* 2006, **102**(2):247-253.

157. Pinheiro E, Gomes B, Ferraz C, Teixeira F, Zaia A, Souza Filho F: **Evaluation of root canal microorganisms isolated from teeth with endodontic failure and their antimicrobial susceptibility**. *Oral microbiology and immunology* 2003, **18**(2):100-103.

158. Brading M, Marsh P: **The oral environment: the challenge for antimicrobials in oral care products**. *International dental journal* 2003, **53**(S6P1):353-362.

159. Busscher HJ, van der Mei HC, Subbiahdoss G, Jutte PC, van den Dungen JJ, Zaat SA, Schultz MJ, Grainger DW: **Biomaterial-associated infection: locating the finish line in the race for the surface**. *Science translational medicine* 2012, **4**(153):153rv110-153rv110.

160. Neu HC: **The crisis in antibiotic resistance**. *Science* 1992, **257**(5073):1064-1073.

161. Hancock RE, Lehrer R: **Cationic peptides: a new source of antibiotics**. *Trends in biotechnology* 1998, **16**(2):82-88.

162. Hancock RE, Diamond G: **The role of cationic antimicrobial peptides in innate host defences**. *Trends in microbiology* 2000, **8**(9):402-410.

163. Costa F, Carvalho IF, Montelaro RC, Gomes P, Martins MCL: **Covalent immobilization of antimicrobial peptides (AMPs) onto biomaterial surfaces**. *Acta Biomaterialia* 2011, **7**(4):1431-1440.

164. Balhara V, Schmidt R, Gorr SU, DeWolf C: **Membrane selectivity and biophysical studies of the antimicrobial peptide GL13K**. *Bba-Biomembranes* 2013, **1828**(9):2193-2203.

165. Godoy-Gallardo M, Wang ZJ, Shen Y, Manero JM, Gil FJ, Rodriguez D, Haapasale M: **Antibacterial Coatings on Titanium Surfaces: A Comparison Study Between in Vitro Single-Species and Multispecies Biofilm**. *Acs Appl Mater Inter* 2015, **7**(10):5992-6001.

166. Godoy-Gallardo M, Mas-Moruno C, Fernandez-Calderon MC, Perez-Giraldo C, Manero JM, Albericio F, Gil FJ, Rodriguez D: **Covalent immobilization of hLf1-11 peptide on a titanium surface reduces bacterial adhesion and biofilm formation**. *Acta Biomaterialia* 2014, **10**(8):3522-3534.

167. Jenssen H, Hamill P, Hancock RE: **Peptide antimicrobial agents**. *Clinical microbiology reviews* 2006, **19**(3):491-511.

168. Billiet L, Gok O, Dove AP, Sanyal A, Nguyen L-TT, Du Prez FE: **Metal-free functionalization of linear polyurethanes by thiol-maleimide coupling reactions**. *Macromolecules* 2011, **44**(20):7874-7878.

169. Phelps EA, Enemchukwu NO, Fiore VF, Sy JC, Murthy N, Sulchek TA, Barker TH, García AJ: **Maleimide cross‐linked bioactive peg hydrogel exhibits improved reaction kinetics and cross‐linking for cell encapsulation and in situ delivery**. *Advanced materials* 2012, **24**(1):64-70.

170. Wu P, Hogrebe P, Grainger DW: **DNA and protein microarray printing on silicon nitride waveguide surfaces**. *Biosensors and Bioelectronics* 2006, **21**(7):1252-1263.

171. Rezania A, Johnson R, Lefkow AR, Healy KE: **Bioactivation of metal oxide surfaces. 1. Surface characterization and cell response**. *Langmuir* 1999, **15**(20):6931-6939.

172. Zhao Y, Zhang J, Wang X, Chen B, Xiao Z, Shi C, Wei Z, Hou X, Wang Q, Dai J: **The osteogenic effect of bone morphogenetic protein-2 on the collagen scaffold conjugated with antibodies**. *Journal of controlled release : official journal of the Controlled Release Society* 2010, **141**(1):30-37.

173. Saha K, Keung AJ, Irwin EF, Li Y, Little L, Schaffer DV, Healy KE: **Substrate modulus directs neural stem cell behavior**. *Biophys J* 2008, **95**(9):4426-4438.

174. Ravi S, Krishnamurthy VR, Caves JM, Haller CA, Chaikof EL: **Maleimide–thiol coupling of a bioactive peptide to an elastin-like protein polymer**. *Acta biomaterialia* 2012, **8**(2):627-635.

175. Collins J, Tanaka J, Wilson P, Kempe K, Davis TP, McIntosh MP, Whittaker MR, Haddleton DM: **In Situ Conjugation of Dithiophenol Maleimide Polymers and Oxytocin for Stable and Reversible Polymer–Peptide Conjugates**. *Bioconjugate chemistry* 2015, **26**(4):633-638.

176. Chen X: **Multi-bioactive Peptide Coatings for Dental Implants**. UNIVERSITY OF MINNESOTA; 2014.

177. Johansson J, Gudmundsson GH, Rottenberg ME, Berndt KD, Agerberth B: **Conformation-dependent antibacterial activity of the naturally occurring human peptide LL-37**. *J Biol Chem* 1998, **273**(6):3718-3724.

178. Park CB, Yi K-S, Matsuzaki K, Kim MS, Kim SC: **Structure–activity analysis of buforin II, a histone H2A-derived antimicrobial peptide: the proline hinge is responsible for the cell-penetrating ability of buforin II**. *Proceedings of the National Academy of Sciences* 2000, **97**(15):8245-8250.

179. Yeaman MR, Yount NY: **Mechanisms of antimicrobial peptide action and resistance**. *Pharmacological reviews* 2003, **55**(1):27-55.

180. Paulsen IT, Banerjei L, Myers GSA, Nelson KE, Seshadri R, Read TD, Fouts DE, Eisen JA, Gill SR, Heidelberg JF *et al*: **Role of mobile DNA in the evolution of vancomycin-resistant Enterococcus faecalis**. *Science* 2003, **299**(5615):2071-2074.

181. Mohamed JA, Murray BE: **Lack of correlation of gelatinase production and biofilm formation in a large collection of Enterococcus faecalis isolates**. *J Clin Microbiol* 2005, **43**(10):5405-5407.

182. Baizman ER, Branstrom AA, Longley CB, Allanson N, Sofia MJ, Gange D, Goldman RC: **Antibacterial activity of synthetic analogues based on the disaccharide structure of moenomycin, an inhibitor of bacterial transglycosylase**. *Microbiology* 2000, **146**(12):3129-3140.

183. Eckhard LH, Sol A, Abtew E, Shai Y, Domb AJ, Bachrach G, Beyth N: **Biohybrid Polymer-Antimicrobial Peptide Medium against Enterococcus faecalis**. *PloS one* 2014, **9**(10):e109413.

184. Iohara K, Imabayashi K, Ishizaka R, Watanabe A, Nabekura J, Ito M, Matsushita K, Nakamura H, Nakashima M: **Complete pulp regeneration after pulpectomy by transplantation of CD105+ stem cells with stromal cell-derived factor-1**. *Tissue Engineering Part A* 2011, **17**(15-16):1911-1920.

185. Galler K, D'souza R, Hartgerink J, Schmalz G: **Scaffolds for dental pulp tissue engineering**. *Advances in dental research* 2011, **23**(3):333-339.

186. Bottino MC, Thomas V, Schmidt G, Vohra YK, Chu T-MG, Kowolik MJ, Janowski GM: **Recent advances in the development of GTR/GBR membranes for periodontal regeneration—a materials perspective**. *Dental materials* 2012, **28**(7):703-721.

187. Peter M, Binulal N, Nair S, Selvamurugan N, Tamura H, Jayakumar R: **Novel biodegradable chitosan–gelatin/nano-bioactive glass ceramic composite scaffolds for alveolar bone tissue engineering**. *Chemical Engineering Journal* 2010, **158**(2):353-361.

188. Bozic KJ, Ries MD: **The impact of infection after total hip arthroplasty on hospital and surgeon resource utilization**. *J Bone Joint Surg Am* 2005, **87**(8):1746-1751.

189. Francolini I, Donelli G: **Prevention and control of biofilm-based medical-device-related infections**. *FEMS Immunology & Medical Microbiology* 2010, **59**(3):227-238.

190. Ruckh TT, Oldinski RA, Carroll DA, Mikhova K, Bryers JD, Popat KC: **Antimicrobial effects of nanofiber poly (caprolactone) tissue scaffolds releasing rifampicin**. *Journal of Materials Science: Materials in Medicine* 2012, **23**(6):1411-1420.

191. Feng K, Sun H, Bradley MA, Dupler EJ, Giannobile WV, Ma PX: **Novel antibacterial nanofibrous PLLA scaffolds**. *Journal of Controlled Release* 2010, **146**(3):363-369.

192.   Amruthwar SS, Janorkar AV: **Preparation and characterization of elastin-like polypeptide scaffolds for local delivery of antibiotics and proteins**. *J Mater Sci-Mater M* 2012, **23**(12):2903-2912.

193.   Kim HW, Knowles JC, Kim HE: **Hydroxyapatite porous scaffold engineered with biological polymer hybrid coating for antibiotic Vancomycin release**. *J Mater Sci-Mater M* 2005, **16**(3):189-195.

194.   D'Britto V, Kapse H, Babrekar H, Prabhune A, Bhoraskar S, Premnath V, Prasad B: **Silver nanoparticle studded porous polyethylene scaffolds: bacteria struggle to grow on them while mammalian cells thrive**. *Nanoscale* 2011, **3**(7):2957-2963.

195.   Javadpour MM, Juban MM, Lo W-CJ, Bishop SM, Alberty JB, Cowell SM, Becker CL, McLaughlin ML: **De novo antimicrobial peptides with low mammalian cell toxicity**. *Journal of medicinal chemistry* 1996, **39**(16):3107-3113.

196.   Putsep K, Carlsson G, Boman HG, Andersson M: **Deficiency of antibacterial peptides in patients with morbus Kostmann: an observation study**. *Lancet* 2002, **360**(9340):1144-1149.